Investigating the Impact of *POLA2* Expression on Cytarabine Efficacy in Acute Myeloid Leukemia (AML)

by

Monika M. Kojic

Department of Pharmacology and Therapeutics

McGill University, Montréal, Québec, Canada

December 2024

A thesis submitted to McGill University in partial fulfillment of the requirements for the degree of Master of Science

Table of Contents:

Abstract:

Despite the availability of novel therapies for acute myeloid leukemia (AML), the frontline, curative treatment for most patients relies on the chemotherapeutic agent - cytarabine (ara-C). As a result, the five-year overall survival rate in AML patients is still ~30%. Thus, there is a critical need to improve the efficacy of cytarabine. However, even after decades of widespread clinical use, the mechanisms responsible for cytarabine's action in AML are poorly understood. Recent studies identified primer RNA as a favourable target of cytarabine incorporation. However, we do not know why ara-C is metabolized into RNA vs DNA or how this impacts AML patient outcomes. We hypothesize that ara-C incorporation into RNA depends on optimal function of the DNA polymerase alpha-primase complex and is particularly dependent on the expression of the alpha subunit B encoding gene – *POLA2*. To test this hypothesis, the following aims were completed: 1) Compare expression data of each subunit of the DNA polymerase alpha-primase complex vs. AML patient survival, 2) Develop *in vitro* AML approaches for altering *POLA2* expression, 3) Determine the impact of altered *POLA2* expression on AML cell death and variable ara-C incorporation into RNA vs DNA.

In the first aim, I analyzed the largest available set of validated AML mRNA expression data from clinical trials and the TCGA AML RNA-seq gene expression dataset. My results indicated a statistically significant correlation between low levels of *POLA2* and longer patient survival, establishing *POLA2* as a potential biomarker for AML prognosis. My second aim was to develop *in vitro* methods for *POLA2* modulation in AML cell lines. Though AML cell lines are notoriously difficult to transfect in vitro, I established new methods for siRNA-based downregulation of *POLA2* in two AML cell lines. Beyond establishing robust methods for siRNA

knockdown in AML cells, these results may facilitate future therapeutic development to improve cytarabine efficacy.

Finally, my last aim was to evaluate the impact of altered *POLA2* expression on cytarabine sensitivity and ara-C incorporation. By measuring both cell viability and proliferation, we confirmed that *POLA2* knockdown increased cell sensitivity to cytarabine treatment. However, using a "clickable" ara-C analog and a biorthogonal chemistry approach, no change in cytarabine uptake was observed. Furthermore, cells consistently displayed parthanatos features regardless of *POLA2* knockdown. Together, our results confirm the importance of *POLA2* in cytarabine efficacy though the mechanism for this response is unknown.

In summary, this thesis establishes a potential therapeutic role for *POLA2* in sensitizing patients to frontline ara-C treatment. By improving our understanding of how ara-C exerts its anti-leukemic effects, we aim to facilitate the development of new co-treatment strategies to improve long-term AML outcomes.

Résumé:

Malgré la disponibilité de nouvelles thérapies pour la leucémie myéloïde aiguë (LMA), le traitement curatif de première ligne pour la plupart des patients repose sur l'agent chimiothérapeutique - cytarabine (ara-C). Par conséquent, le taux de survie global à cinq ans chez les patients atteints de LMA est toujours d'environ 30 %. Il est donc essentiel d'améliorer l'efficacité de la cytarabine. Cependant, même après des décennies d'utilisation clinique généralisée, les mécanismes responsables de l'action de la cytarabine dans la LMA sont mal compris. Des études récentes ont identifié l'ARN de l'amorce comme cible favorable pour l'incorporation de la cytarabine. Cependant, nous ne savons pas pourquoi l'ara-C est métabolisé en ARN vs. ADN ni comment cela affecte les résultats des patients atteints de LMA. Nous supposons que l'incorporation de l'ara-C dans l'ARN dépend de la fonction optimale du complexe alpha-primase de l'ADN polymérase et est particulièrement tributaire de l'expression du gène codant pour la sous-unité alpha B, *POLA2*. Pour tester cette hypothèse, les objectifs suivants ont été réalisés : 1) Comparer les données d'expression de chaque sous-unité du complexe ADN polymérase alpha-primase contre la survie des patients LMA, 2) Développer des approches *in vitro* LMA pour modifier l'expression de la *POLA2*, 3) Déterminer l'impact de l'altération de l'expression de *POLA2* sur la mort cellulaire de la LMA et l'incorporation variable d'ara-C dans l'ARN contre l'ADN.

Dans le premier objectif, j'ai analysé le plus grand ensemble de données validées d'expression des ARNm LMA provenant d'essais cliniques et l'ensemble de données sur l'expression des gènes ARN-séq. Mes résultats ont indiqué une corrélation statistiquement significative entre les faibles niveaux de *POLA2* et la survie plus longue du patient, établissant *POLA2* comme biomarqueur potentiel pour le pronostic de LMA. Mon deuxième objectif était de

développer des méthodes *in vitro* pour la modulation *POLA2* dans les lignées cellulaires LMA. Bien que les lignées cellulaires LMA soient notoirement difficiles à transfecter *in vitro*, j'ai établi de nouvelles méthodes pour la régulation de *POLA2* basée sur siRNA dans deux lignées cellulaires LMA. Au-delà de l'établissement de méthodes robustes pour la transfection des siARN dans les cellules LMA, ces résultats peuvent faciliter le développement thérapeutique futur pour améliorer l'efficacité de la cytarabine.

Enfin, mon dernier objectif était d'évaluer l'impact de l'altération de l'expression de *POLA2* sur la sensibilité à la cytarabine et l'incorporation d'ara-C. En mesurant la viabilité et la prolifération des cellules, nous avons confirmé que la réduction de *POLA2* augmentait la sensibilité cellulaire au traitement par la cytarabine. Cependant, en utilisant un analogue ara-C « cliquable » et une approche chimique biorthogonale, aucun changement dans l'absorption de la cytarabine n'a été observé. De plus, les cellules affichaient systématiquement des traits parthanatos indépendamment de la réduction de *POLA2*. Ensemble, nos résultats confirment l'importance de la *POLA2* dans l'efficacité de la cytarabine bien que le mécanisme de cette réponse soit inconnu.

En résumé, cette thèse établit un rôle thérapeutique potentiel pour la *POLA2* dans la sensibilisation des patients au traitement de première ligne ara-C. En améliorant notre compréhension de la façon dont ara-C exerce ses effets anti-leucémiques, nous visons à faciliter le développement de nouvelles stratégies de co-traitement pour améliorer les résultats à long terme de la LMA.

Acknowledgments:

My M.Sc. journey has been one of most challenging and rewarding experiences in my academic career. I would like to express my deepest gratitude to my supervisor, Prof. Maureen McKeague, for her invaluable guidance, constant encouragement and support throughout the course of my research project. Maureen – thank you for your incredible mentorship and I am really looking forward to continuing my graduate research work under your guidance! I would also like to acknowledge my advisor, Prof. Jason Tanny, as well as my committee members, Prof. Bastien Castagner and Prof. Bernard Robaire for their valuable insights pertaining to my project.

A special thank you to all members of the McKeague lab, especially Olivia and Bruk, for all of their assistance, insightful discussions, and for creating an inspiring and collaborative research environment. Bruk and Olivia - your unwavering support and kind words made this journey so much more enjoyable. Additionally, I greatly appreciate the funding provided by NSERC PROMTOTE, the Cole Foundation, CIHR, and CRBS that made this work possible.

I am eternally grateful to my family and friends, whose unconditional support and belief in me has been a constant source of motivation. To my partner Blair, my parents, Izabella and Sinisa, and my sister Lidia - thank you for your unconditional love and encouragement. Lastly, I would like to thank everyone who, in one way or another, contributed to the completion of this thesis. Your kindness and generosity did not go unnoticed. You have made this a truly unforgettable and fulfilling journey.

Contribution of Authors:

All chapters presented in this thesis are authored by Monika M. Kojic and edited by Prof. Maureen McKeague.

Experimental work was executed by Monika M. Kojic and guided by Prof. Maureen McKeague.

List of Abbreviations:

53BP1	p53-binding protein 1
AB/AM	Antibiotic-antimycotic
Ago	Argonaute
AML	Acute myeloid leukemia
ANOVA	Analysis of variance
APL	Acute promyelocytic leukemia
Aph	Aphidicolin
Ara-C	Cytarabine
ASO	Antisense oligonucleotide
ATP	Adenosine triphosphate
ATCC	American Type Culture Collection
ATO	Arsenic trioxide
ATRA	All-trans retinoic acid
BCA	Bicinchoninic acid
BCL-2	B-cell lymphoma 2
BH3	BCL-2 homology 3
BSA	Bovine serum albumin
cDNA	Complementary DNA
CR	Complete remission
CuAAC	Copper-catalyzed azide-alkyne cycloaddition
DAPI	4',6-diamidino-2-phenylindole
DMSO	Dimethyl sulfoxide
DMEM	Dulbecco's modified eagle medium
DNMT3A	DNA (cytosine-5)-methyltransferase 3 alpha
DSB	Double-strand break
ECL	Enhanced chemiluminescence
EFS	Event-free survival
EFSI	Event-free survival interval

Etp	Etoposide
FDA	Food and Drug Administration
FBS	Fetal bovine serum
FGL-2	Fibrinogen-like protein 2
FLT3	FMS-like tyrosine kinase 3
GAPDH	Glyceraldehyde-3-phosphate dehydrogenase
GBM	Glioblastoma multiforme
GEPIA	Gene expression profiling interactive analysis
GFP	Green fluorescent protein
GRB2	Growth factor receptor-bound protein 2
HCC	Hepatocellular carcinoma
HCl	Hydrochloric acid
HOVON	Stichting Hemato-Oncologie voor Volwassenen Nederland
HPRT	Hypoxanthine-guanine phosphoribosyltransferase
HR	Hazards ratio
HR	Homologous recombination
HRP	Horseradish peroxidase
IC50	Half-maximal inhibitory concentration
Ida	Idarubicin
IDH	Isocitrate dehydrogenase
IR	Ionizing radiation
ITD	Internal tandem duplication
IV	Intravenous
mRNA	Messenger RNA
MLL	Mixed-lineage leukemia
mTat	Modified HIV-1 Tat peptide
nTPM	Normalized transcripts per million
NHEJ	Non-homologous end-joining
NSCLC	Non-small-cell lung carcinoma
OS	Overall survival

OSI	Overall survival interval
PARP1	Poly(ADP-ribose) polymerase 1
PBS	Phosphate buffered saline
PBMC	Peripheral blood mononuclear cells
PEI	Polyethylenimine
PFA	Paraformaldehyde
PML-RARA	Promyelocytic leukemia-retinoic acid receptor alpha
POL-PRIM	Polymerase-alpha-primase
POLA1	DNA polymerase alpha 1
POLA2	DNA polymerase alpha 2
PRIM1	DNA primase subunit 1
PRIM2	DNA primase subunit 2
PVDF	Polyvinylidene difluoride
RIPA	Radioimmunoprecipitation assay
RISC	RNA-induced silencing complex
RNAa	RNA activation
RNAi	RNA interference
RNR	Ribonucleotide reductase
RPMI 1640	Roswell Park Memorial Institute 1640
RT-qPCR	Quantitative reverse transcription polymerase chain reaction
saRNA	Small activating RNA
SF	Serum-free
SiR-alkyne	Silicon rhodamine alkyne dye
siRNA	Small interfering RNA
SPAAC	Strain-promoted azide-alkyne cycloaddition
SDS-PAGE	Sodium dodecyl sulfate - polyacrylamide gel electrophoresis
TCGA	The cancer genome atlas
TGFβ	Transforming growth factor beta
THTPA	Tris(3-hydroxypropyltriazolylmethyl)amine
XIAP	X-linked inhibitor of apoptosis protein

List of Figures:

List of Tables:

Chapter 1 - Introduction:

1.1 Acute myeloid leukemia – pathogenesis and prognosis:

Albeit rare, acute myeloid leukemia is still the most common leukemia affecting adults and the leading cause of leukemia-related deaths [1]. The global incidence of this myeloid leukemia has increased by 15 % over the last few decades to about 1.54 per 100,000 person/year [2]. Acute myeloid leukemia – commonly referred to as AML – is an extremely aggressive and highly heterogeneous cancer of the blood and bone marrow. AML develops as a consequence of a series of genomic or cytogenetic abnormalities that occur in the hematopoietic stem cells which trigger the formation of leukemic blasts [3]. In AML, the myeloid stem cells become leukemogenic and in most cases this disease arises as a *de novo* malignancy [1]. Over time, these abnormal, immature myeloid cells accumulate in the bone marrow and peripheral blood, crowding out the healthy blood cells and impairing their function. This leads to inadequate production of healthy blood cells and platelets, eventually leading to bone marrow failure [3].

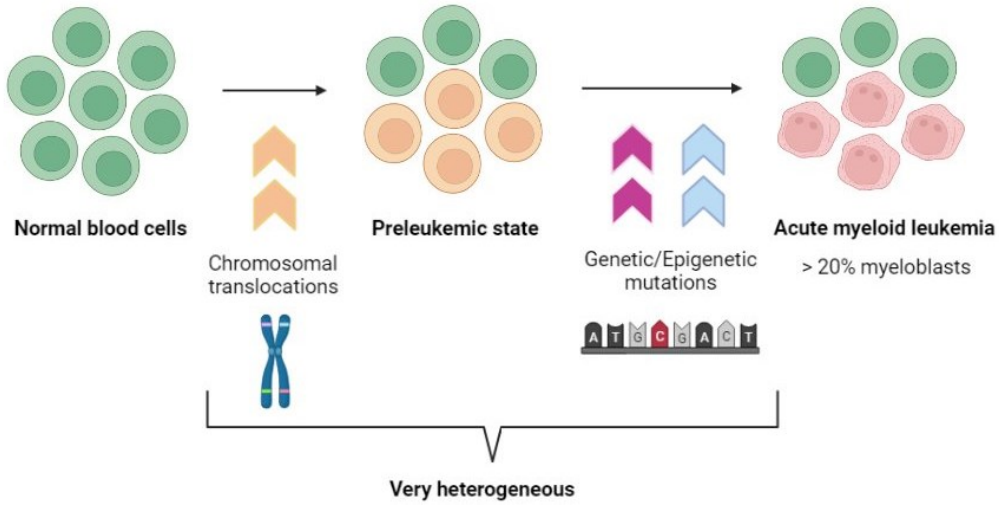

Figure 1: Schematic of AML Pathogenesis. Highly heterogeneous combination of genetics & epigenetic changes or chromosomal abnormalities lead to the formation of a preleukemic state and eventually to the accumulation of immature myeloblasts in the bone marrow and peripheral blood.

Unlike chronic, slowly progressing leukemias, AML is an acute disease and thus involves a sudden on-set of aggressive symptoms. Due to the fast pace of disease progression in AML, immediate treatment following diagnosis is essential. Approximately 10% of AML patients are diagnosed with a specific subtype of AML – acute promyelocytic leukemia (APL) that has achieved an >90% survival rate because of an extremely effective chemo-free regimen [4, 5]. APL patients can benefit from a combination of all-trans retinoic acid (ATRA) and arsenic trioxide (ATO) that degrades the promyelocytic leukemia-retinoic acid receptor alpha (PML-RARA) fusion protein caused by the t(15;17) translocation, removing the disease-causing myeloid differentiation block [4, 5]. Unfortunately, the remaining 90% of AML patients diagnosed with one of the other seven subtypes of AML are faced with cytotoxic chemotherapies that have limited efficacy and high relapse rates (Table 1) [6-9]. Despite the availability of AML therapies, the net five-year survival rate for AML is still only approximately 30% [10, 11]. Thus, the challenge of developing novel therapeutics for this heterogeneous and deadly disease is on-going.

Table 1: French-American-British (FAB) Classification of Acute Myeloid Leukemia [9].

Subtype	**Description**	**Percentage of AML patients**
M0	AML with no cytochemical evidence of differentiation	5%
M1	Myeloblastic leukemia with little maturation	15%
M2	Myeloblastic leukemia with maturation	25%
M3	Acute promyelocytic leukemia (APL)	10%
M4	Acute myelomonocytic leukemia	25%
M5	Acute monoblastic and monocytic leukemia	10%
M6	Erythroleukemia	5%
M7	Acute megakaryoblastic leukemia	5%

1.2 *Acute myeloid leukemia – current treatment strategies:*

The frontline treatment for AML remains relatively unchanged over the past four decades and consists of two primary phases: remission induction and post-remission consolidation [11-14]. The standard induction therapy consists of a continuous 7-day intravenous (IV) infusion of the chemotherapeutic agent, cytarabine (ara-C) and three days of a single IV dose of an anthracycline [11-14]. This is referred to as the "7+3 regimen." Cytarabine (ara-C) - a cytosine analogue – acts as a DNA damaging agent by interfering with DNA synthesis in an S-phase specific manner (Figure 2)[15-17]. The mechanism of action of cytarabine relies on its incorporation into DNA or RNA, leading to inhibition of DNA strand elongation, which in turn, results in cell cycle block and eventually apoptosis (Figure 2) [16-18]. Anthracyclines also disrupt DNA and do so by inhibiting topoisomerase activity which is critical for the unwinding of DNA during replication and synthesis, thereby causing programmed cell death [19]. Although several studies have investigated varying the dosage of cytarabine, anthracyclines and the addition of other agents for AML treatment, clinicians agree that the "7+3 regimen," will likely remain the frontline treatment for the foreseeable future [20]. If a patient reaches remission, they may be offered additional chemotherapy or an allogeneic stem cell transplantation as consolidation therapy. Age and performance status are just a few factors affecting chemotherapy effectiveness. AML patients that are deemed poor candidates for intensive chemotherapy are typically offered less-intensive therapy or palliative care to relieve symptoms, improve quality of life and potentially extend survival [21].

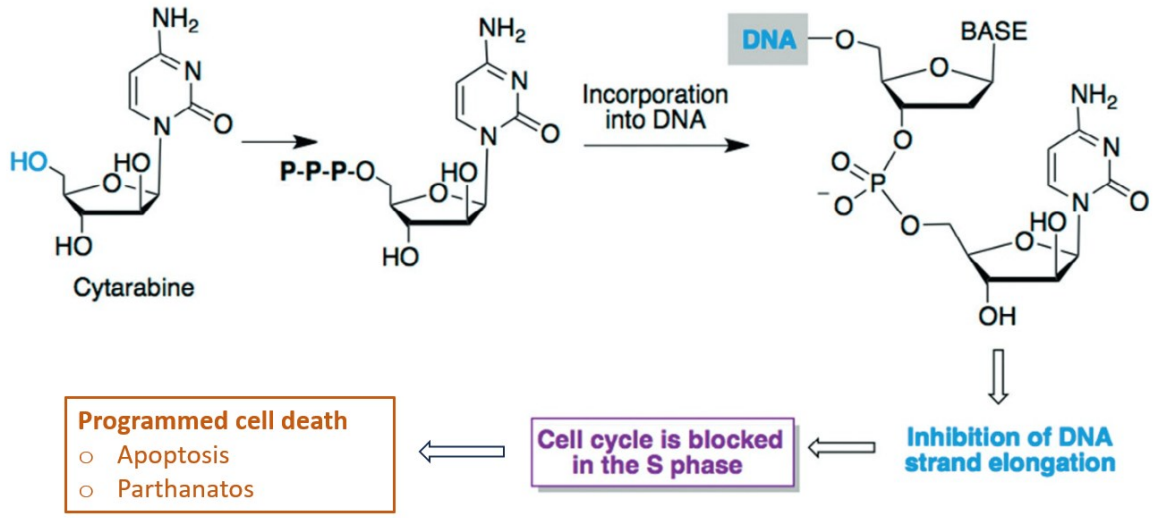

Figure 2: Traditional DNA-targeting mechanism of action of cytarabine (Ara-C). Ara-C undergoes metabolic activation via phosphorylation yielding its cytotoxic triphosphate active form. The active form is incorporated into DNA in place of deoxycytidine triphosphate. This results in inhibition of DNA polymerase, chain termination and stalling of DNA and RNA synthesis. Consequently, a blockage in cell cycle ensues from G_1 to the S phase triggering programmed cell death. Figure adapted from [17].

A more targeted approach has guided the development of novel AML therapeutics leading to the approval of small molecule inhibitors such as FMS-like tyrosine kinase 3 (FLT3) inhibitors, isocitrate dehydrogenase (IDH) inhibitors, and B-cell lymphoma 2 (BCL-2) inhibitors. Frequently mutated genes leading to the pathogenesis of AML have been exploited as targets for these inhibitors such as in the case of FLT3-targeting and IDH-targeting drugs. FLT3 inhibitors (ie. Midostaurin, Gilteritinib) competitively inhibit adenosine triphosphate (ATP)-binding sites in the receptor of mutated FLT3 protein, leading to cell cycle arrest and cell death [22]. Mutations in IDH lead to abnormal epigenetic regulation and can be treated with inhibitors selectively targeting IDH-mutant proteins (ie. Enasidenib, Ivosidenib), inducing myeloid differentiation in AML cells [23]. Meanwhile other classes of inhibitors, such as BCL-2 inhibitors, use advantage of the apoptotic pathway for their mechanism of action [24]. BCL-2 inhibitors (ie. Venetoclax) mimic the action of certain pro-apoptotic BCL-2 homology 3 (BH3)-only proteins to combat the BCL-2

protein overexpression responsible for reducing malignant cell apoptosis and resultant chemotherapy resistance [24].

Due to the highly heterogeneous nature of AML, many patients will not be eligible to benefit from a targeted inhibitor drug. Moreover, even in patients that do achieve complete remission (CR), the risk of relapse ranges from 35-85%, with age being a prominent risk factor [6, 8]. Thus, there is a clear need for the development and clinical implementation of novel therapeutic strategies for the treatment of this aggressive cancer. The high genetic heterogeneity seen among the AML patient population calls for personalized, genetically targeted treatment [25, 26]. As such, RNA therapeutics, with their ability to modulate gene expression and target specific mutations, may serve as an effective therapeutic strategy to improve AML patient treatment.

1.3 *Oligonucleotide therapeutics for AML treatment – progress and challenges:*

The emergence of oligonucleotide therapeutics has revolutionized the field of precision medicine by unlocking new mechanisms to target previously "undruggable" proteins, transcripts and genes [27, 28]. Currently, there are several classes of oligonucleotide therapeutics FDA-approved for the treatment of various diseases including but not limited to hypercholesterolemia, muscular dystrophies, and neuropathies [27-29]. Antisense oligonucleotides (ASOs) – the most mature of these therapies – comprise the majority of the FDA-approved oligonucleotide therapeutics, while the more recent approval of small interfering RNAs (siRNAs) as well as additional short, single-stranded DNA or RNA molecules that bind specific targets with high affinity known as aptamers and mRNA technologies have further established the utility of oligonucleotide drugs in precision medicine. However, important considerations - namely cellular uptake, tissue-specific delivery and stability – present prominent challenges in the development of these therapeutics [28, 30].

Pharmacological challenges slow the progress of targeted therapeutic development, particularly in the context of myeloid malignancies such as AML. Namely, the cellular uptake of RNA sequences is greatly limited in AML cell lines. One factor limiting this uptake is that immature AML cells generally exhibit compromised endocytic activity [31, 32]. The non-adherent nature of AML cells presents an additional challenge in targeting these suspension cells with transfection complexes [33]. Electroporation-based methods are able to introduce small RNAs into some AML cell lines but are greatly limited by both cell line and the high rates of cell death incurred [34, 35]. Beyond challenges in the cellular uptake of RNA, the genetic heterogeneity observed in AML along with the lack of preclinical models representative of intra- and interpatient heterogeneity also significantly hinder the development of these therapies for use in AML treatment [36].

Despite the aforementioned challenges, nucleic acid therapies have immense potential to broaden the pool of available therapeutic targets for AML treatment. AML-treating therapeutic oligonucleotides have yet to be approved and applied in the clinic, but some candidate drugs have already advanced to clinical trials [37]. For instance, cenersen is a p53-targeting antisense oligonucleotide that sensitizes AML cells to low levels of different DNA-damaging agents including chemotherapy drugs that typically fail to exert an effect on leukemic cells [38]. Results from phase II clinical trials suggest that the combination of cenersen with chemotherapy may have clinical efficacy in patients with refractory or relapsed AML [38]. Currently, clinical trial recruitment is ongoing for two other oligonucleotide drug candidates for AML: BP1001, a liposome-incorporated growth factor receptor-bound protein 2 (GRB2)-targeting ASO, and AS1411, an anti-nucleolin aptamer that localizes to tumor cells overexpressing nucleolin. [37, 39, 40]

Table 2: Oligonucleotide Therapeutics in Active, Recruiting or Completed Clinical Trial Phase for Acute Myeloid Leukemia.

Drug Name	Oligonucleotide	Target	Phase	Identifier	Reference
Cenersen	ASO	TP53	II	NCT00074737	Cortes et al.[38]
G4460	ASO	C-MYB	I	NCT00780052	
GTI-2040	ASO	R2 subunit of RNR	II	NCT00565058	
oblimersen sodium	ASO	BCL-2	I/III	NCT00085124 NCT00039117	Walker et al., Yin et al. [41-43]
AEG35156	ASO	XIAP	I/II	NCT00363974	
BP1001	ASO	GRB2	I/II	NCT01159028 NCT02781883	Ohanian et al. [39]
AS1411	Aptamer	Nucleolin	II	NCT00512083	

Classes of small RNAs such as small interfering RNAs (siRNAs) and small activating RNAs (saRNAs) have also garnered interest as therapeutic tools but have yet to be evaluated for clinical use in AML. Structurally identical, siRNAs and saRNAs are small 20-24 nucleotide noncoding RNAs with opposing functions in gene regulation. While siRNAs silence genes by degrading complementary target mRNA through the RNA interference (RNAi) pathway, saRNAs increase gene expression by binding to complementary genomic loci of their targets using the RNA activation (RNAa) pathway [44]. Although advancements in RNAi biology and siRNA design have led to the approval of novel siRNA therapeutics, there are currently no siRNAs approved or in clinical trials for myeloid leukemias [30, 45]. However, several *in vitro* studies suggest a role for siRNA-mediated silencing of key leukemic oncogenes and anti-apoptotic proteins in improving clinical outcomes in AML therapy [46, 47]. saRNAs have yet to be clinically approved but evidence of their efficacy in treating hepatocellular cancer has already been demonstrated through clinical trials [48]. Our research group is interested in further investigating saRNAs, more specifically with the purpose of applying them for targeted AML treatment.

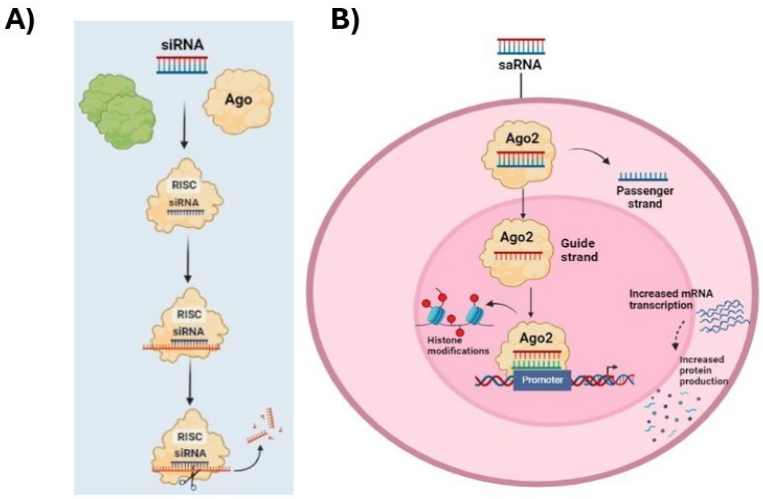

Figure 3: siRNA-induced gene silencing & saRNA-induced gene activation. A) Once the RNA duplex binds with Argonaute (Ago) protein to form the RNA-induced-silencing-complex (RISC), the sense strand of the siRNA is discarded. The RISC complex then scans through the cytoplasm looking for target mRNA complementary to the antisense strand of the siRNA. Upon binding to a complementary sequence, the RISC complex cleaves the mRNA, preventing its translation into protein. B) In brief, the saRNA duplex is loaded onto an Argonaute (Ago) protein in the cytoplasm where the passenger strand (blue) is cleaved and discarded, resulting in an active Ago-RNA complex. The active complex is guided to its target regions by the guide strand, which may bind to complementary promoter regions. Transcriptional machinery and histone modifying enzymes are recruited to the promoter to activate transcriptional expression.

1.4 *Small RNAs for probing therapeutic targets and biomarkers*:

Despite their potential promise, oligonucleotide therapeutics are challenging to design and develop [49, 50]. Nonetheless, they represent a promising class of therapeutics to be exploited for AML treatment. Beyond their therapeutic potential, RNA sequences also hold value as biological tools for probing possible drug targets or disease biomarkers. For example, siRNA and saRNA duplexes may serve as a robust pair for controlled exogenous gene knockdown and upregulation [51-54]. Compared to ASOs, small RNA duplexes like siRNAs have generally proven to be a more robust technology in cell culture, driving their use in gene expression studies [55]. The discovery and validation of novel therapeutic targets and biomarkers is of particular importance for the treatment of extremely genetically heterogeneous diseases such as AML.

The utility of siRNA sequences for oncogenic target screening and validation has already been demonstrated in the context of leukemia [52]. Several leukemia-associated downstream targets have also been revealed through RNAi-mediated gene silencing of known targets such as leukemogenic fusion gene *MLL-AF9* [56]. In terms of studying gene upregulation, saRNAs represent a recent yet powerful addition to nucleic acid tools. Though less established in their mechanism, these saRNAs possess several advantages over conventional vector-based methods including mitigating risk of insertional mutagenesis and more targeted gene activation [57]. For instance, saRNAs have been shown to serve as a more attractive method to reprogram human mesenchymal stem cells compared with the standard lentiviral based method due to the lack of insertional mutagenesis risk, induction of interferon response as well as activation of transforming growth factor beta (TGFβ) signaling, which could decrease reprogramming efficacy [58]. Additionally, saRNAs offer the option of transient overexpression and thus reversible gene overexpression as compared to conventional gain-of-function techniques [57]. Since siRNAs and saRNAs may be designed to target a broad range of genetic targets, bioinformatic analysis paired with subsequent *in vitro* screening in relevant cell line models could serve as an effective strategy for identifying therapeutically interesting targets.

1.5 *Bioinformatics and in vitro screening tools in target identification and validation:*

The development of novel RNA therapeutics often follows the bioinformatic discovery and *in vitro* validation of genetic targets whose modulation produces pharmacological benefit. The AML patient population which suffers from great genetic heterogeneity in leukemogenic mutations or translocations stands to benefit greatly from this drug discovery approach. Improvements in predicting patient outcomes and prognosis will also follow the identification of novel biomarkers [59]. Thus, the integration of bioinformatic analysis and *in vitro* screening is

vital in advancing AML treatment strategies. Bioinformatic analysis supports a better understanding of the molecular landscape of AML. Leveraging large-scale genomic, transcriptomic, and proteomic datasets allows researchers to identify aberrant gene expression patterns, mutations, and to predict clinical responses in the AML patient population [60-62]. By employing a computational approach, this enables the prioritization of candidate genes and pathways that may serve as potential therapeutic targets whilst saving precious time and resources [63]. For example, bioinformatic analysis has enabled the identification of prognostic biomarkers and novel targets for AML patients with the unfavourable DNA (cytosine-5)-methyltransferase 3 alpha *(DNMT3A)* mutation [64]. Moreover, bioinformatic strategies were also harnessed to reveal *TSC22D3* expression as a new prognostic biomarker and potential therapeutic target for AML [65].

Supporting bioinformatic analysis, *in vitro* screening is a useful tool to validate bioinformatic findings by allowing functional studies of identified targets [62, 63]. In particular, *in vitro* studies enable researchers to evaluate the efficacy of RNA therapeutics or validate potential biomarkers/therapeutic targets in relevant AML cell lines or patient-derived cells via relatively rapid screening assays. To illustrate, researchers leveraged the bioinformatic analysis of a large TCGA AML patient dataset coupled with *in vitro* experiments to establish fibrinogen-like protein 2 (*FGL2)* as a novel biomarker for the prognosis and treatment of AML [66]. Furthermore, *in vitro* assays not only confirm the biological relevance of bioinformatically predicted targets but also yield the opportunity to optimize the delivery, stability, and potency of these RNA sequences [67, 68]. Additionally, these cell-based experiments allow for the assessment of potential off-target effects, which are critical for ensuring the safety and long-term utility of RNA-based treatments [69]. Although it is likely that not all hits from *in vitro* screening will be clinically pursued if, no

therapeutic effect or damaging off-target effects are observed *in vivo*, this screening approach remains the most feasible option for the identification of potential drug targets or biomarkers [70].

By systematically identifying and validating RNA therapeutic targets, this integrated approach can enable the development of more precise and personalized treatment strategies, ultimately improving outcomes for AML patients. Indisputably, the major shift towards personalized cancer therapy requires the identification of novel biomarkers to be able to predict whether patients will respond well to frontline treatment or alternative therapies without compromising patient health and quality of life.

1.6 *The importance of the POL-alpha-PRIM complex in cytarabine sensitivity:*

Given the discussed importance of new medicines but our continued reliance on cytarabine, there is a significant effort to improve patient response to ara-C. Recently, studies demonstrated an alternate, non-DNA target of incorporation for cytarabine and showed its importance in improving survival outcomes in the M4/M5 AML patient population [18]. Using an azide-containing drug analog of cytarabine, termed "AzC", the biological target of Ara-C was revealed using a strain-promoted azide-alkyne cycloaddition (SPAAC) click-down-and-release pulldown experiment where samples were treated with either DNase, RNase A/T, RNase H or no enzyme [18, 71]. RNA hybridized to DNA primers was identified as another target of Ara-C and this alternative incorporation was found to be correlated to AML patient survival [18]. In patients that incorporated AzC into both the RNA and DNA rather than only the DNA, a three-fold improvement in overall survival was observed [18].

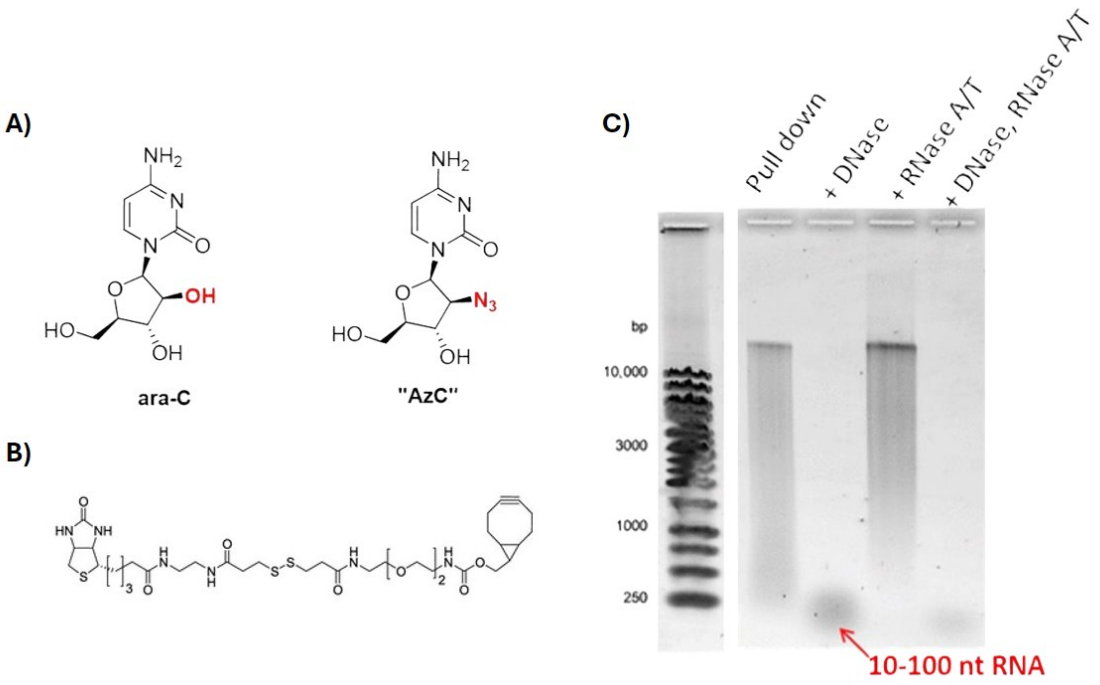

Figure 4: SPAAC Click-Pulldown-and-Release Capture of AzC-Containing Materials. A) Structures of ara-C and azide-containing ara-C analog, AzC. **B**) Structure of the new click, pull-down and release agent "Biot-SS-BCN" used to reversibly capture AzC-containing materials from treated cells using copper-free SPAAC reactions. C) Agarose gel displaying AzC-containing materials isolated from OCI-AML3 cells treated with 15 μM AzC for 24 hours. Lane 1: materials captured from cells treated with AzC; lane 3: materials captured from AzC-treated cells treated with DNase; lane 4: materials captured from AzC-treated cells treated with RNase A/T; lane 5: materials captured from AzC-treated cells treated with DNase + RNase A/T. Adapted from [18].

Messikommer *et al*. performed some of these AzC incorporation studies using nonspecific B-family polymerase inhibitor, aphidicolin, treatment. Surprisingly, aphidicolin-treated cells showed increased incorporation of AzC, suggesting the importance of the polymerase-alpha-primase complex in determining Ara-C incorporation [18]. The *POL-alpha-PRIM* complex plays a central role in eukaryotic DNA metabolism, active in DNA repair and replication pathways [72]. It generates *de novo* RNA-DNA primers through intricate regulation and coordination of four subunits - *POLA1, POLA2, PRIM1* and *PRIM2*. The primase domain (*PRIM1-PRIM2*) works to *de novo* synthesize a short (7-11 nt) RNA primer, which is then extended by the DNA polymerase

domain (*POLA1-POLA2*) to form hybrid RNA-DNA primers [72]. While *PRIM1* plays an essential role in template binding and positioning the template for RNA primer initiation, *PRIM2* regulates this RNA primer initiation and is responsible for transferring the primer to *POLA1* for DNA elongation [72]. *POLA2* regulates the DNA elongation performed by the *POLA1* polymerase subunit [72]. Although cryo-EM structures have elucidated some mechanistic details of POL-alpha-PRIM activity, the overall physical mechanism of how POL-alpha-PRIM complex performs dynamic, multistep enzymatic actions is still unknown [72].

Following polymerase inhibition, comparable enhancements in AzC incorporation were observed in AML cell lines as well as peripheral blood mononuclear cells (PBMCs) from human donors [18]. Although, the mechanism(s) responsible for the variable incorporation of AzC into DNA versus RNA are currently unknown, given the role of the Pol α-primase complex in synthesizing RNA-DNA primers for AzC incorporation, cell-type-specific differences in its expression and associated DNA damage response pathways likely play a role [18]. To further unveil the role of the different protein subunits of the Pol α-primase complex in Ara-C incorporation and resultant sensitivity, more specific polymerase inhibition is required. Nonetheless, these AzC incorporation studies clearly imply the importance of this dynamic protein complex in increasing Ara-C incorporation and perhaps drug sensitivity.

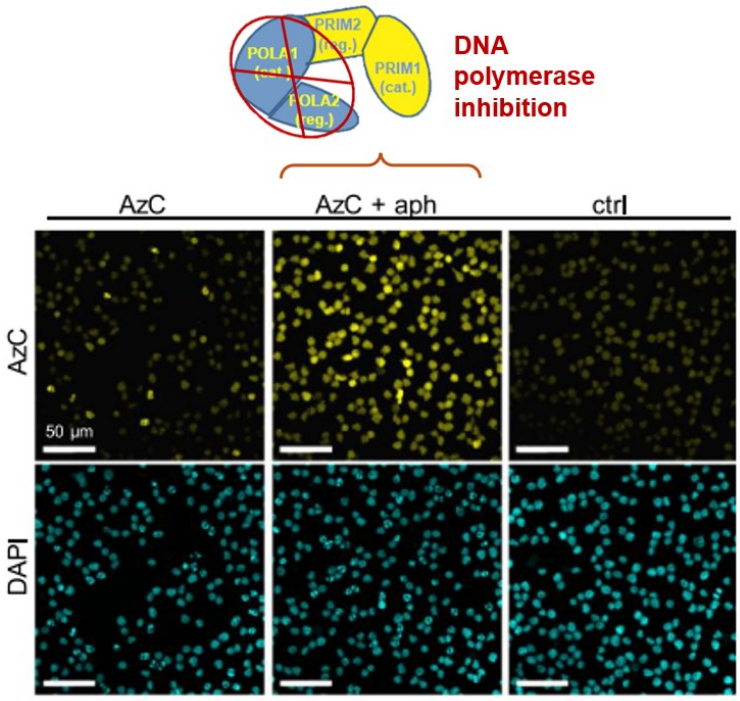

Figure 5: Enhanced AzC incorporation into OCI-AML3 cells following aphidicolin (aph) treatment. The AzC-treated AML cells were fixed, washed, and stained with fluorescent alkyne dye using CuAAC and DAPI, and cytospun onto slides prior to analysis by fluorescence microscopy. The control sample (ctrl) was treated with aphidicolin but no AzC. Adapted from [18].

1.7 *Loss of POLA2 sensitizes cells to genomic insult:*

Together, recent work divulging the role of *POLA2* in double-strand break (DSB) repair coupled with the surprising findings demonstrating enhanced ara-C AML cell incorporation upon DNA polymerase inhibition, suggests the particular importance of *POLA2* expression in altering ara-C incorporation and sensitivity. To illustrate, decreasing *POLA2* levels was shown to increase DSB formation in cells [73]. *POLA2*-deficient cells displayed an increase in p53-binding protein 1 (53BP1) foci formation which is indicative of an increase in endogenous double strand breaks (DSBs) [73]. Thus, *POLA2* deficiency was associated with delayed DNA repair kinetics *in vitro*.

Interestingly, loss of *POLA2* was revealed to inhibit both of the major double strand break repair pathways: non-homologous end-joining (NHEJ) and homologous recombination (HR) [73]. Data from green fluorescent protein (GFP) reporter cell lines where GFP expression was used to determine a successful repair event showed a 70% and 35% loss in HR and NHEJ repair efficiency, respectively, in cells transfected with a *POLA2*-targeting siRNA [73]. These results delineate a clear role for *POLA2* in DNA repair. Since NHEJ repair is functional throughout the cell cycle while HR is restricted to the S and G2 phase, the requirement for *POLA2* in DSB repair is seemingly cell-cycle independent [73]. Furthermore, siRNA knockdown of *POLA2* levels was confirmed to sensitize cells to exogenous genomic insults. As evidence of the contribution of *POLA2* expression in cell protection, cells lacking *POLA2* displayed decreased survival in response to ionizing radiation (IR), etoposide (etp) and poly(ADP-ribose) polymerase 1 (*PARP1)* small molecule inhibitor Niraparib [73].

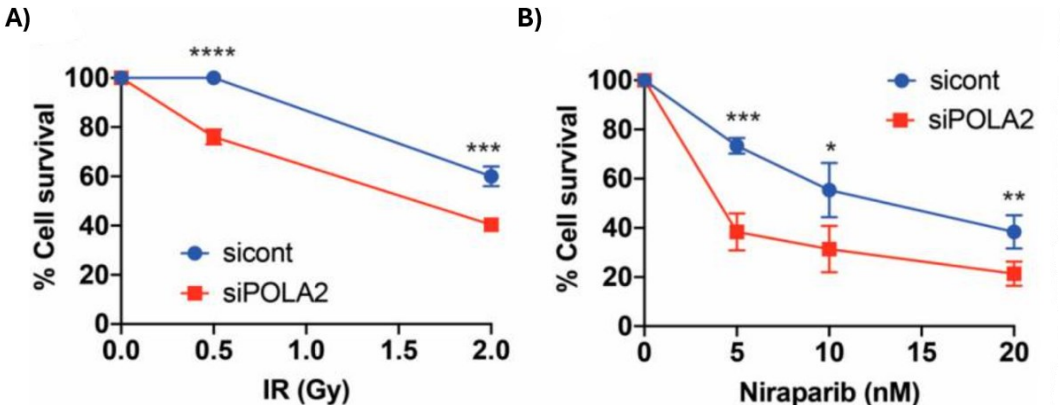

Figure 6: LN229 cells with *POLA2* knockdown demonstrated increased sensitivity to ionizing radiation (IR) exposure and PARP1 inhibition. Percent cellular survival was measured in LN229 cells exposed to control (cont) and *POLA2* siRNAs. Following siRNA transfection, these cells were then treated with (**A**) ionizing radiation (IR) or (**B**) Niraparib, a PARP1 small-molecule inhibitor, at the displayed doses. Statistical analysis was performed using the student's *t* test. * $p < 0.05$, ** $p < 0.01$, *** $p < 0.001$ and **** $p < 0.0001$. Adapted from [73].

1.8 *Overexpression of POLA2 correlated with negative disease-related outcomes:*

In line with the *POLA2* knockdown studies, Arabidopsis research shows that overexpression of *POLA2* could lead to various negative effects. It was found that ectopic expression of *POLA2* causes dominant negative effects, including defective gametogenesis and embryo lethality [74]. This suggests that the tight regulation of *POLA2* expression is especially critical in reproductive or DNA replication-centric events. Therefore, *POLA2* is likely highly regulated to avoid or limit aberrant expression yielding negative consequences.

Interestingly, the unfavourable outcomes associated with high *POLA2* expression have been extended to include poorer cancer prognosis. For example, microarray data from glioblastoma multiforme (GBM) patients show elevated *POLA2* levels in GBM tumour samples as compared to normal brain tissue [73]. Using the same Kawaguchi dataset, elevated *POLA2* expression was also correlated with poor overall survival of GBM patients, suggesting the therapeutic relevance of *POLA2* knockdown in GBM which could be potentially extrapolated to broader cancer treatment [73]. Notably, *POLA1* levels were also found to be elevated in this patient cohort; however, there was no correlation found with overall GBM patient survival [73].

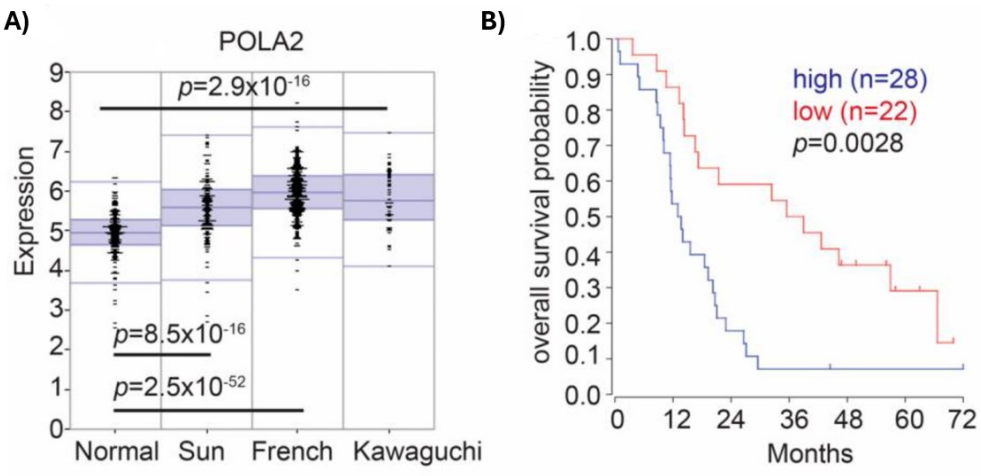

Figure 7: Higher *POLA2* expression correlated with poorer overall glioblastoma patient survival. (**A**) Expression of *POLA2* in normal vs. tumor datasets. (**B**) Overall patient survival in high vs low *POLA2* patient populations. Gene expression analysis was performed using the R2 genomics analysis and visualization platform using the default settings.

Similarly, studies have linked *POLA2* overexpression to poor prognosis and low overall survival in hepatocellular carcinoma (HCC) [75-77]. *POLA2* was found to be significantly highly expressed in HCC compared to normal liver tissue in both the cancer genome atlas (TCGA) and collected HCC samples [75-77]. Furthermore, *POLA2* was revealed to be a potential molecular biomarker for prognostic evaluation or a therapeutic target for HCC due to its influence on the immune micro-environment and tumor progression in this cancer [75-77]. Unfavourable effects of *POLA2* upregulation have also been observed in the context of non-small-cell lung carcinoma (NSCLC) [78]. Furthermore, *POLA2* expression was found to have an impact on both erlotinib and gemcitabine drug sensitivity in lung cancer cells, implying a role for *POLA2* as a biomarker for drug resistance in patients with NSCLC [78, 79]. Bioinformatic analyses have also identified *POLA2* as a prognostic biomarker in ovarian cancer as well as in gastrointestinal stromal tumors [80, 81]. The mounting evidence of *POLA2* as a disease biomarker suggests an important yet unexplored role for this protein in cancer progression and modulating sensitivity to therapeutic agents.

1.9 *Thesis objectives and rationale:*

Non-specific inhibition of the alpha subunit B of the DNA polymerase alpha-primase, responsible for synthesizing short RNA primers, has been shown to alter cytarabine incorporation in AML. This suggests that the polymerase domain of the POL-alpha-PRIM complex may hold particular significance in the RNA incorporation of ara-C in AML. Moreover, the clear evidence of the role of *POLA2* in cell protection against genomic insult, implies a significant role for *POLA2* in mediating the effects of DNA-damaging agents like cytarabine. Furthermore, studies correlating *POLA2* overexpression with poor cancer survival outcomes also imply an important role for this DNA synthesis-regulating protein. However, there are no studies evaluating the impact of *POLA2* expression on ara-C incorporation and ara-C-induced cell death. It is also still not known why cytarabine is sometimes metabolized into RNA or why this correlates with AML patient outcomes. Thus, I hypothesize that cytarabine incorporation into RNA depends on optimal function of the DNA polymerase alpha-primase complex and is particularly dependent on the expression of the alpha subunit B encoding gene – *POLA2*. Hence, the overarching objective of my thesis project will be to investigate the impact of *POLA2* expression on cytarabine efficacy in acute myeloid leukemia.

My first aim was to investigate how the expression levels of POL-PRIM subunits correlate with AML patient survival. To this end, I harnessed comprehensive bioinformatic datasets to compare expressional data of each subunit of the DNA polymerase alpha-primase complex against AML patient survival. I analyzed the largest available set of validated mRNA expression data from clinical trials (the Haemato Oncology Foundation for Adults in the Netherlands) and the TCGA RNA-sequencing gene expression dataset. From these datasets, I stratified patients according to expression levels and compared overall survival (OS) and event free survival (EFS). These results

will allow for relationships between subunit expression and AML patient survival to be elucidated, guiding the development of novel strategies to stratify and improve AML patient outcomes.

For my second aim, I sought to develop *in vitro* methods that allow for the specific modulation of *POLA2* expression in relevant AML cell lines. To alter gene expression, I chose to use pairs of siRNAs and saRNAs to decrease and increase, respectively, the expression of target genes. siRNAs are well-studied with regards to their mechanism and design and are poised to become a standard modality of pharmacotherapy [45]. Unlike siRNAs, saRNAs are less established but still very promising in their gene-upregulating function and therapeutic potential [57]. I screened a panel of saRNAs designed via a prediction algorithm to identify an saRNA that could upregulate *POLA2* expression. Given that AML cells are notoriously difficult to transfect *in vitro*, I first screened and developed new chemical transfection methods for diverse AML cell lines available in our lab. This work will facilitate both the validation of various therapeutic targets in AML cell lines, including *POLA2*, and the future development of small RNAs therapeutics for the improvement of cytarabine efficacy.

My third aim was to assess the impact of altered expression of *POLA2* on AML cell death and the variable incorporation of cytarabine into RNA vs DNA. To test whether certain expressional levels of *POLA2* are required for the targeting of AML via cytarabine, I used model cell lines OCI-AML3 and THP1 that we have previously validated in our lab for various responses to cytarabine treatment [18, 53]. The most significant siRNA transfection efficiencies were also obtained in these two cell lines, as revealed in my second aim. The AML cells were treated with a clinically-relevant 17:1 ratio of cytarabine and idarubicin. Changes in sensitivity towards cytarabine were evaluated in a dose-response manner using resazurin fluorescence and trypan blue exclusion assays. I further examined cells via confocal microscopy for the presence of apoptotic

bodies or parthanatos features to determine the mechanism of cell death. Parthanatos, a caspase-independent form of programmed cell death mediated by poly(ADP-ribose) polymerase 1 (PARP-1), has been observed in AML cells treated with cytarabine and idarubicin [53]. This non-apoptotic form of cell death is characterized by distinct features including nuclear "ring" morphologies and PARP-dependent changes in drug sensitivity [53]. To measure cytarabine incorporation into RNA primers vs DNA, I used a "biorthogonal chemistry" approach [18, 71] . Specifically, I treated AML cells with a "clickable" cytarabine analog "AzC" which exhibits the same potencies and characteristic effects on cellular proliferation, cell cycle progression, DNA damage formation, caspase activation, and DNA synthesis inhibition in AML cell cultures and animals [18, 71].

Throughout the course of this project, I aimed to further uncover the role of the POL-alpha-PRIM complex in cancer by examining the relationship between *POLA2* expression and cytarabine incorporation and sensitivity in AML. My results will aid in establishing a potential therapeutic target and important biomarker for predicting patient response to the frontline cytarabine treatment. Furthermore, this study exposed important mechanistic details of cytarabine's therapeutic action following variable RNA/DNA incorporation. Characterizing these unexplored mechanisms of cytarabine-induced leukemic cell death using therapeutic RNA will also enable the development of new co-treatment strategies to improve long-term AML outcomes.

Chapter 2 - Materials and Methods:

2.1 - Materials:

2.1.1 Bioinformatic datasets:

The TCGA RNA-seq AML dataset was accessed using Gene Expression Profiling Interactive Analysis (GEPIA) 2: http://gepia2.cancer-pku.cn/#index. Validated mRNA microarray data from the Stichting Hemato-Oncologie voor Volwassenen Nederland (HOVON) clinical trials was provided by P.J.M. Valk.

2.1.2 Commercial kits and assays:

The RNA Miniprep Kit was purchased from New England Biolabs. GoScript™ Reverse Transcription Mix, Oligo(dT) was purchased from Promega. TaqMan Fast Advanced Master Mix, 20x HPRT TaqMan Expression Assay Hs02800695_m1 (FAM-MGB: S – 250 rxns), 20x POLA2 TaqMan Expression Assay Hs00160242_m1 (FAM-MGB: M – 750 rxns), 20x GAPDH TaqMan Expression Assay Hs02786624_g1 (FAM-MGB: L – 2900 rxns), Pierce BCA Protein Assay kit, Pierce™ ECL Western Blotting Substrate, and LIVE/DEAD™ Fixable Green Dead Cell Stain Kit were all purchased from Thermo Fisher Scientific. SF Cell Line 4D X Kit L was purchased from VWR International Co. MycoFluor Mycoplasma Detection Kit was purchased from Invitrogen.

2.1.3 Cell lines:

MV4-11, U-937, OCI-AML3, OCI-AML2, MOLM-13 and MOLM-14 cell lines were obtained from the Leibniz Institute DSMZ-German Collection of Cell Cultures GmbH. THP-1 cell line was obtained from the American Type Culture Collection (ATCC).

Table 3: Summary of AML Cell Lines Used in This Study [82].

Cell Line	Origin	Morphology	Characteristic Mutations
MV4-11	Derived from the peripheral blood of a 10-year-old male with biphenotypic B-myelomonocytic leukemia (AML FAB M5)	Suspension	FLT3-ITD
U-937	Established from the pleural effusion of a 37-year-old male with histiocytic lymphoma (reclassified as monocytic leukemia)	Suspension	TP53
OCI-AML3	Derived from the peripheral blood of a 57-year-old male with acute myeloid leukemia (AML FAB M4)	Suspension	NPM1, DNMT3A
OCI-AML2	Established from the peripheral blood of a 65-year-old male with acute myeloid leukemia (AML FAB M4)	Suspension	DNMT3A
MOLM-13	Derived from the peripheral blood of a 20-year-old male with relapsed acute monocytic leukemia (AML FAB M5)	Suspension	FLT3-ITD
MOLM-14	Derived from the peripheral blood of a 20-year-old male with acute monocytic leukemia (AML FAB M5)	Suspension	FLT3-ITD
THP-1	Established from the peripheral blood of a 1-year-old male with acute monocytic leukemia (AML FAB M5)	Suspension	NRAS, TP53

2.1.4 RNA sequences:

Cy3-labelled siRNA, *POLA2*-targeting siRNA, and non-targeting control siRNA duplexes were purchased from Integrated DNA Technologies.

2.1.5 Reagents:

RPMI 1640 media, fetal bovine serum (FBS), antibiotic-antimycotic (AB/AM), Dulbecco's Modified Eagle Medium (DMEM), trypan blue, phosphate buffered saline (PBS) (pH 7.4), and Gibco™ DMEM media were purchased from Gibco. ViaFect™ and FuGENE® HD transfection reagents were purchased from Promega. Lipofectamine™ 3000 and Lipofectamine™ RNAiMAX transfection reagents were purchased from Thermo Fisher Scientific. INTERFERin® transfection reagent was purchased from VWR International Co. The silicon rhodamine alkyne dye (SiR-alkyne) was purchased from Spirochrome. Triton X-100 was purchased from Sigma-Aldrich. Trypsin, Fluoromount-G™ mounting medium and Image-IT FX Signal Enhancer were purchased from Thermo Fisher Scientific.

2.1.6 Chemicals and proteins:

AzC was synthesized and provided by the Luedtke lab at McGill University (Montréal, QC, CA). Cytosine β-D-arabinofuranoside (ara-C) and idarubicin were purchased from Sigma Aldrich. Resazurin sodium salt, Bovine Serum Albumin (BSA), 4′,6-diamidino-2-phenylindole (DAPI), dimethyl sulfoxide (DMSO), sodium tetraborate decahydrate, glycine, ammonium chloride, and Triton X-100 were purchased from Sigma-Aldrich. Copper (II)- sulfate pentahydrate, sodium ascorbate, tris(3-hydroxypropyltriazolylmethyl)amine (THTPA), and aminoguanidine hydrochloride were kindly provided by the Luedtke lab. Hydrochloric acid (HCl) was purchased from Biobasic. DNase I was obtained from the RNA Miniprep Kit purchased from New England Biolabs. RNase H and paraformaldehyde (PFA) were purchased from Thermo Fisher Scientific.

2.1.7 Antibodies:

POLA2 Polyclonal Antibody, rabbit/ IgG was purchased from Thermo Fisher Scientific and horseradish peroxidase (HRP)-conjugated anti-rabbit secondary antibody was purchased from New England Biolabs.

2.2 - Methods:

2.2.1 Bioinformatic analysis of TCGA data:

Firstly, the TCGA RNA-seq AML dataset was accessed using Gene Expression Profiling Interactive Analysis (GEPIA) 2: http://gepia2.cancer-pku.cn/#index. The gene expression profiles of all POL-PRIM subunits - *POLA2*, *POLA1*, *PRIM1* and *PRIM2* - were searched for using the GEPIA2 database. Under the "Expression Analysis," function on GEPIA2, the "General," pane was selected. Subsequently, the bar plots depicting gene expression profiles across all tumor samples and paired normal tissues were analyzed for each subunit. The height of each bar in the plot represents the median expression of certain tumor type or normal tissue.

To investigate the correlation between gene expression and AML patient survival, survival analysis was performed based on the expressional data for each POL-PRIM gene. This was done using the AML (LAML) dataset to construct Kaplan-Meier survival curves. For this analysis, the "Survival Analysis," pane was selected on GEPIA2. After inputting "*POLA2*," "*POLA1*," "*PRIM1*," or "*PRIM2*," as the gene of interest, the rest of the survival analysis parameters were selected as follows. For the method, "overall survival" or "disease-free survival" was selected while the group cutoff was selected as either "median," or "quartile." The hazards ratio (HR) and 95% confidence interval were selected for calculation. X-axis units were set to "months". The TCGA AML dataset was chosen for analysis, labeled as "LAML". Once all parameters were fixed,

the survival package in the R program was used to generate Kaplan Meier survival curves plotting percent survival of a high/low gene expression group over time. The logrank test was employed for statistical analysis of the survival curves. Hazard ratios were generated to quantify the effect of POL-PRIM gene expression on AML patient survival.

2.2.2 Bioinformatic analysis of HOVON trials data:

To further investigate the impact of POL-PRIM subunit expression on AML patient survival but this time in the context of a large patient population treated with the 7+3 regimen, bioinformatic data from HOVON clinical trials was analyzed. The validated mRNA microarray data from the HOVON clinical trials was accessed and provided by P.J.M. Valk. Patient data including mRNA expression for each POL-PRIM complex subunit was filtered according to various patient population characteristics (ie. AML FAB subtype, presence/absence of mutation). Data from each patient included target gene expression, overall survival (OS), event-free survival (EFS), overall survival interval (OSI) and event-free survival interval (EFSI). OSI was assigned as either "dead," or "alive," depending on whether the patient survived until the end of the clinical study. Next, patient data in the chosen sub-group (ie. M4/M5 subtype, FLT3-ITD negative) was ordered from lowest to highest expression of the selected POL-PRIM complex gene. For the overall survival analysis, each patient OSI designated as "dead," was assigned a numerical value of "1," while each patient OSI designated as "alive," was assigned a value of "0". For event-free survival analysis, each patient EFSI denoted as "event-free survival" was assigned a "0" while all other EFSIs such as "Relapse/Disease Progression" or "Death" were assigned a "1". Ordered patient data, ascending in terms of target expression, was divided into equal groups. To construct survival curves in GraphPad Prism, OS/EFS values were plotted on the x-axis against two groups of converted OSI/EFSI values corresponding to "high," and "low," expression of the selected POL-

PRIM gene. Statistical analysis of the resultant survival curves was performed using the log-rank test as well as the Gehan Breslow Wilcoxon test in GraphPad Prism software. Hazard ratios were generated following each statistical test to quantify the effect of POL-PRIM gene expression on the survival of the AML patients.

2.2.3 Mammalian tissue culture:

All cell culture work was performed in a biological safety cabinet using proper aseptic technique. OCI-AML2, MOLM-13, MOLM-14, MV4-11 and THP-1 cells were cultured in RPMI 1640 media to which FBS) and AB/AM were added to a final concentration of 10% FBS and 1% AB/AM in the complete media. OCI-AML3 cells were also cultured in complete RPMI 1640 media but supplemented with 20% FBS. Adherent cell culture was performed using DMEM media supplemented with 10% FBS and 1% ABAM.

To thaw AML cells from freezer stock, complete media was first warmed in a 37˚C bead bath and then 9 mL of warm media was pipetted in a 50-mL Falcon tube. A freezer stock containing 1 mL of ~4-5 x 10^6 AML cells was thawed and added to the media in the Falcon tube. The thawed cells were centrifuged at 300 xg for 5 minutes at room temperature. Subsequently, pelleted cells were resuspended in fresh, warm RPMI media and stored in a T-25 cell culture flask. Cell culture flasks were stored in a 37˚C incubator with 5% CO_2.

Prior to experimental use, cells were left to recover and grow for a few days. Cells were counted using the Cell Counter Model R1 (Olympus) of the Tecan Spark microplate reader. For each cell count, 10 µL of cell suspension was mixed thoroughly with 10 µL of trypan blue dye and then 10 µL of this mixture was loaded onto a Tecan Cell Chip™ and placed into the Tecan Spark microplate reader. Each measurement produced an output including but not limited to the cell

density (number of cells per milliliter) as well as the percent cell viability. Cell density values were multiplied by two to account for Trypan Blue dilution and then used for cell seeding calculations for experimental work or cell passaging.

Cell lines were grown to confluency and passaged every 2–4 days. While THP-1 cells were passaged using a 1:2 dilution in complete RPMI media, all other AML cell lines were typically passaged using a 1:10 dilution in complete RPMI media, depending on the experimental conditions required. To passage or seed adherent cells, DMEM media was first aspirated. The cells were then washed with PBS, detached with 2 mL of trypsin and finally diluted in 8 mL of fresh complete DMEM media. All cultured cells were tested monthly for mycoplasma infections using the MycoFluor Mycoplasma Detection Kit (Invitrogen).

2.2.4 Lipofectamine 3000 Transfection:

24 hours before transfection, adherent HEK293T cells were seeded in a 6-well plate to ensure 70–90% confluency at the time of transfection, in 1 mL of 10% FBS DMEM media. Suspension cells were plated at a density of 1 X 10^6 per well, two hours before transfection in a 6-well plate, resuspended in 1 mL of serum-free and antibiotic-free RPMI media. On the day of transfection, two tubes were prepared for each condition. Tube A contained 250 µL of Opti-MEM and 5 uL of 20 uM *POLA2* saRNA, *POLA2* siRNA or control siRNA, while Tube B contained 250 µL of Opti-MEM and 5 µL of Lipofectamine 3000 reagent (Thermo Fisher Scientific). The contents of each tube were mixed by pipetting, and 250 µL of the solution from Tube B was added to Tube A. The complexation mixture was then thoroughly mixed and incubated for 10–15 minutes at room temperature to allow for the formation of transfection complexes. During this incubation, the media in the 6-well plate was removed, and 1.5 mL of fresh DMEM was added to each well of adherent cells. Suspension cells were kept in the original seeding media. After incubation, 500 µL

of transfection mix was added to each well, resulting in a final volume of 2 mL per well and a final siRNA concentration of 50 nM (HEK293T cells) or 100 nM (AML cells). Then, the plate was gently rocked to ensure even distribution of the mixture. Approximately 8 hours post-transfection, 1 mL of RPMI media supplemented with FBS and ABAM, to reach 10% and 1% conditions respectively, was added to each well of suspension cells to restore optimal growth conditions. For adherent cells, the media was replaced 6 hours later with 2 mL of complete DMEM, and the transfection procedure was repeated at the 24-hour time point. RNA was extracted 48–72 hours after the initial transfection.

2.2.5 RNAiMAX Transfection:

Cells were plated at a density of 5 x 10^4 per well of complete RPMI media, in a 24-well plate. siRNA-Lipofectamine RNAiMAX complexes were prepared for each well by first diluting 18 pmol of *POLA2* or negative control siRNA in 50 µL of Opti-MEM reduced serum media and mixing gently. Separately, 1 µL of Lipofectamine RNAiMAX (Thermo Fisher Scientific) was also diluted in 50 µL of Opti-MEM reduced serum media. The diluted siRNA and Lipofectamine RNAiMAX were combined and incubated for 15 minutes at room temperature to allow for complex formation. 500 µL of the transfection complexes were then added to each well of cells, bringing the total volume to 600 µL and the final siRNA concentration to 30 nM. The plate was gently rocked to evenly distribute the complexes. The transfected cells were incubated at 37°C in a CO_2 incubator for 24–48 hours, after which gene knockdown was analyzed.

2.2.6 INTERFERin Transfection:

Cells were seeded at a density of 1.8 x 10^5 cells per well in a 24-well plate and resuspended in 200 µL of RPMI media. Subsequently, 0.021 µg of *POLA2* or control siRNA was diluted in 100

µL of OptiMEM reduced serum media or serum-free RPMI 1640 media and mixed gently by pipetting. Before use, INTERFERin (VWR) was vortexed for 5 seconds and briefly spun down. Following this, 4 µL of INTERFERin was added to the 100 µL of siRNA solution, and the mixture was vortexed immediately for 10 seconds. The siRNA-INTERFERin complex mixture was incubated at room temperature for 15 minutes. Following the incubation period, the 100 µL of siRNA-INTERFERin mix was added to the each well of cells, yielding a final volume of 300 µL per well and a final siRNA concentration of 7 nM. The plate was gently swirled or placed on a plate shaker at low speed to ensure even distribution of the transfection mixture. The transfection plate was then incubated at 37°C for 4–6 hours, after which 0.7 mL of growth media was added to each well to bring the final volume to 1 mL. Cells were further incubated for 16–48 hours prior to fluorescence microscopy, RNA or protein extraction.

2.2.7 *Nucleofection:*

1 x 10^6 cells were harvested from culture, centrifuged at 90 x g for 10 minutes and resuspended in 20 µL of SF or SG buffer/siRNA solution (VWR). Experimental cells were nucleofected with 100 nM of *POLA2* siRNA while control cells were nucleofected with an equivalent concentration of non-targeting negative control siRNA, using the Lonza 4D-Nucleofector X Unit (AAF-1003X) with 16-well nucleocuvette strips. THP-1 cells were nucleofected in the SG cell line solution using the FF-100 nucleofection program. Meanwhile, OCI-AML3 cells were nucleofected in the SF cell line solution using the EH-100 nucleofection program. Lastly, U937 cells were nucleofected in the SF cell line solution using the ER-100 nucleofection program. Nucleofected cells were pipetted into warmed complete RPMI media to recover and incubated at 37°C for 24–48 hours prior to gene expression analysis.

2.2.8 ViaFect Transfection:

On the day of transfection, 2 x 10^5 cells were harvested by centrifugation and resuspended in 90 µL of complete RPMI media then, transferred to a 96-well plate. To create the transfection complexation mix, 0.1 µg of *POLA2* siRNA or respective controls and 0.8 µL of ViaFect transfection reagent (Promega) were mixed with 10 µL of Opti-MEM reduced serum media. The transfection mixture was incubated at room temperature for 15 minutes to allow complex formation. Next, 10 µL of DNA/ViaFect/Opti-MEM mixture was then added to the 90 µL of cells in each well, and the plate was incubated at 37°C in a 5% CO2 incubator for 24–72 hours. Cy3-siRNA -transfected cells were incubated for 16 hours before analysis via fluorescence microscopy. *POLA2* siRNA-transfected samples were incubated for 24–72 hours, for gene expression analysis via RT-qPCR and Western blot.

2.2.9 FuGENE HD transfection:

Cells were harvested by centrifugation at 300 x g for 5 minutes and resuspended in 95 µL of full culture media at a density of 200,000 cells/mL. 0.1 µg *POLA2* or control siRNA was combined with 0.3 µL of FuGENE transfection reagent (Promega) and 5 µL of Opti-MEM reduced serum media. The mixture was incubated at room temperature for 15 minutes to allow the formation of transfection complexes. Following the incubation, 5 µL of the DNA/reagent complex was added to the 95 µL of cells. The transfected cells were incubated at 37°C in a 5% CO_2 incubator for 16–48 hours, depending on the experimental endpoint(s). Cells were prepared for RNA extraction or fluorescence microscopy after a 16-hour, or 24-hour incubation period, respectively.

2.2.10 RNA extraction:

AML cells were pelleted then transferred to microcentrifuge tubes for RNA isolation. Prior to RNA extraction, adherent HEK293T cells were washed with PBS, detached from the bottom of the well using a cell scraper, lysed with lysis buffer and then transferred directly to a microcentrifuge tube. Total RNA was extracted from the AML cells with Monarch Total RNA Miniprep Kit (New England Biolabs) and quantified using a BioSpectrometer Fluorescence (Eppendorf) according to manufacturer's instruction.

2.2.11 Quantitative reverse transcription polymerase chain reaction (RT-qPCR):

Briefly, RT master mix was made with a 2:2:1 ratio of nuclease-free water, GoScript Reaction Buffer, Oligo(dT) and GoScript Enzyme Mix. In PCR tubes, RNA was diluted in the appropriate concentration using nuclease-free water, incubated at 70 °C for 5 minutes then chilled on ice for 5 minutes. 5 µL of RT master mix was added to 5 µL of diluted RNA and then the mixture was incubated in a C1000 Touch Thermal Cycler (Bio-Rad) under the following conditions: 25°C (5 minutes), 42 °C (60 mins), and 70 °C for 15 minutes. qPCR master mixes were made respecting a 1:10:4:5 ratio of 20x TaqMan Gene Expression Assays (Thermo Fisher Scientific), 2x TaqMan Fast Advanced Master Mix (Thermo Fisher Scientific), cDNA template and nuclease-free water. 16 µL of the selected gene expression master mix was added to each corresponding well in a 96-well qPCR plate (Bio-Rad). Next, 4 µL of the appropriate cDNA template was added to each well, the qPCR plate was sealed using Microseal B PCR plate seals (Bio-Rad). qPCR was conducted using CFX96 Real-Time System (Bio-Rad) under the following conditions: denaturation (50 °C for 2 minutes), annealing (95 °C for 2 minutes), and extension (60 °C for 20 seconds → repeated for 40 cycles). DDCt values were calculated to compare the expressions by the (2-DDCt) method.

2.2.12 Fluorescence microscopy:

To assess the uptake of fluorescently labeled RNA by cells following transfection, the contents of each transfection plate were carefully pipetted into correspondingly labeled microcentrifuge tubes. The samples were centrifuged at 400 x g for 3 minutes to pellet the cells. The pelleted cells were then resuspended and washed 2–3 times with PBS. After the final PBS wash, the cells were resuspended in 100 µL of PBS. From each tube, 10 µL of the resuspended cells were pipetted onto a microscope slide, forming a neat droplet. The slides were transferred to the microscope platform for imaging. The appropriate fluorescent channel (e.g., green for GFP-labeled plasmids or red for Cy3-labeled siRNA) was selected on the microscope. Both brightfield and corresponding fluorescence images were captured for each sample.

2.2.13 Western blot:

Cells were washed with PBS and then lysed using ice-cold radioimmunoprecipitation assay (RIPA) buffer supplemented with protease inhibitors. The resultant lysates were centrifuged at 16,000 x g for 15 minutes at 4 °C to pellet cell debris, and the supernatant containing the protein lysate was collected. Protein concentrations were determined using the Pierce BCA Protein Assay Kit (Thermo Fisher Scientific) following the manufacturer's protocol. To reduce and denature the extracted protein samples prior to gel electrophoresis, samples were boiled in 2x Laemmli sample buffer at 70°C for 10 minutes. A total of 10–20 µg of protein from each sample was loaded onto a 10% SDS-PAGE separating gel with a 6% stacking gel. Proteins were separated by electrophoresis and then transferred onto a polyvinylidene difluoride (PVDF) membrane. Membranes were incubated overnight at 4°C with a primary antibody targeting *POLA2* (POLA2 Polyclonal Antibody, rabbit polyclonal, 1:1000, Thermo Fisher Scientific). The following day, the membrane was incubated at room temperature for 1–2 hours with a horseradish peroxidase (HRP)-conjugated

anti-rabbit secondary antibody (1:2000, New England Biolabs). Protein visualization was carried out using the Pierce ECL Western Blotting Substrate (Thermo Fisher Scientific) according to the manufacturer's protocol. Protein was visualized via chemiluminescence using an Amersham Imager 600 system (GE Healthcare Life Sciences). The relative integrated density values of the protein bands were quantified using Fiji ImageJ software (version 1.54b, National Institutes of Health), and statistical analysis was performed using GraphPad Prism (version 9.5.0).

2.2.14 Resazurin cell viability assay:

In preparation for the resazurin dye reduction assay, THP-1 cells were seeded in 96-well plates at a density of 200,000 cells/mL and a volume of 50 µL. Nine cytarabine and idarubicin (17:1) drug concentrations were prepared over the selected range, using five-fold dilutions starting from the maximum concentration (Figure 8). A 50 µL volume of the appropriate drug treatment solution was added to each well, resulting in a final volume of 100 µL per well. The experimental layout for the drug treatments followed the design illustrated in Figure 8. The treated THP-1 cells were incubated with ara-C/idarubucin for 24 hours. After the incubation period, 2 µL of Triton-X-100 was added to each of the Triton-X positive control wells, for a final concentration of approximately 2%. Next, resazurin dye was used to assess cell viability in experimental samples. A working solution of resazurin was prepared by diluting 4 mL of 10X resazurin stock with 2 mL of PBS. The 10X resazurin solution was made from a 1000X stock, which had been previously prepared by dissolving 0.1 g of resazurin sodium salt in 9 mL of PBS. Next, 40 µL of the resazurin working solution was added to each well containing treated cells. Dye only control wells were given 100 µL media and 40 µL resazurin dye. No dye control wells contained 100 µL of treated cells but were given an additional 40 µL of media rather than dye. The plates were incubated for

3 hours at 37°C to allow for the reduction of resazurin by metabolically active cells. Fluorescence was then measured using a TECAN Spark plate reader, with excitation and emission wavelengths set at 550 nm and 590 nm, respectively. The fluorescence intensity values were normalized to the respective controls and were used to calculate cell viabilities.

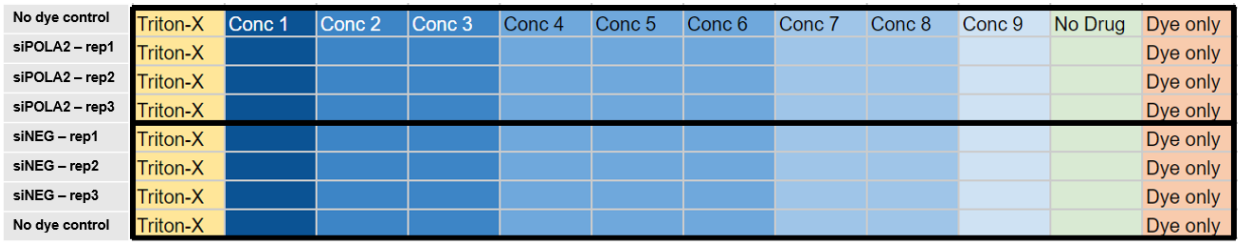

Figure 8: Well plate overview for resazurin cell viability assay.

2.2.15 Trypan blue cell counting assay:

THP-1 cells were seeded in 96-well plates at a density of 160,000 cells/mL and a volume of 50 µL. Ten cytarabine drug concentrations were prepared over the selected range, using five-fold dilutions starting from the maximum concentration. A 50 µL volume of the appropriate drug treatment solution was added to each well, resulting in a final volume of 100 µL per well. Each day post ara-C treatment, for a total of five days, the number of viable THP-1 cells in each well was counted using the trypan blue exclusion assay. Briefly, for each cell count, 10 µL of cell suspension was mixed thoroughly with 10 µL of trypan blue dye. Then 10 µL of this mixture was loaded onto a Tecan Cell Chip™ and placed into the Tecan Spark microplate reader. The Cell viability module was used to generate viable cell density values which were multiplied by two to account for dye dilution.

2.2.16 DAPI nuclei staining:

THP-1 cells were seeded in 6-well plates at a density of 5 x 10^5 cells per well in 2 mL of complete RPMI media. Treated cells were incubated with 0.5 μM or 1 μM ara-C and idarubicin in a 17:1 ratio for 24 hours. After 24-hour drug treatment, the cells were transferred to 15 mL centrifuge tubes and centrifuged at 300 x g for 5 minutes. The pelleted cells were ressuepnded and washed with 500 μL of PBS. Next, cells were fixed using 300 μL of 3.7% PFA in PBS and incubated at room temperature for 15 minutes with occasional gentle mixing. After fixation, cells were washed three times with PBS. Then, cells were resuspended in 500 μL of a 5 μM DAPI solution, prepared in PBS, and incubated overnight at 4°C, protected from light. After nuclei staining, cells were transferred to microscope slides using a cytospin centrifuge (2000 rpm for 8 minutes). Slides were mounted with coverslips using Fluoromount-G™ mounting medium (Thermo Fisher Scientific) and allowed to dry overnight at room temperature, protected from light. The following day, the mounted samples were analyzed using confocal microscopy.

2.2.17 CuAAC click staining:

To examine variable ara-C incorporation, THP-1 cells were first seeded in 24-well plates at a density of 4 × 10^5 cells per well in 500 μL of media and then treated with 15 μM azide-containing cytarabine analog, AzC, for 8–10 hours. Following AzC treatment, cells were transferred to microcentrifuge tubes and fixed in 300 μL of 3.7% paraformaldehyde (PBS) for 15 minutes at room temperature (RT), then washed twice with PBS. Fixed cells were transferred onto microscope slides via cytospin centrifugation for 8 minutes at 2,000 rpm. Next, cells were quenched with quenching buffer (50 mM glycine and 50 mM ammonium chloride in PBS) for 5 minutes at RT and washed twice with PBS. Then, the THP-1 cells were permeabilized twice with

0.2% Triton-X-100/PBS for 5 minutes at RT. DNA denaturation was carried out with 2 M HCl for 30 minutes, followed by neutralization in 0.1 M borax for 10 minutes, with PBS washes after each step. For DNase digest, cells were incubated in 100 μL DNase buffer for 5 minutes, followed by treatment with DNase I (1 mg/mL) for 30 minutes at 37°C. For hybridized RNA degradation, RNase H digestion was performed in 250 units/mL RNase H-containing buffer for 30 minutes at 37°C. Cells were washed three times with PBS after each digestion step. To enhance fluorescent signal, cells were incubated with Image-iT FX Signal Enhancer (Thermo Fisher Scientific) for 30 minutes at RT, followed by three PBS washes and blocking in 3% BSA/PBS solution for 15 minutes. Cells were then incubated with 100 μL of click staining solution (10 μM alkyne dye, 1 mM $CuSO_4$, 2 mM THTPA, 10 mM aminoguanidine hydrochloride, 10 mM sodium ascorbate in PBS or 1% BSA/PBS) for 2–3 hours at RT, followed by consecutive washes with PBS, 0.2% Triton-X-100/PBS, and 0.1% Tween-20/PBS. After the CuAAC staining, cell nuclei were stained with 100 μL of DAPI solution (5 μM in PBS) for 15 minutes, followed by washes with PBS, 0.2% Triton-X-100/PBS, and milliQ water. Resultant samples were mounted with Fluoromount-G and analyzed using confocal microscopy.

Chapter 3 – Results and Discussion:

3.1 - Bioinformatic Comparison of POL-PRIM Expression in AML Patient Survival

Recent work has implied an important role for the POL-PRIM complex in variable ara-C incorporation which has been shown to impact AML patient survival. However, more specific probing of the POL-PRIM subunits – *POLA1, POLA2, PRIM1 and PRIM2* – is needed to further investigate the impact of this complex on cytarabine efficacy and patient survival. Considering the powerful nature of bioinformatic analysis in identifying potential drug targets or biomarkers, we decided to leverage available AML datasets to help elucidate the therapeutic potential of the individual POL-PRIM subunits as well as their impact on AML outcomes. Thus, two large datasets were analyzed - TCGA RNA sequencing-derived data and HOVON clinical trials mRNA patient data – for patient survival trends in groups with "high" or "low" expression of *POLA2*. Survival curves and corresponding hazard ratios were used to draw quantitative conclusions about any changes in AML patient survival observed as a function of differential *POLA2* expression.

3.1.1 *Bioinformatic analysis of POL-PRIM in AML - TCGA dataset:*

Before investigating the impact of POL-PRIM on AML survival, we aimed to determine whether the average expression of each subunit was higher or lower in AML samples as compared to healthy, normal samples. For this goal, the TCGA AML dataset was leveraged as the HOVON trials data provided did not include data from healthy individuals. The Cancer Genome Atlas (TCGA) is a collaborative project that has compiled genomic and clinical data from thousands of cancer patients across a wide range of cancer types. It includes information such as gene expression profiles, DNA mutations, copy number variations, and clinical outcomes. TCGA data is publicly available and widely used for cancer research as it is comprised of large cancer patient datasets.

For this reason, we chose to analyze the AML TCGA dataset which contains data from 173 AML tumour samples as well as paired normal tissues. The resultant bar plot created using GEPIA2 depicts *POLA2* expression in transcripts per million (TPM) across all tumor samples and paired normal tissues. (Figure 9). The y-axis of the plot represents the median expression of the target gene found in the tumor type or normal tissue while the x-axis shows the different TCGA cancer types included in the analysis.

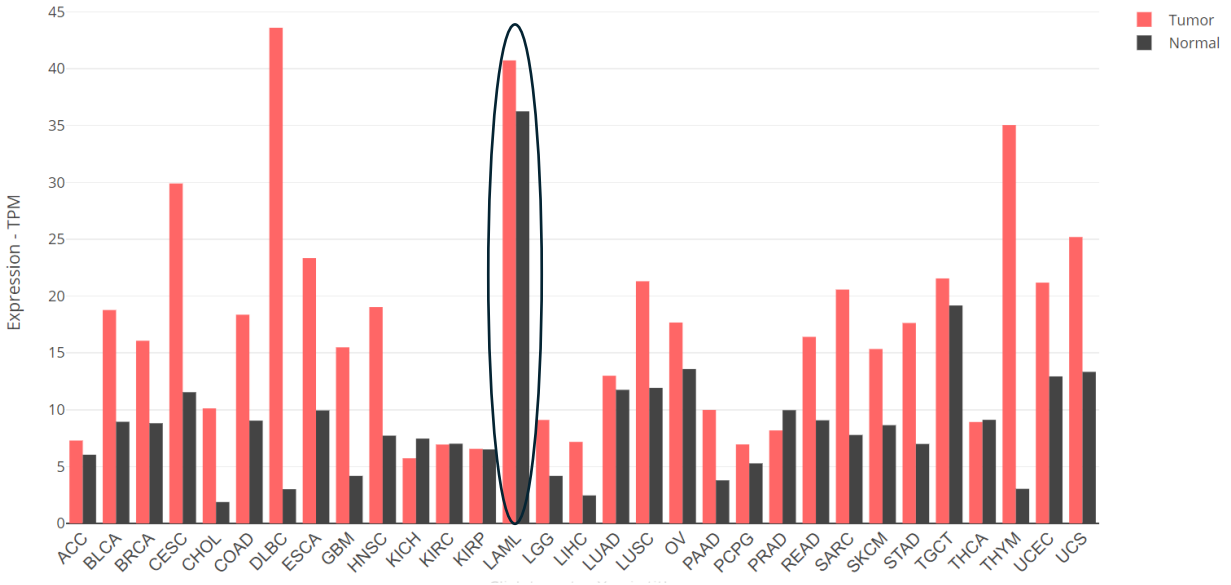

Figure 9: *POLA2* gene expression profile derived from TCGA AML dataset reveals elevated *POLA2* expression in AML (LAML) tumour. The height of each bar represents the median *POLA2* expression of a certain tumour type or normal tissue. The AML dataset represents 173 AML tumour samples and paired normal tissues samples. LAML represents AML dataset. AML tumour samples (red) reveal a higher median *POLA2* expression (40.73 TPM) as compared to matched normal tissue (black) (36.25 TPM).

As depicted in Figure 9, the AML dataset depicted as "LAML," unveils a modest difference in median *POLA2* expression between AML cancer tissues and paired normal bone marrow tissue. AML tissue samples exhibit a median *POLA2* expression of 40.73 transcripts per million while normal bone marrow tissue samples exhibit a lower median *POLA2* expression of 36.25 transcripts per million. This difference in median expression between AML and healthy bone marrow samples

may suggest *POLA2* as a possible therapeutic target and biomarker, with lower *POLA2* levels potentially linked to favorable outcomes. Subsequent functional studies, particularly gene knockdown strategies, would be essential to explore these findings and fully probe the biological and therapeutic relevance of *POLA2* expression in AML

Interestingly, bioinformatic analysis of TCGA RNA-seq data for all three other POL-PRIM subunits demonstrates higher median subunit expression in the normal tissue as compared to AML cancer samples (Figure S1). In the case of *POLA1*, the gene expression profile shows a median *POLA1* expression of 10.65 TPM for AML samples while normal bone marrow tissue exhibits a median expression of 13.18 TPM (Figure S1). For *PRIM1*, the respective bar plot depicts a median *PRIM1* expression value of 30.16 TPM for AML samples compared to normal bone marrow samples indicate an expression value of 67.03 TPM (Figure S1). Finally, the *PRIM2* bar plot constructed demonstrates a median *PRIM2* expression value of 13.39 TPM in AML samples while normal tissue exhibits a median gene expression of 21.52 TPM (Figure S1). This expressional trend may point to a potential relevance of the POL-PRIM complex in the context of AML, although further investigation is needed to confirm its role in improving patient outcomes.

Having established that AML and healthy bone marrow samples exhibited differential expression of the POL-PRIM complex genes, the respective gene expression data from the TCGA AML dataset was analyzed for survival trends. Survival analysis was performed using the Log-rank or Mantel Cox test which compares the survival distributions of two populations, assuming a proportional hazards model. Corresponding hazards ratios were also derived based on this statistical approach. Survival analysis of the four POL-PRIM subunits revealed that only the polymerase subunits – *POLA1* & *POLA2* – displayed a statistically significant difference in survival curves, with the survival difference between low and high *POLA2*-expressing groups

being the most significant (Figure 10). Mantel Cox statistical analysis revealed the highest statistical significance for the elevated patient survival observed in the low *POLA2* group (p=0.03), while the *POLA1* survival analysis was less significant (p=0.044), and analysis concerning the primase subunits revealed no statistically significant survival trend (PRIM1: p=0.62; PRIM2: p=0.15) (Figure 10). The *POLA1* expression survival curve demonstrated a slightly significant impact on AML patient survival due to variable *POLA1* expression, with higher *POLA1* expression correlating to an 80% increase in AML patient death (HR(high) =1.8; p=0.047). Similarly, the survival curves for *POLA2* demonstrate an 80% increase in AML patient death associated with higher *POLA2* expression (HR(high) =1.8; p=0.034) however this impact of *POLA2* expression on survival is more statistically significant and thus more compelling for future analysis.

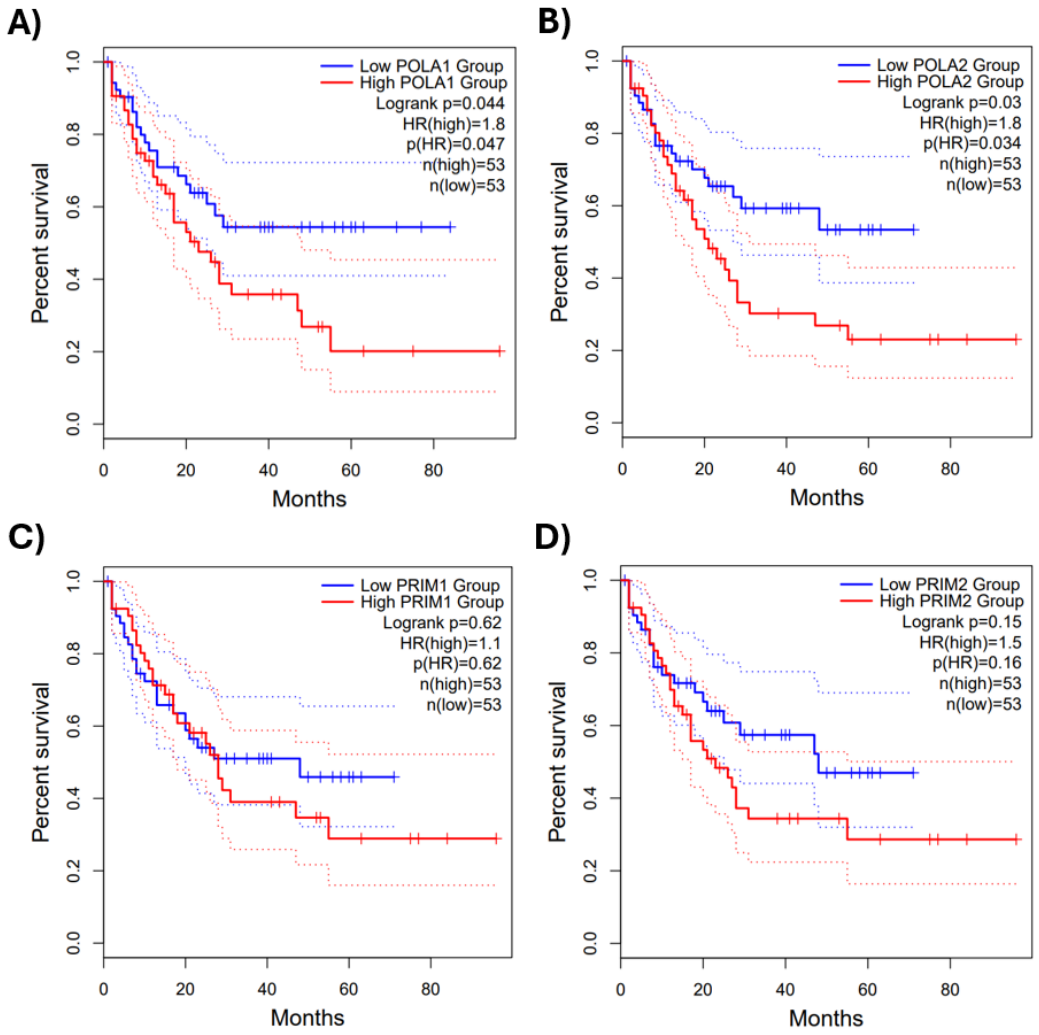

Figure 10: TCGA Kaplan Meier overall survival curves for TCGA patient groups with high/low POL-PRIM subunit expression. Among the four subunits, only the polymerase subunits demonstrate that the lower-expressing AML patient population (n=53; blue) exhibited enhanced overall survival as compared to the higher-expressing group (n=53; red). Dotted lines represent 95% confidence intervals. **A)** *POLA1* overall survival analysis showed a less significant (p=0.044; HR (high) = 1.8) correlation between low POLA1 group and elevated overall survival. **B)** Mantel Cox statistical analysis revealed the highest statistical significance for the elevated overall survival observed in the low *POLA2* group (p=0.03; HR (high) =1.8). **C) & D)** Analysis concerning the primase subunits revealed no statistically significant survival trend (*PRIM1*: p=0.62; HR (high)=1.1 & *PRIM2*: p=0.15; HR (high) =1.5).

3.1.2 *Survival analysis of POL-PRIM in AML – HOVON trials data:*

Resultant survival trends derived from the TCGA data consolidate a statistically significant relationship between low *POLA2* expression and improved AML patient survival. To further investigate this relationship in a more clinically relevant context, microarray data from a large (n=512) AML patient clinical trial (HOVON trials) was analyzed for survival trends. It is important to note that the data was derived from different HOVON trials (HO4/HO29/HO43) where a standard chemotherapy approach based on two remission induction cycles with a "7+3" regimen and intermediate dose of cytarabine were examined. Patients in these clinical trials received chemotherapy/autologous stem cell transplantation or allogeneic stem cell transplantation as post-remission treatment based on a risk assessment approach. Standardization of the type of AML treatment across the analyzed patient cohort combined with the specific use of the "7+3" frontline regimen allows the survival analysis of this data to yield insights more specific to cytarabine-related patient outcomes. Given that the "7+3" cytarabine/anthracycline treatment is likely to remain the frontline treatment option for AML, this would render subsequent survival analysis particularly valuable in identifying relevant biomarkers or therapeutics targets for improving cytarabine treatment.

To extract clinically relevant survival data, microarray data derived from a 512 AML patient cohort from HOVON trials was analyzed for trends in overall survival related to the expression of POL-PRIM subunits. Prior to analysis, the patient data was further stratified by factors such as AML subtype and the presence/absence of key leukemic mutations. Given that the favourable incorporation of cytarabine into RNA primers and associated improvement in AML patient survival was identified in the context of an M4/M5 subtype AML patient group, the HOVON microarray data was first filtered for M4/M5 patient data. Subsequent OS analysis of the

M4/M5 patient data was performed by stratifying the data into two subunit expression groups of equal size, denoted as "high" or "low" expression, with a median subunit expression level of 48.9, 125.6, 198.7 and 76.7 for *POLA2*, *POLA1*, *PRIM1* and *PRIM2*, respectively. Kaplan-Meier survival curves were constructed and analyzed by log-rank (Mantel-Cox) & Gehan-Breslow-Wilcoxon test. Although the analysis of the HOVON trials includes the testing of multiple hypotheses (e.g. with or without FLT3/ITD mutation), it must be noted that the statistical analysis was conducted without correction for multiple comparisons, thus the probability of false positives is increased. Additionally, hazard ratios (Mantel-Haenszel) were calculated as well. Thus, patients were divided into two groups according to low POL-PRIM subunit (lower-expressing 50% of patient population) versus high POL-PRIM subunit (higher-expressing 50% of patient population).

As shown for *POLA2*, lower expression was significantly correlated with lower OS (Gehan-Breslow-Wilcoxon, p=0.0443; log-rank, p=0.0819) (Figure 11). Although statistical significance was achieved only with the Gehan-Breslow-Wilcoxon test, it is still compelling as this statistical method is more powerful in the event that the two survival curves cross. Furthermore, the microarray data of *POLA1* was analyzed for potential correlation with OS. Hence, the OS of patients with low *POLA1* (lower-expressing 50% of patient population) were compared to patients with high *POLA1* (higher-expressing 50% of patient population). Unexpectedly, the difference of OS in these two patient groups was not found to be statistically significant with either statistical test (Gehan-Breslow-Wilcoxon, p=0.2454; log-rank, p=0.4542) (Figure 11). Therefore, unlike the OS analysis of the *POLA1* TCGA data, this result supports no correlation between *POLA1* expression and the overall survival of this patient population. For a complete analysis of all POL-PRIM subunits, the HOVON patient data was also analyzed for trends between OS and primase expression. Consistent with the TCGA OS curves, the microarray data for the primase subunits –

PRIM1 and *PRIM2* – also revealed a lack of significant correlation between OS and *PRIM1* subunit expression (Gehan-Breslow-Wilcoxon, p=0.6961; log-rank, p=0.1835) or *PRIM2* expression (Gehan-Breslow-Wilcoxon, p=0.9510; log-rank, p=0.7176).

Analysis of event-free survival (EFS) within the same M4/M5 AML patient cohort reinforces the overall survival trends identified (Figure S2). Statistically significant correlation was found between low *POLA2* levels and higher EFS (Gehan-Breslow-Wilcoxon, p=0.0505; log-rank, p=0.0462; HR (high) (Mantel-Haenszel) =1.39 (Figure S2). Reflective of the OS results, POLA1 (Gehan-Breslow-Wilcoxon, p=0.1355; log-rank, p=0.3733; HR (high) (Mantel-Haenszel) = 1.157), PRIM1 (Gehan-Breslow-Wilcoxon, p=0.9185; log-rank, p=0.7254; HR (high) (Mantel-Haenszel) =0.9441), and PRIM2 (Gehan-Breslow-Wilcoxon, p=0.5195; log-rank, p=0.8875; HR (high) (Mantel-Haenszel) = 1.023) EFS survival curves yielded no statistically significant correlation between the corresponding subunit expression and EFS (Figure S2).

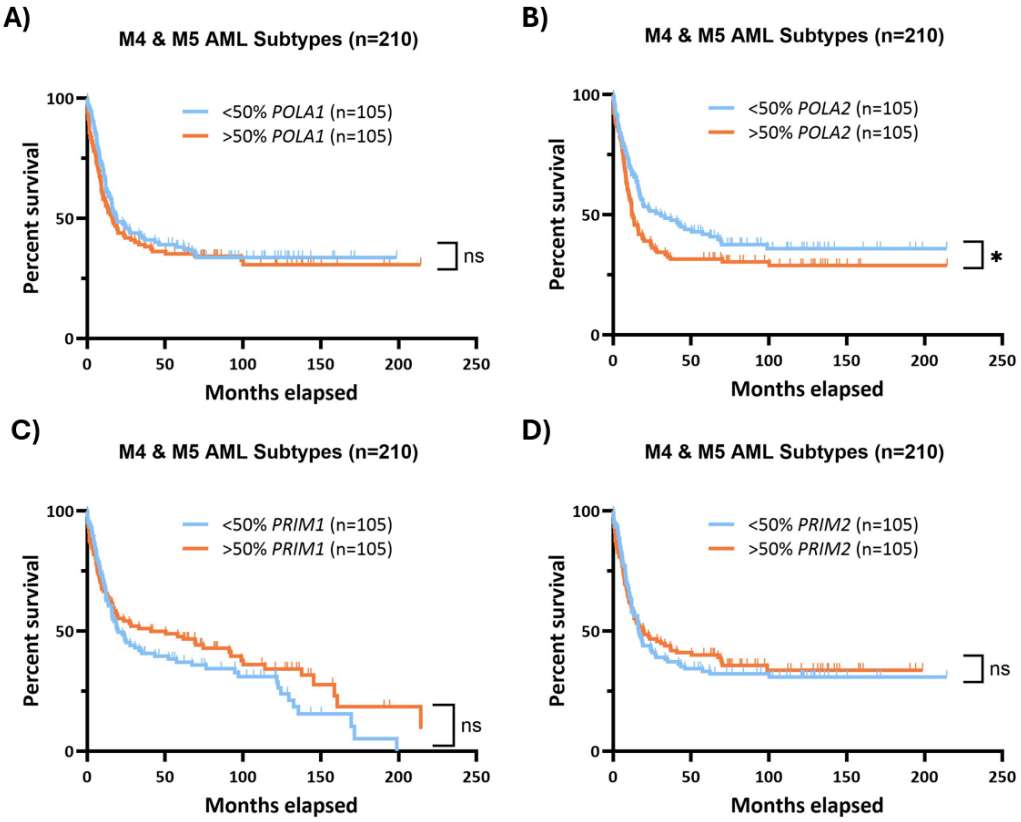

Figure 11: Kaplan Meier event-free survival curves for HOVON trials M4/M5 patient groups with high/low POL-PRIM subunit expression. Significant difference in overall survival between the lower-expressing POL-PRIM subunit patient population (n=210; blue) and the higher-expressing group (n=210; red) were identified only for *POLA2*. **A)** Log-rank and Gehan-Breslow-Wilcoxon tests revealed no correlation between *POLA1* levels and overall survival (Gehan-Breslow-Wilcoxon, p=0.2454; log-rank, p=0.4542; HR (high) (Mantel-Haenszel) = 1.135). **B)** The only statistically significant correlation was found between low *POLA2* levels and enhanced survival (Gehan-Breslow-Wilcoxon, p=0.0443; log-rank, p=0.0819; HR (high) (Mantel-Haenszel) = 1.345). **C)** No relationship was identified between *PRIM1* expression and AML patient survival (Gehan-Breslow-Wilcoxon, p=0.6961; log-rank, p=0.1835; HR (high) (Mantel-Haenszel) = 0.7968). **D)** Survival analysis in the context of *PRIM2* levels also failed to produce a significant correlation (Gehan-Breslow-Wilcoxon, p=0.9510; log-rank, p=0.7176; HR (high) (Mantel-Haenszel) = 0.9406).

To ensure thorough exploration of the impact of POL-PRIM subunit expression on survival (OS) in acute myeloid leukemia (AML) patients, an additional expanded analysis of the HOVON patient data was performed. Here, all AML subtypes were included, but patients who were positive for the FLT3/ITD (Internal Tandem Duplication) mutation were excluded due to extremely poor outcomes in AML [83]. Again, patient data was divided into two subunit expression groups of

equal size, denoted as “high” or “low” expression, with a median subunit expression level of 48.6, 130.3, 198.6 and 77 for *POLA2*, *POLA1*, *PRIM1* and *PRIM2*, respectively. From the analysis, lower expression of *POLA2* was significantly correlated with improved overall survival (OS). Both the Gehan-Breslow-Wilcoxon test ($p = 0.0181$) and the log-rank test ($p = 0.0426$) indicated statistically significant associations between *POLA2* expression and OS (Figure 12). The significance observed in both tests in the current analysis strengthens the evidence that *POLA2* expression may serve as an effective prognostic biomarker. The hazard ratio (HR) for *POLA2* was 1.306, indicating a 30.6% higher risk of death in patients with higher expression levels compared to those with lower expression levels. These findings further support the knockdown of *POLA2* as a potential therapeutic strategy in improving AML patient treatment. In contrast, analysis of *POLA1* did not reveal any significant correlations with OS. Neither the log-rank test ($p = 0.8932$) nor the Gehan-Breslow-Wilcoxon test ($p = 0.6050$) showed statistically significant results (Figure 12), consistent with earlier analyses in which *POLA1* also failed to achieve significance. The hazard ratio for *POLA1* was 1.01, suggesting no meaningful increase in risk between patient groups with differing expression levels. The consistent lack of significance indicates that *POLA1* does not appear to impact AML survival in this patient cohort, and its expression is unlikely to influence OS. Further analysis was conducted to assess the potential impact of *PRIM1* and *PRIM2* expression on OS. For *PRIM1*, neither the Gehan-Breslow-Wilcoxon test ($p = 0.4695$) nor the log-rank test ($p = 0.4411$) indicated any statistically significant association between expression levels and survival outcomes (Figure 12). These results are consistent with previous findings, suggesting that *PRIM1* is not associated with significant differences in OS. The HR for *PRIM1* was 0.905, indicating a modest 9.5% reduction in risk, though this was not statistically significant. Similarly, for *PRIM2*, both the Gehan-Breslow-Wilcoxon test ($p = 0.5947$) and the log-rank test ($p = 0.5757$)

yielded nonsignificant results (Figure 4), with an HR of 0.93, indicating a slight 7% decrease in risk. These findings also align with prior analyses, further reinforcing the conclusion that neither *PRIM1* nor *PRIM2* expression has a substantial impact on OS in this patient population. In conclusion, while *POLA2* consistently shows a statistically significant association with reduced survival, *POLA1*, *PRIM1*, and *PRIM2* do not exhibit such correlations.

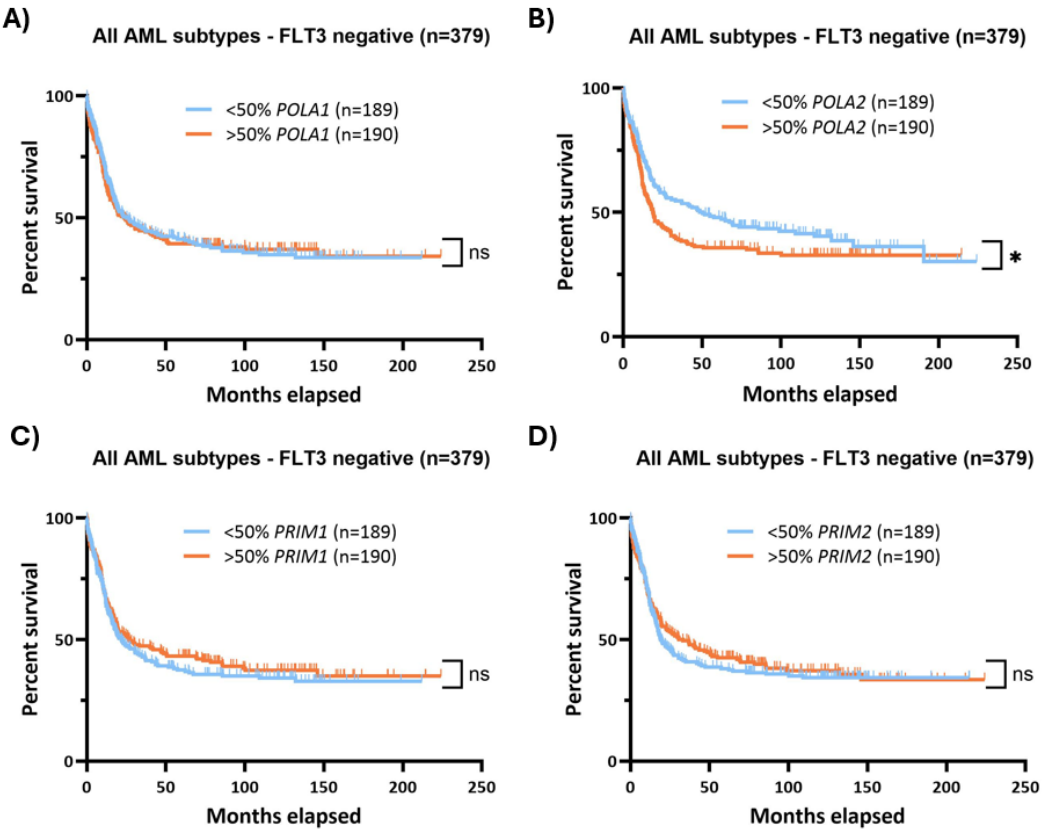

Figure 12: Kaplan Meier overall survival curves for HOVON trials FLT-negative patient groups with high/low POL-PRIM subunit expression. Significant difference in overall survival between the lower-expressing POL-PRIM subunit patient population (n=189; blue) and the higher-expressing group (n=190; red) were identified only for *POLA2*. **A)** Log-rank and Gehan-Breslow-Wilcoxon tests revealed no correlation between *POLA1* levels and overall survival (Gehan-Breslow-Wilcoxon, p = 0.6050; log-rank, p = 0.8932; HR(high) (Mantel Haenszel) = 1.017). **B)** The only statistically significant correlation was found between low *POLA2* levels and enhanced survival (Gehan-Breslow-Wilcoxon, p = 0.0181; log-rank, p = 0.0426; HR(high) (Mantel Haenszel) = 1.306). **C)** Neither statistical test revealed a significant relationship between *PRIM1* expression and AML patient survival (Gehan-Breslow-Wilcoxon, p = 0.4695; log-rank, p = 0.4411; HR(high) (Mantel Haenszel) = 0.9052). D) Survival analysis in the context of *PRIM2* levels also failed to produce a significant correlation (Gehan-Breslow-Wilcoxon, p = 0.5947; log-rank, p = 0.5757; HR(high) (Mantel Haenszel) = 0.9302).

For a thorough survival analysis, event-free survival (EFS) trends within the same FLT3/ITD -negative AML patient cohort were also analyzed. Interestingly, this EFS analysis supported the OS trends identified earlier for *POLA1, PRIM1, and PRIM2*; however, did not yield a significant EFS correlation with *POLA2* expression, unlike all of the previous bioinformatic analysis (Figure S3). Similarly to the FLT3/ITD-negative OS results, *POLA1* (Gehan-Breslow-Wilcoxon, p=0.2586; log-rank, p=3354; HR (high) (Mantel-Haenszel) = 1.125), *PRIM1* (Gehan-Breslow-Wilcoxon, p=0.3968; log-rank, p=0.4763; HR (high) (Mantel-Haenszel) =0.9167), and *PRIM2* (Gehan-Breslow-Wilcoxon, p=0.9521; log-rank, p=0.7397; HR (high) (Mantel-Haenszel) = 1.041) EFS survival curves yielded no statistically significant correlation between the corresponding subunit expression and EFS (Figure S3) Unexpectedly, EFS analysis of *POLA2* data did not reach statistical significant (Gehan-Breslow-Wilcoxon, p=0.0979; log-rank, p=0.1219; HR (high) (Mantel-Haenszel) =1.209) (Figure S3). It could be that by discriminating for FLT3/ITD negative patients and considering event-free survival, we may be potentially diminishing the impact of *POLA2* expression on survival. Perhaps, excluding FLT-positive patients which are prone to very poor outcomes and grouping relapse, no response and death, altogether, as one event, masks some of *POLA2's* impact on patient survival.

3.1.3 *Validation of basal POLA2 expression in AML cell lines:*

Ultimately, comprehensive survival analysis revealed a significant correlation between lower expression of the *POLA2* gene and improved overall survival in AML patients. This finding highlights the potential role of *POLA2* as a therapeutic target in enhancing AML treatment outcomes. To further investigate this, we aimed to identify suitable AML cell lines that would serve as effective models for *in vitro* studies testing the impact of reduced *POLA2* expression on drug efficacy and different AML-related endpoints. Therefore, we measured the basal expression

levels of *POLA2* in several commonly used AML cell lines available in our lab —THP-1, AML3, MOLM-13, and U937. By confirming which cell lines have sufficient *POLA2* expression to facilitate knockdown experiments, we can ensure that our selected models are appropriate for investigating the effects of *POLA2* modulation on drug response and leukemic cell death. Hence, the expression levels of the *POLA2* gene were assessed across THP-1, AML3, MOLM-13, and U937 cell lines by qPCR mRNA expression analysis. The normalized *POLA2* expression levels, with MOLM-13 set as 1.0, revealed that THP-1, AML3, and U937 exhibited lower *POLA2* expression levels of 0.77, 0.85, and 0.74, respectively (Figure 13). One-way ANOVA followed by Tukey's test revealed that all basal expression levels between the cell lines were statistically different excluding the difference between THP-1 and U-937. Tukey's test p-values: $p=0.0093$ (THP-1 vs. OCI-AML3), $p<0.0001$ (THP-1 vs. MOLM-13), $p=0.3213$ (THP-1 vs. U-937), $p<0.0001$ (OCI-AML3 vs. MOLM-13), $p=0.0005$ (OCI-AML3 vs. U-937), and $p<0.0001$ (MOLM-13 vs. U-937).

Although MOLM-13 displayed the highest *POLA2* expression among the tested cell lines and thus may be preferred for *POLA2* knockdown experiments, all cell lines display expression levels within a relatively similar range, indicating that they may also serve as suitable models for the *in vitro* probing of *POLA2* modulation in AML.

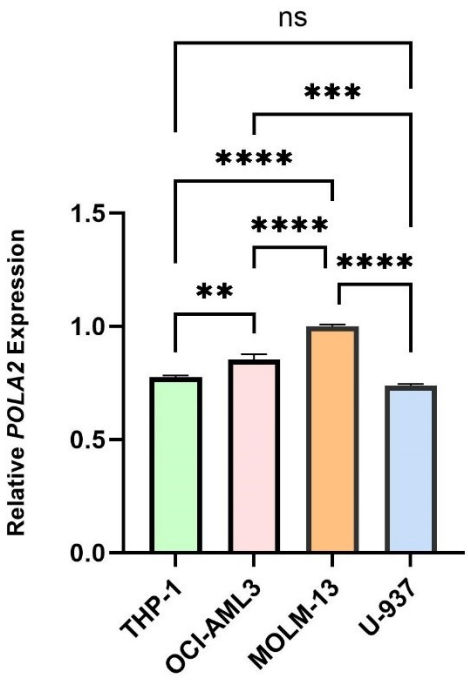

Figure 13: Normalized *POLA2* basal expression levels in THP-1, OCI-AML3, MOLM-13 and U937 cell lines. MOLM-13 exhibited the highest basal expression set as 1.0 for relative POLA2 expression, while THP-1, AML3, and U937 exhibited lower *POLA2* expression levels of 0.77, 0.85, and 0.7, respectively. One-way ANOVA followed by Tukey's test revealed that all basal expression levels between the cell lines were statistically different excluding the difference between THP-1 and U-937. Tukey's test p-values: $p=0.0093$ (THP-1 vs. OCI-AML3), $p<0.0001$ (THP-1 vs. MOLM-13), $p=0.3213$ (THP-1 vs. U-937), $p<0.0001$ (OCI-AML3 vs. MOLM-13), $p=0.0005$ (OCI-AML3 vs. U-937), and $p<0.0001$ (MOLM-13 vs. U-937). The number of biological replicates tested (n) was 4.

As a reference, *POLA2* expression levels derived from the Human Protein Atlas Project were used, where MOLM-13 exhibited the highest *POLA2* expression of 37.5 normalized transcripts per million (nTPM) and basal *POLA2* expression was reported as 32.1 nTPM for OCI-AML3, 29.2 nTPM for THP-1, and 27.9 nTPM for the U937 cell line. When comparing the experimental trend in basal *POLA2* expression obtained via qPCR to the relative expression levels of *POLA2* shown in the human protein atlas for leukemia cell lines, we find a consistent trend in expression levels of this gene. This comparison serves as an additional control, affirming our confidence in the suitability of these AML cell lines for *in vitro* investigations into *POLA2* modulation. Ultimately, while MOLM-13 may be the most suitable cell model for future *POLA2*

knockdown experiments, the similar expression levels across all tested cell lines suggest that they could all be effectively employed to explore the effects of modifying *POLA2* expression on AML drug incorporation, sensitivity and drug-induced cell death.

In summary, the bioinformatic results derived from the TCGA dataset combined with the analysis of the HOVON microarray data provide a strong foundation for the correlation between *POLA2* expression and AML survival. Moreover, these results shed light on the potential of *POLA2* as a biomarker for predicting AML prognosis. This bioinformatic analysis highlights *POLA2* as a potentially critical protein among the POL-PRIM subunits, whose activity has the potential to be exploited for novel AML treatments. The hazard ratios from both datasets correlate higher *POLA2* expression with a 30.6 – 80% increase in the risk of death and a 39% increase in experiencing the events such as death, relapse, or treatment failure, suggesting that the reduction of *POLA2* levels as a possible therapeutic strategy in improving AML patient outcomes. Thus, our aim 1 results offer clear evidence for why *POLA2* knockdown may be therapeutically valuable, specifically for AML patient prognosis, the design of novel therapies as well as the improvement of existing treatments.

3.2 - Screening methods for siRNA uptake into diverse difficult-to-transfect AML cells

Given the significant relationship revealed between reduced *POLA2* expression and improved AML patient survival, modulation, but more specifically the knockdown, of *POLA2* in AML has potential to be an attractive therapeutic strategy. However, *in vitro* AML gene expression studies are greatly hindered by challenges in the uptake of RNA in AML cells. Since immature AML cells exhibit compromised endocytic activity and RNA cargos generally rely on endocytic pathways for successful cellular uptake, chemical transfection in AML cells is inefficient [31, 32]. Furthermore, AML cells are also naturally in suspension which renders the targeting of these cells

by transfection complexes much more difficult [33]. As chemical transfection methods are generally ineffective for RNA transfection in AML cells, physical transfection methods such as electroporation are more commonly relied upon. Unfortunately, although electroporation methods bypass the need for endocytosis, they are only able to introduce small RNAs into some AML cell lines by creating transient pores in cell membranes which result in high rates of cell death [34, 35]. Thus, my second aim in this project was to develop *in vitro* methods that could facilitate the modulation of *POLA2* expression in relevant AML cell lines.

3.2.1 *Validation of POLA2 siRNA Activity in easy-to-transfect HEK-293T Cells:*

To investigate the cellular effects of *POLA2* knockdown, siRNA sequences were selected. As *POLA2*-targeting siRNA sequences are commercially available, we selected and ordered the *POLA2* siRNA sequence with the highest transfection efficiency from Integrated DNA Technologies. Nonetheless, before the *POLA2* siRNA could be used for *in vitro* studies, its activity needed to be validated *in vitro*. For this validation experiment, we chose to transfect HEK293T cells as they are widely used in gene expression studies for their high transfection efficiency, especially when employing chemical-based methods like Lipofectamine. Lipofectamine 3000 transfection of the *POLA2* siRNA sequence in HEK-293T cells resulted in approximately 80% knockdown ($p<0.0001$) of the *POLA2* gene at the mRNA level (Figure 14). The significant decrease in *POLA2* mRNA achieved confirms the knockdown activity of this siRNA and its utility for future *in vitro* experiments. Additionally, this siRNA screening also establishes a benchmark for the transfection efficiency that can be attained with this siRNA, without prominent challenges in cellular RNA uptake.

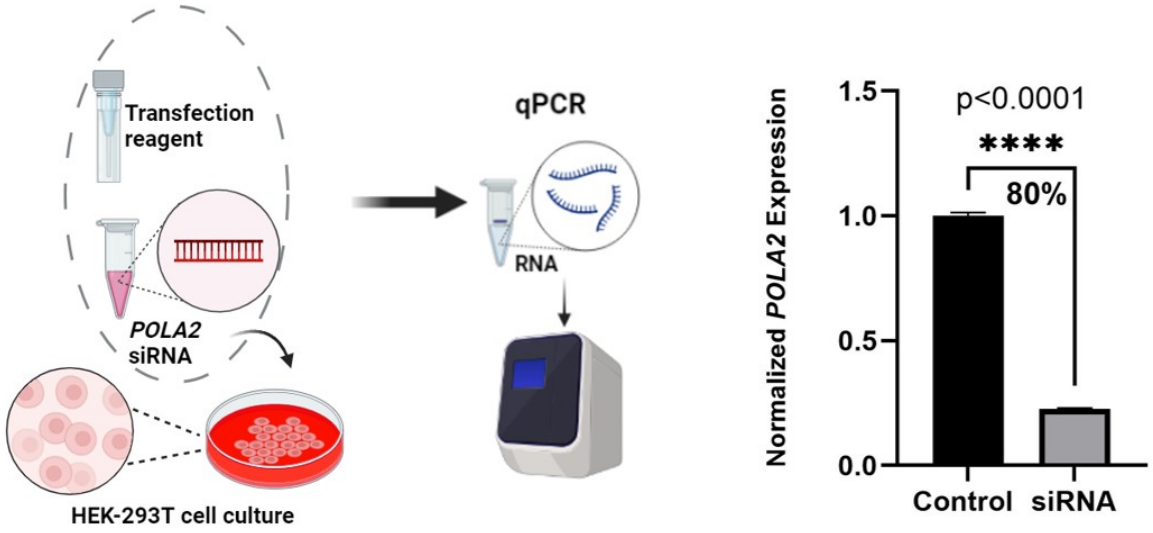

Figure 14: Validation of *POLA2* siRNA activity in HEK293T cells. A) Experimental workflow for screening of *POLA2* siRNA knockdown in HEK-293T cells. Following Lipofectamine 3000 transfection twice, incubated HEK-293T cells were harvested 48 hours later for RNA extraction and RT-qPCR. **B)** Screening of *POLA2* siRNA activity resulted in an ~80% knockdown of *POLA2* mRNA expression in Lipofectamine 3000-transfected HEK-293T cells. Changes in *POLA2* mRNA expression were normalized against housekeeping genes – HPRT and GAPDH. Statistical analysis performed using the unpaired t-test; n=4, reveals high statical significance ($p<0.0001$).

3.2.2 *Visualization of RNA uptake in AML cells:*

Once the knockdown activity of the selected *POLA2* siRNA was validated by qPCR, it could be employed for the testing of transfection methods for siRNA delivery in AML cell lines. Based on a comprehensive literature review, several chemical transfection methods were selected for their demonstrated effectiveness in either AML cell lines or cell lines that are similarly difficult-to-transfect. The following transfection reagents were primarily chosen based on their chemical formulations, toxicity profiles, and compatibility with RNA-based delivery. Based on our success with this reagent for plasmid transfection in AML cells and its low toxicity, the ViaFect™ lipid-based transfection reagent was tested [84]. Also reported to have low toxicity in published studies, the lipid-based FuGENE® HD formulation was also tested [85]. Recent work

also demonstrates the non-liposomal cationic amphiphilic lipid-based transfection reagent, INTERFERin, as one of the most efficient reagents for siRNA delivery [86-88]. It also offers the additional advantage of reduced off-target effects by enabling high transfection efficiency at low RNA concentrations. Moreover, Lipofectamine® 3000, one of the most traditional lipid-based transfection reagents, and RNAiMAX, specifically optimized for RNA delivery, were another two reagents that were included in these experiments. These cationic lipid-based reagents function by forming complexes with negatively charged nucleic acid molecules to allow them to overcome the electrostatic repulsion of the cell membrane. Although traditional Lipofectamine-based transfections typically demonstrate very limited transfection efficiency in AML cell lines, few studies have reported the transfection of MV4-11 cells with Lipofectamine and/or RNAiMAX -based protocols [89]. Lastly, a nucleofection method was included in the testing as electroporation-based physical transfection methods are still considered the gold standard for difficult-to-transfect AML cell lines. Nucleofection harnesses electrical pulses to create transient pores in the cell membrane, thereby allowing the RNA to enter the cell without the need for a carrier molecule. Unfortunately, the electrical pulses are harsh on cells, causing extensive cell death.

While efficient *POLA2* knockdown must be verified quantitatively using RT-qPCR and Western blot (Figure 15), we first sought to test a more rapid method for optimizing RNA uptake. Fluorescent dye labeling of DNA and RNA oligonucleotides is a well-established technique for the assessment of RNA/DNA uptake and localization inside cells [90]. This fluorescence-based RNA visualization technique could allow for more rapid, resource-efficient screening for the evaluation of transfection methods in several AML cell lines. Briefly, AML cells were transfected with the appropriate chemical reagent and a Cy3 dye-labelled siRNA which could be visualized through the red fluorescent channel. For some combinations of cell lines and transfection methods,

the bright red fluorescence signal emitted from the Cy3-siRNA appeared to overlap with corresponding cells, indicating successful siRNA uptake.

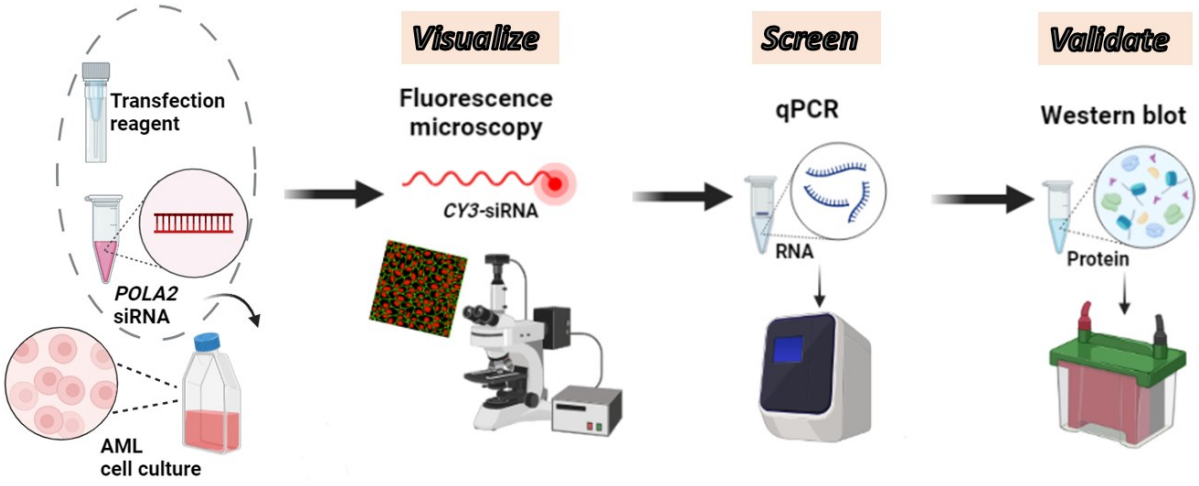

Figure 15: Experimental workflow of transfection method screening. AML cells were transfected with Cy3-siRNA and analyzed via fluorescent microscopy. For more quantitative analysis, AML cells were transfected with *POLA2*-siRNA and changes in *POLA2* mRNA and protein expression were quantified after 24-48 hours by RT-qPCR and Western blot, respectively.

This Cy3 fluorescence signal can be observed in the microscopy images of FuGENE-transfected U-937 cells (Figure 16). The lack of red fluorescence signal observed in the control sample without Cy3-siRNA confirms that the source of the red fluorescence is the Cy3 dye conjugated to the siRNA. Surprisingly some Cy3-associated fluorescence was also observed in the control samples where the respective transfection reagent was excluded (Figure 16). It is unlikely that the fluorescence observed in the control samples was due to residual siRNA given that three washes with performed. We therefore hypothesize that the fluorescence observed in the control sample without transfection reagent is attributed to the uptake of cleaved Cy3 dye from RNA. Indeed, Cy3 dye molecules are small and able to cross the cellular membrane without the help of a carrier molecule. In fact, recent studies show that nuclease degradation of unmodified DNA/RNA

strands results in a misleading intracellular fluorescent signal which is saturated by the fluorescence of the degradation product (phosphorylated dye) [90]. Since our siRNA are not chemically-modified they are highly susceptible to degradation in the cell media (with serum), thereby releasing some of the dye. As such, we concluded that microscopy was not suitable for testing RNA uptake.

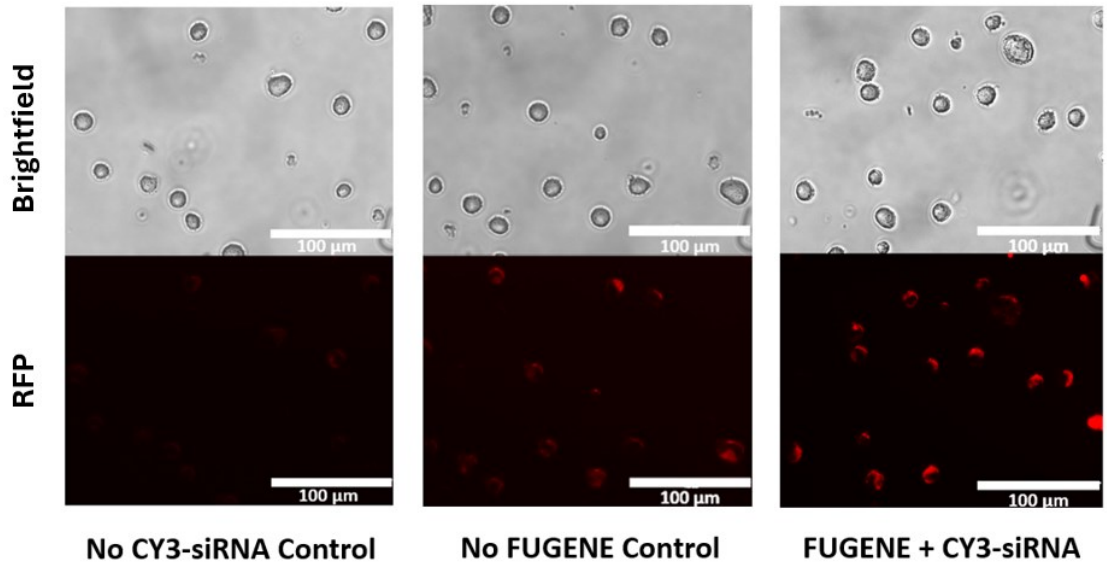

Figure 16: Visualization of Cy3-siRNA uptake in FuGENE HD-transfected U-937 cells. Red fluorescence of Cy3-labelled siRNA could be detected in U-937 cells transfected with FuGENE HD reagent for 16 hours. While the no Cy3-siRNA control confirms that the fluorescence signal is derived from the Cy3 dye molecule, the no FuGENE sample indicates that the red fluorescence could be attributed to both siRNA uptake and uptake of the Cy3 dye alone.

3.2.3 *Functional transfection method screening in diverse AML cells:*

Given that microscopy was not a suitable method for testing RNA uptake efficiency, all transfection methods were tested by directly measuring RNA and protein alterations. For improved efficiency, all transfection methods were compared by first measuring mRNA levels by RT-qPCR. Given the number of methods and conditions tested, results displayed here represent those with the highest activity.

Overall, the liposomal INTERFERin formulation greatly outperformed all of the other reagents, vectors, and the nucleofector device tested. The highest siRNA transfection efficiency as measured by RNA knockdown, without significant optimization, was approximately 60% ($p<0.0001$) siRNA knockdown in THP-1 cells transfected with INTERFERin for 24 hours (Figure 17). The second highest transfection efficiency achieved with INTERFERin was in OCI-AML3 cells, yielding approximately 48% ($p<0.0001$) *POLA2* mRNA knockdown (Figure 17). INTERFERin was significantly less efficient in the rest of the AML cell lines - MOLM-14, MOLM-13, MV4-11 and OCI-AML2 – yielding 20% ($p=0.0201$), <10% ($p=0.0886$), <10% ($p=0.0323$), and 12% ($p=0.0132$) *POLA2* knockdown, respectively. It is not surprising that THP-1 and OCI-AML3 cell lines resulted in the highest knock down because these are the most differentiated AML cell lines among those tested.

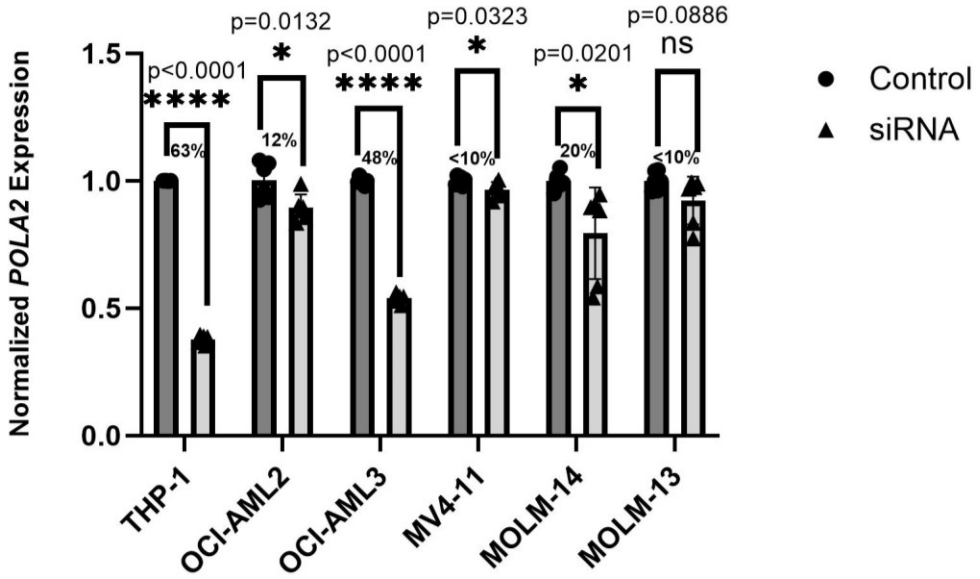

Figure 17: Average transfection efficiencies achieved with INTERFERin formulation in diverse AML cell lines. POLA2 mRNA knockdown of 63%, 48%, 12%, 20%, <10%, and <10% was achieved in THP-1, OCI-AML3, OCI-AML2, MOLM-14, MV4-11, and MOLM-13, respectively. Differences in mRNA expression were found statistically significant (unpaired t-test; THP-1, OCI-AML3: $p<0.0001$; OCI-AML2: $p=0.0132$; MV4-11: $p=0.0323$; MOLM-14: $p=0.0201$) for all cell lines except MOLM-13 ($p=0.0886$). Three biological replicates were tested per cell line (n=3).

We next aimed to develop new protocols functional for more diverse AML cell lines. In particular, protocols for important AML cell lines U-937, MV4-11 and MOLM-14 were highly desired due to their common mutations and uses for testing numerous therapeutic agents. As such we investigated the transfection of MV4-11 and MOLM-14 with several different lipid-based formulations – ViaFect, FuGENE, RNAiMAX and Lipofectamine 3000 due to their marketed promise for RNA uptake [89]. Unfortunately, little-to-no transfection efficiency was obtained with ViaFect (<10%; p=0.2930) and FuGENE (<10%; p=0.1352) reagents as demonstrated by the lack of statistically significant *POLA2* mRNA knockdown demonstrated (Figure 18). Similarly, RNAiMAX lipid-based transfection also failed to produce sufficient transfection efficiency in MV4-11 (<10%; p=0.0045) and MOLM-14 cells (10%; p=0.1741) (Figure 19). Although the *POLA2* knockdown generated from RNAiMAX-transfected MV4-11 cells was statistically significant, a mRNA knockdown of <10% is too low to reliably elicit any *POLA2*-silencing effect on AML drug sensitivity, drug incorporation or leukemic cell death. Furthermore, the final lipid-based reagent screened for efficacy in AML cells was the Lipofectamine 3000 reagent. Consistent with the ViaFect, FuGENE HD, and RNAiMAX transfection results, Lipofectamine siRNA transfection produced less than 10% (MV4-11: p=0.8024; MOLM-14: p=0.4636) *POLA2* mRNA knockdown in both MV4-11 and MOLM-14 cells (Figure 20).

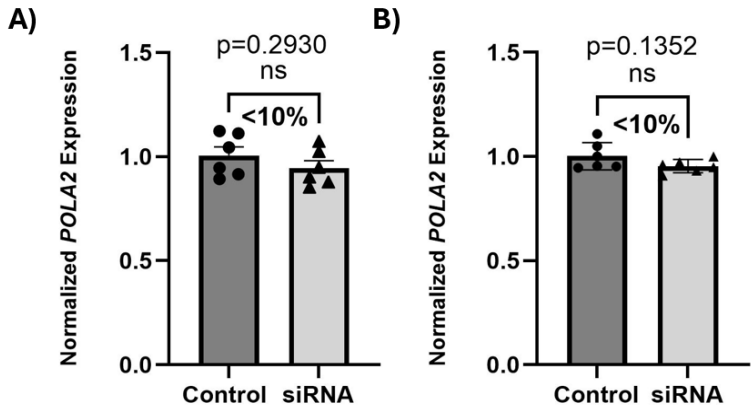

Figure 18: Average transfection efficiencies achieved with ViaFect and FuGENE HD reagents in U-937 cells. *POLA2* mRNA knockdown of <10% was attained in U-937 cells with both **A)** ViaFect and **B)** FuGENE reagents. Differences in mRNA expression were found to be statistically non-significant (unpaired t-test; ViaFect: p=0.2930; FuGENE: p=0.1352) for both methods. Three biological replicates were tested (n=3) for each condition.

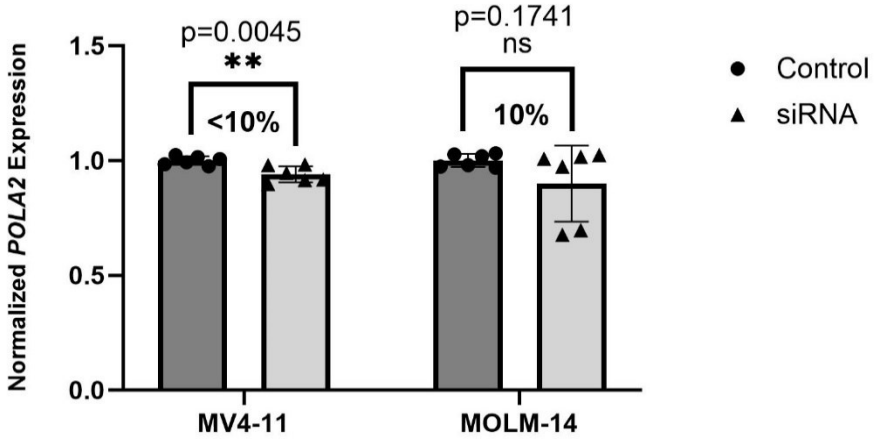

Figure 19: Average transfection efficiencies achieved with RNAiMAX reagent in MV4-11 and MOLM-14 cells. *POLA2* mRNA knockdown of <10% and 10% were attained in MV4-11 and MOLM-14 cells, respectively. Differences in mRNA expression were found to be statistically significant (unpaired t-test; MV4-11: p=0.0045; MOLM-14: p=0.1741) for *POLA2* knockdown in MV4-11 but not for MOLM-14. Three biological replicates were tested (n=3) for each cell line.

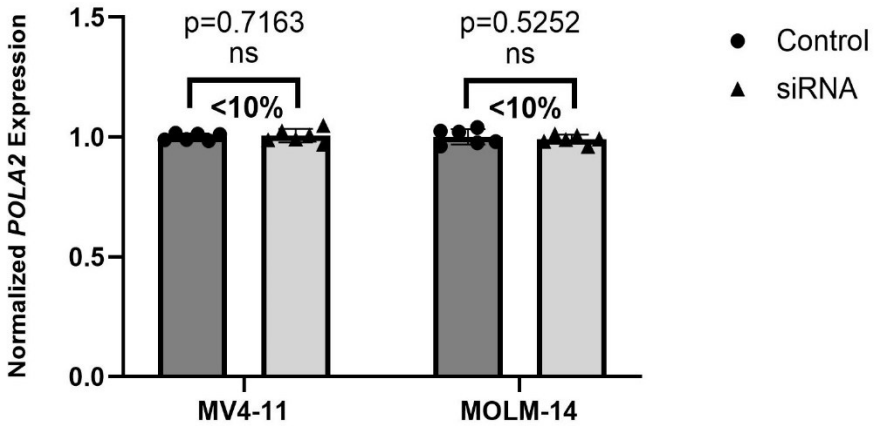

Figure 20: Average transfection efficiencies achieved with Lipofectamine 3000 reagent in MV4-11 and MOLM-14 cells. *POLA2* mRNA knockdown of < 10% were attained in both MV4-11 and MOLM-14 cells. Differences in mRNA expression were found to be statistically nonsignificant (unpaired t-test; MV4-11: p=0.7163; MOLM-14: p=0.5252) for *POLA2* knockdown for both MV4-11 and MOLM-14 cells. Three biological replicates were tested (n=3) for each cell line.

Finally, although our focus was to develop chemical transfection methods for the delivery of siRNA into AML cells to avoid compromising cell viability, we included nucleofection in our screening as a benchmark for currently available *in vitro* AML transfection methods. Nucleofection of *POLA2* siRNA into U-937 cells yielded the highest transfection efficiency of 55%, followed by 32% efficiency in OCI-AML3 cells and 20% efficiency in THP-1 cells (Figure 21). All differences in *POLA2* mRNA expression were identified as highly statistically significant ($p<0.0001$) (Figure 21). These transfection efficiencies fall in the range of those acquired with INTERFERin; however, for cell lines such as THP-1 and OCI-AML3 which exhibited improved siRNA uptake with INTERFERin. However, nucleofection is very harsh, resulting in significant cell death (see below), as such we concluded that the less-abrasive, INTERFERin method is favourable for siRNA-based cell death studies.

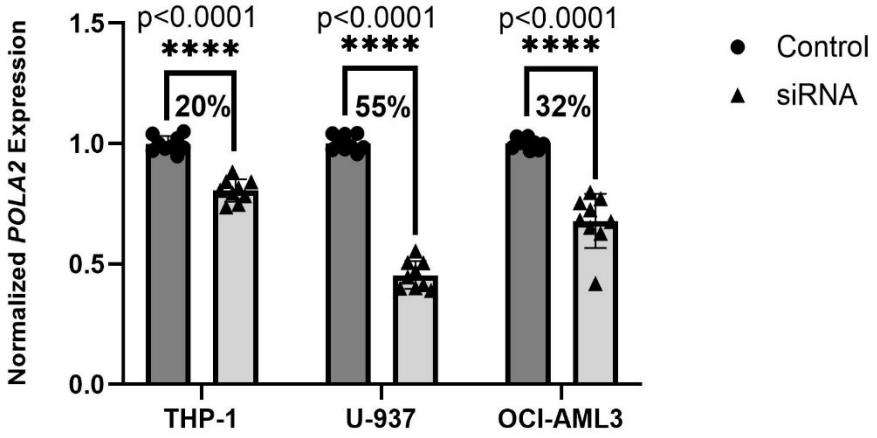

Figure 21: Average transfection efficiencies achieved with Nucleofection in THP-1, U-937, and OCI-AML3 cells. *POLA2* mRNA knockdown of 20%, 55%, and 32% were achieved in THP-1, U-937, and OCI-AML3 cells, respectively. Differences in mRNA expression were found to be highly statistically significant (unpaired t-test; $p<0.0001$) for *POLA2* knockdown in all three cell lines. Three biological replicates were tested (n=3) for each cell line.

3.2.4 *Optimization of AML cell transfection – RNA concentration:*

Following the completion of comprehensive transfection method screening, we sought to further enhance transfection efficiencies across various AML cell lines through optimization. Several factors may influence RNA transfection efficiency *in vitro* including but not limited to RNA concentration, cell culture density, transfection reagent to RNA ratio, and serum conditions [91]. Given that certain cell types and transfection reagents require higher RNA concentrations for maximal transfection efficiency, we attempted to optimize our RNAiMAX protocols for the MV4-11 cell line by increasing the initial RNA concentration of 30 nM to 100 nM. Interestingly, increasing the *POLA2* siRNA concentration by more than triple its original value did not alter the transfection efficiency (<10%; $p=0.7644$) of RNAiMAX in MV4-11 cells (Figure 22). The same optimization strategy was applied to the INTERFERin transfection of MV4-11 cells. Consistent with the RNAiMAX results, raising the siRNA concentration to 100 nM failed to improve INTERFERin transfection efficiency (<10%; $p=0.1582$) in MV4-11 cells (Figure 23). These

results together indicate that siRNA concentration is not a limiting factor in achieving maximal transfection efficiency with these two lipid-based transfection methods.

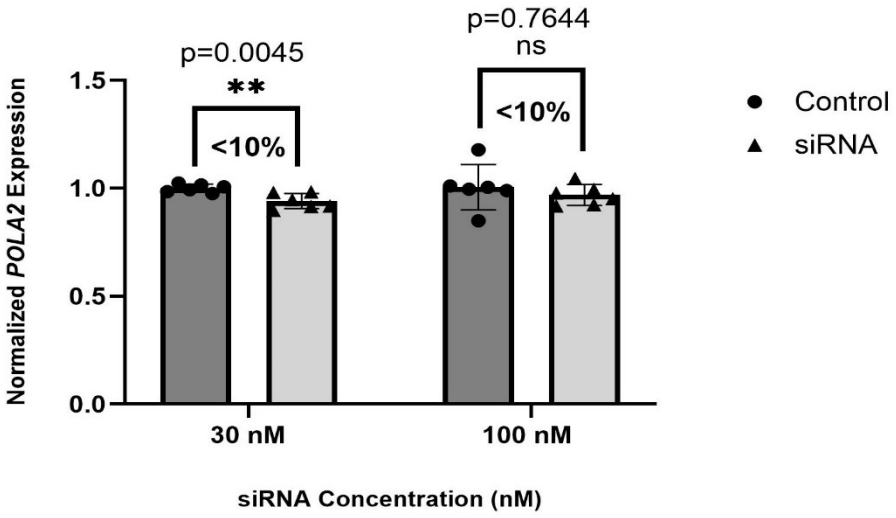

Figure 22: Average transfection efficiencies achieved with RNAiMAX reagent and 100 nM siRNA in MV4-11 cells. *POLA2* mRNA knockdown of <10% was achieved in MV4-11 cells even with increased siRNA concentration (100 nM). Following an increase in siRNA concentration, differences in mRNA expression were found to be statistically nonsignificant (unpaired t-test; p=0.7644) for *POLA2* knockdown in MV4-11. Three biological replicates were tested (n=3) for each cell line.

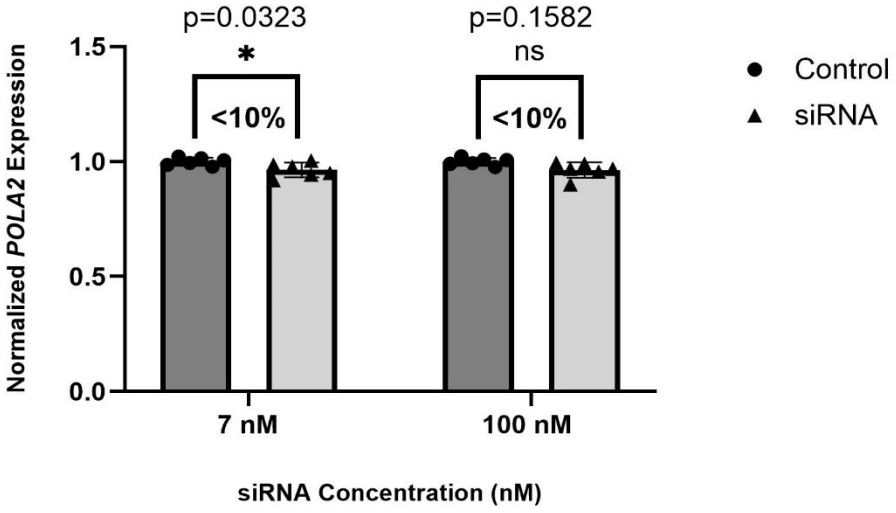

Figure 23: Average transfection efficiencies achieved with INTERFERin reagent and 100 nM siRNA in MV4-11 cells. *POLA2* mRNA knockdown of <10% was achieved in MV4-11 cells even with increased siRNA concentration (100 nM). Following an increase in siRNA concentration, differences in mRNA expression were found to be statistically nonsignificant (unpaired t-test; p=0.1582) for *POLA2* knockdown in MV4-11. Three biological replicates were tested (n=3) for each cell line.

3.2.5 *Optimization of AML cell transfection – Addition of lipopolypeptide vector:*

The next optimization strategy employed to improve INTERFERin transfection efficiency was the addition of a promising lipopolypeptide hybrid vector which utilizes a combination of a modified HIV-1 Tat peptide (mTat), jetPEI (PEI), and INTERFERin. Literature reports ≈100% siRNA knockdown of β-actin expression compared to non-treated cell with little cytotoxicity when using this mTat/PEI/INTERFERin transfection method [92]. Unfortunately, addition of mTat and PEI did not increase INTERFERin transfection efficiency in any of the cell lines tested (THP-1, MV4-11, MOLM-14 (Figure 24).

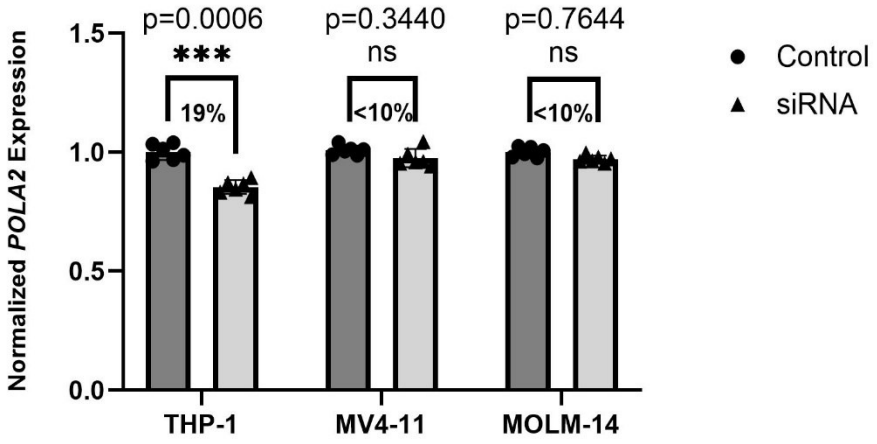

Figure 24: Average transfection efficiencies achieved with mTat/PEI/INTERFERin method in THP-1, MV4-11, and MOLM-14 cells. *POLA2* mRNA knockdown of ~19% was achieved for THP-1 cells using the mTat/PEI/INTERFERin lipopolypeptide vector. For MV4-11 and MOLM-14 cells, <10% (MV4-11 *POLA2* knockdown was achieved with the mTat/PEI/INTERFERin method. Addition of mTat/PEI resulted in differences in mRNA expression that were statistically significant (unpaired t-test) for *POLA2* knockdown in THP-1 (p=0.0006), but non-significant for MV4-11 (p=0.3440) and MOLM-14 (p=0.7644). Three biological replicates were tested (n=3) for each cell line.

3.2.6 *Optimization of AML cell transfection – serum conditions:*

As a final optimization strategy, we explored modified serum conditions. Completely eliminating or reducing serum in cell culture media used for transfection can be employed as a strategy to maximize transfection efficiency, particularly in difficult-to-transfect cell lines [93, 94].

Adopting serum-free or reduced-serum conditions during transfection 1) minimizes interference with transfection reagents as serum proteins can bind to transfection reagents, inhibiting the formation of lipid-RNA/DNA complexes and 2) reduces degradation of nucleic acids since serum contains nucleases that can degrade RNA/DNA [91, 95, 96]. Thus, we hypothesized that introducing serum-free conditions during siRNA transfection would increase transfection efficiency in AML cells. Complete, serum-containing media was added after the six-hour timepoint to improve cell viability.

Interestingly, in AML cells like THP-1 and OC-AML3, for which INTERFERin was already effective alone, an increase of 10-20% in transfection efficiency was observed (Figure 25). As a product of the serum-free conditions, INTERFERin transfection efficiency increased to ~80% in THP-1 cells ($p<0.0001$), and ~60% in OCI-AML3 cells ($p<0.0001$) (Figure 25). In contrast, MV4-11 cells, which were not susceptible to INTERFERin transfection in serum conditions, did not exhibit an increased transfection efficiency from <10% ($p=0.1206$), with a serum-free approach (Figure 25). Unexpectedly, Lipofectamine transfection combined with serum-free conditions resulted in an 17-19% increase in transfection efficiency in MV4-11 and MOLM-14 cells (Figure 26). Although this significant ~20% *POLA2* knockdown achieved in MV4-11 and MOLM-14 cells is promising, it may not elicit the full *in vitro* effect of the target on the endpoints of interest. Similarly, these methods would not be suitable for an RNA drug screen where we may be testing sequences with lower gene-modulating activity. Essentially, these results combined with those concerning INTERFERin transfection, suggest that minimizing serum in transfection conditions can serve as a viable strategy for optimizing chemical transfection efficiency in AML cell lines.

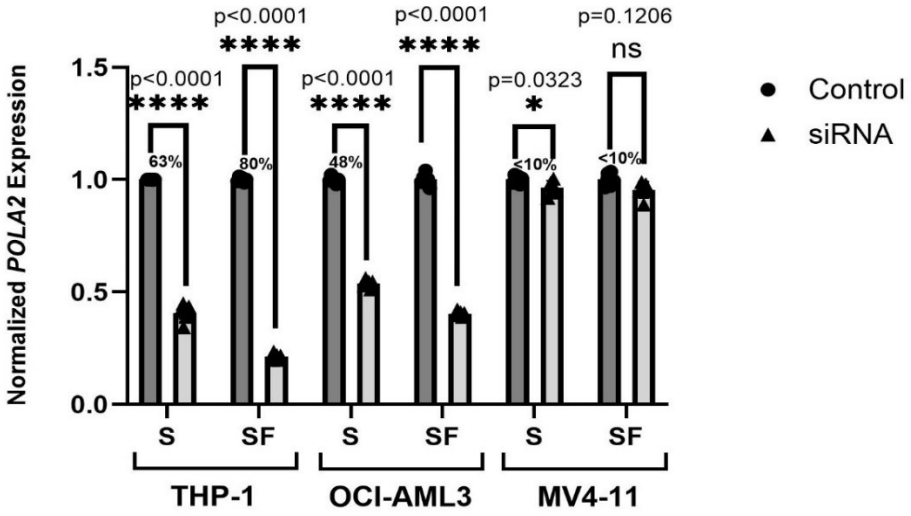

Figure 25: Average transfection efficiencies achieved with INTERFERin method and serum-free conditions in THP-1, OCI-AML3, and MV4-11 cells. Serum-free (SF) conditions resulted in ~10-17% increase in transfection efficiency in THP-1 and OCI-AML3 cell lines that were susceptible to INTERFERin alone. Serum-free/INTERFERin transfected THP-1 cells yielded ~80% *POLA2* mRNA knockdown while SF/INTERFERin transfected OCI-AML3 cells yielded ~60% *POLA2* mRNA knockdown. No significant (<10%) *POLA2* knockdown was achieved in MV4-11 INTERFERin transfected cells even with serum-free conditions. Differences in *POLA2* mRNA expression were highly statistically significant (unpaired t-test) for *POLA2* knockdown in THP-1 ($p<0.0001$) and OCI-AML3 ($p<0.0001$), but non-significant for MV4-11 ($p=0.1206$). Three biological replicates were tested (n=3) for each cell line.

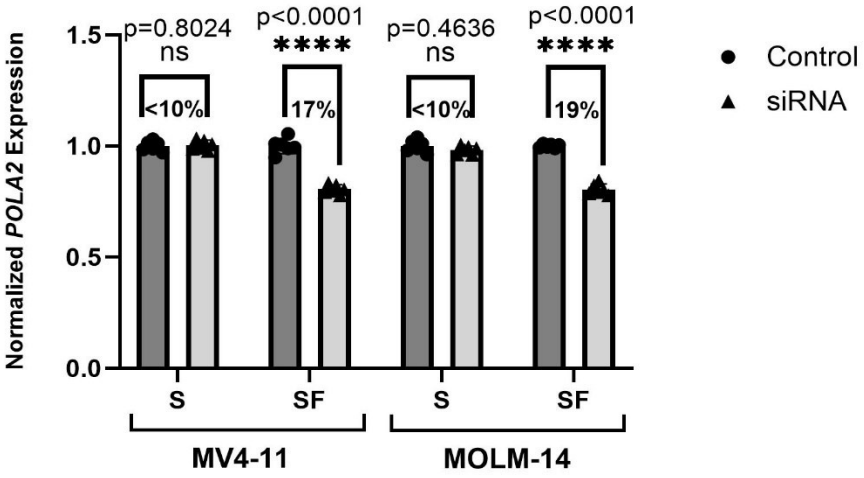

Figure 26: Average transfection efficiencies achieved with Lipofectamine method and serum-free conditions in MV4-11, and MOLM-14 cells. Serum-free (SF) conditions resulted in ~17-19% increase in transfection efficiency in MV4-11 and MOLM-14 cell lines that were not susceptible to Lipofectamine in serum conditions. Serum-free/Lipofectamine transfected MV4-11 cells yielded ~17% *POLA2* mRNA knockdown while SF/Lipofectamine transfected MOLM-14 cells yielded ~19% *POLA2* mRNA knockdown. Differences in *POLA2* mRNA expression were highly statistically significant (unpaired t-test) for *POLA2* knockdown in both MV4-11 ($p<0.0001$) and MOLM-14 ($p<0.0001$). Three biological replicates were tested (n=3) for each cell line.

Ultimately, the extensive *in vitro* AML transfection method qPCR screening performed was successful in developing two novel protocols for siRNA knockdown in THP-1 and OCI-AML3 cells. Optimization experiments also revealed minimal serum conditions to be effective in improving transfection efficiency in some AML cell lines. Since many transfection methods reaction conditions and cell lines were tested, the results of all *in vitro* AML transfection method screening are summarized in Table 2.

Table 4: Summary of *in vitro* AML Transfection Method qPCR Screening Results

Cell line	**Lipofectamine 3000 (100 nM)**		**ViaFect (100 nM)**	**FuGENE HD (100 nM)**	**INTERFERin (7 nM)**			**mTat/PEI with INTERFERin (30 nM)**	**RNAiMAX (30 nM)**			**Nucleofection**
Serum Conditions	Serum	Serum-free	Serum	Serum	Serum	Serum-free	100 nM siRNA	Serum-free	Serum	Serum-free	100 nM siRNA	Serum
OCI-AML3	N/A	N/A	N/A	N/A	~48%	~60%	N/A	N/A	N/A	N/A	N/A	~32%
OCI-AML2	N/A	N/A	N/A	N/A	~12%	~14%	<10%	N/A	N/A	N/A	N/A	N/A
THP-1	N/A	N/A	N/A	N/A	~63%	~80%	N/A	~19%	N/A	N/A	N/A	~20%
MOLM-14	<10%	~19%	N/A	N/A	~20%	N/A	N/A	<10%	~10%	~19%	N/A	N/A
MV4-11	<10%	~17%	N/A	N/A	<10%	<10%	<10%	<10%	<10%	~20%	<10%	N/A
U-937	N/A	N/A	<10%	<10%	N/A	N/A	N/A	N/A	N/A	N/A	N/A	~55%

Note: Percentages refer to transfection efficiencies measured in terms of *POLA2* mRNA knockdown.

3.2.7 *Protein validation of in vitro AML transfection methods:*

Having established chemical transfection methods that enable sufficient *POLA2* knockdown at the mRNA level, we validated these methods at the protein level via western blotting. Western blot gel images obtained demonstrate clear knockdown of *POLA2* protein in both transfected THP-1 and OCI-AML3 cells (Figure 27). However, to analyze these protein expression results more quantitatively, the relative integrated density values of the protein bands were quantified using Fiji ImageJ software (version 1.54b, National Institutes of Health), and statistical

analysis was performed using GraphPad Prism (version 9.5.0). Quantified protein expression results indicated that *POLA2* siRNA transfection using INTERFERin resulted in ~53% ($p<0.0001$) and ~42% ($p<0.0001$) reduction in *POLA2* protein production in THP-1 and OCI-AML3 cells respectively (Figure 28). These reductions in *POLA2* protein reflect the level of *POLA2* mRNA knockdown achieved with INTERFERin in these two cell lines, further corroborating our earlier mRNA results. Thus, our results at the protein level confirm that THP-1 and OCI-AML3 cell transfection with *POLA2* siRNA and INTERFERin yields functional knockdown of the target gene and is this suitable for use in downstream assays.

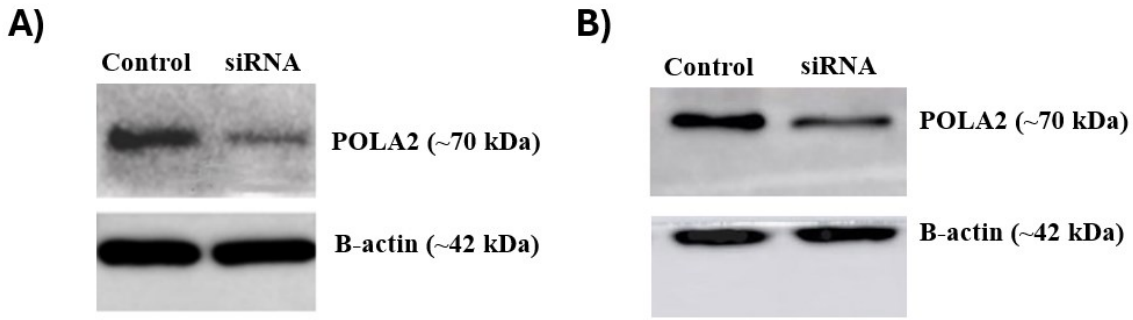

Figure 27: Western blot images depicting changes in *POLA2* protein expression following INTERFERin transfection of *POLA2* siRNA in A) THP-1 cells and B) OCI-AML3 cells.

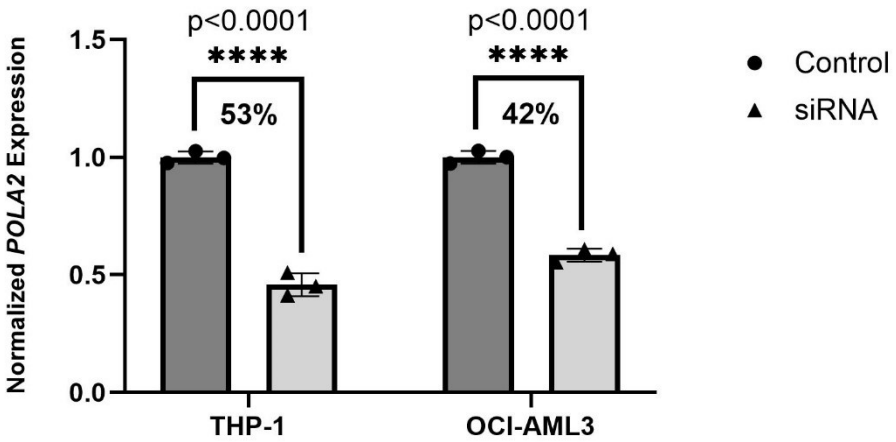

Figure 28: *POLA2* protein knockdown achieved with INTERFERin transfection in THP-1 and OCI-AML3 cells. *POLA2* protein knockdown of ~53% was achieved for INTERFERin-transfected THP-1 cells. For OCI-AML3 cells, ~42% *POLA2* protein knockdown was achieved via INTERFERin transfection. Differences in protein expression were highly statistically significant (unpaired t-test) for both THP-1 ($p<0.0001$) and OCI-AML3 ($p<0.0001$). Three biological replicates were tested ($n=3$) for each cell line.

3.2.8 *Impact of transfection method on AML cell viability:*

Lastly, preserving cell viability is an essential goal during transfection, not only to ensure good transfection efficiency but also to ensure that transfected cells or extracted cellular components are of good quality for downstream assays. Hence, we aimed to test the effects of some of the transfection formulations or devices investigated on the viabilities of diverse AML cell lines. Most of the lipid-based chemical reagents assessed did not display a harsh impact on AML cell viabilities, with the viabilities of the transfected AML cells ranging from 84 - 96% (Table 3). On the other hand, the physical nucleofection method tested demonstrated a significant decrease in AML cell viabilities as compared to the chemical reagents (Table 3). Cell viabilities reported 24 hours post-nucleofection were 64%, 52%, and 35% for OCI-AML3, THP-1, and U-937 cells, respectively (Table 3). These results further corroborate the literature showing elevated rates of cell death following physical transfection approaches such as nucleofection. Moreover, these differences in cell viabilities post-transfection further reinforce the importance of developing novel *in vitro* methods that allow for efficient siRNA uptake while also maintaining healthy cell viabilities.

Table 5: Impact of Chemical Transfection Reagents on AML Cell Viability

Cell line	Lipofectamine 3000	ViaFect	FuGENE HD	INTERFERin	RNAiMAX	Nucleofection
OCI-AML3	N/A	92%	N/A	96%	N/A	64%
OCI-AML2	N/A	88%	N/A	92%	N/A	N/A
THP-1	N/A	86%	N/A	89%	N/A	52%
MOLM-14	94%	N/A	N/A	95%	90%	N/A
MV4-11	90%	N/A	N/A	92%	84%	N/A
U-937	N/A	91%	85%	N/A	N/A	35%

Note: Percentages refer to cell viabilities post-transfection and subsequent 24-hour incubation.

Overall, we succeeded in completing our second aim by developing two robust chemical transfection protocols that will allow for siRNA knockdown in THP-1 and OCI-AML3. Our protocols for siRNA INTERFERin transfection facilitate the specific modulation of *POLA2*, demonstrated both at the mRNA and protein level. Although thorough optimization revealed increased transfection efficiency in serum-free conditions, INTERFERin transfection conducted in serum-containing conditions would be favourable for downstream in vitro assays for which cell viability must be preserved. To conclude, these methods will enable us to interrogate the impact of *POLA2* expression on several AML endpoints including cytarabine sensitivity, cell death mechanism, and cytarabine incorporation.

3.3 – Investigating the impact of *POLA2* expression on cytarabine sensitivity, incorporation and leukemic cell death

3.3.1 *Impact of POLA2 on cytarabine sensitivity:*

With *in vitro* protocols that allow for sufficient siRNA knockdown of *POLA2*, we could investigate the impact of altering *POLA2* expression on cytarabine-induced cell death, drug sensitivity and drug incorporation. We hypothesized that *POLA2* knockdown could sensitize AML cells to the DNA damaging drug – cytarabine [73]. Thus, we evaluated AML cell sensitivity to ara-C (cytarabine and idarubicin in a 17:1 ratio) following knockdown of *POLA2* by siRNA. The resultant viability assay (using resazurin) showed an IC_{50} of 1.4×10^{-6} M in the control cells vs 9.0×10^{-7} M in *POLA2* siRNA-treated THP-1 cells. This ~1.6-fold decrease in ara-C/ida IC_{50} following *POLA2* knockdown (Figure 29) support our hypothesis that reducing *POLA2* expression increases THP-1 cell sensitivity to ara-C/ida frontline treatment, rendering this frontline regimen more potent in these AML cells.

Although the resazurin cell viability offers a time and resource-effective approach, one key limitation of this assay in evaluating cytarabine sensitivity stems from its use of metabolic activity as an indirect measure of cell viability. Cytarabine exerts its cytotoxic effects primarily by inhibiting DNA synthesis during the S-phase of the cell cycle, which directly impairs proliferation rather than immediately disrupting cellular metabolism. Consequently, cells may remain metabolically active even after cytarabine has halted their division or induced DNA damage, leading to underreported cytotoxic effects. Moreover, the resazurin assay does not differentiate between cells that are merely non-proliferating and those undergoing apoptosis.

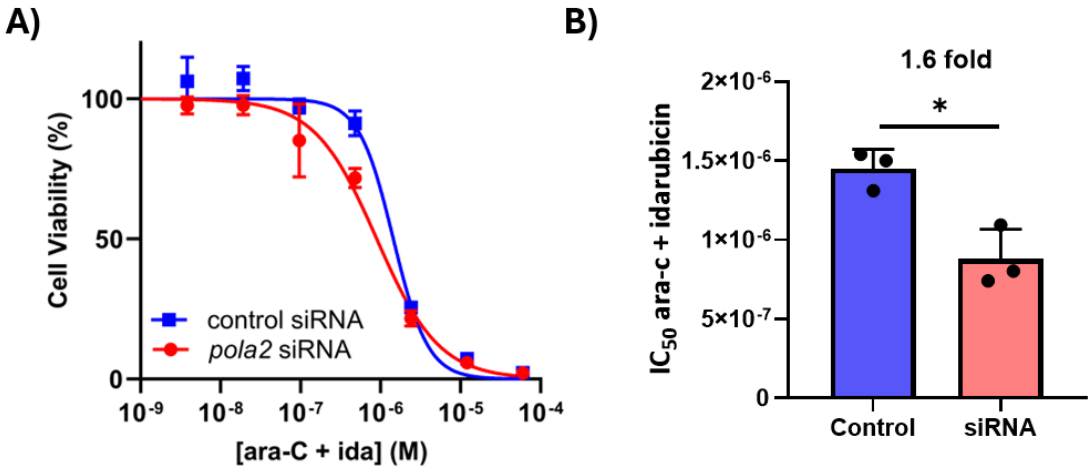

Figure 29: Ara-C/Ida dose-response curves for *POLA2* knockdown and control THP-1 cells. A) 72-hour *POLA2* siRNA transfection followed by 24-hour ara-C/ida drug treatment and resazurin cell viability assay revealed a ~1.6-fold decrease in IC50 values. Nonlinear regression analysis was used to fit dose-response curves and data points were averaged from technical triplicates. **B)** The average of three experimental replicates resulted in a statistically significant (unpaired t-test) ~1.6-fold decrease in ara-C/ida IC50, indicating an increase in THP-1 cell ara-C/ida sensitivity.

To circumvent the limitations of the resazurin assay, we further investigated the effect of decreasing *POLA2* expression on ara-C-induced leukemic cell death by trypan blue exclusion assay. Following *POLA2* siRNA transfection and subsequent ara-C treatment, THP-1 cells were counted over multiple days. Here, idarubicin was excluded from the drug treatment as it is still

unclear whether its high cytotoxicity may partially mask the effect of cytarabine alone on leukemic cell death.

One to five days after ara-C treatment, trypan blue THP-1 cell counts revealed a consistent trend in decreased ara-C IC50 values for *POLA2* siRNA-treated cells compared to control cells (Figure 23). The large error bars, representing standard deviation, reflect inherent variability in manual cell counting methods (Figure 30). While statistical analysis was not performed for these experiments, the observed trend in the data suggest an increase in ara-C sensitivity in siRNA-treated cells. Further experiments could be pursued to confirm these findings and to quantify any significant effect.

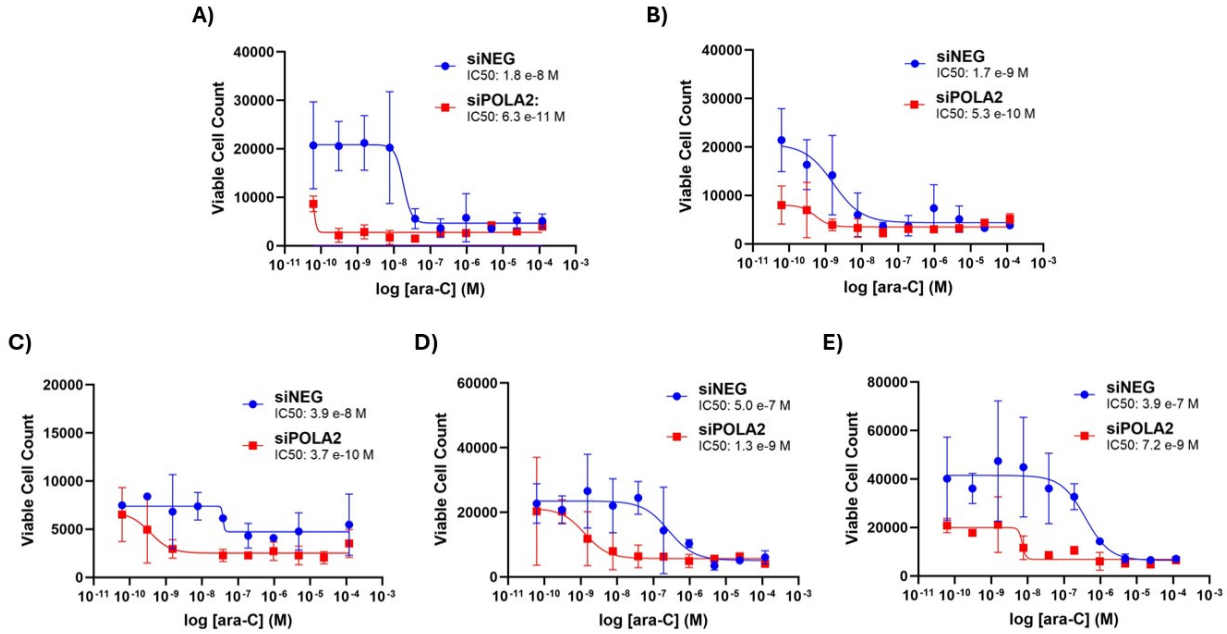

Figure 30: Ara-C dose-response curves for *POLA2* knockdown and control THP-1 cells after 1-5 days of drug treatment. Trypan blue exclusion cell counting reveals consistently lowered ara-C IC50 values for *POLA2* knockdown THP-1 cells. **A)** One day of ara-C drug treatment revealed ara-C IC50 values of 1.8 x 10^{-8} M (control) and 6.3 x 10^{-11} M (*POLA2* siRNA). **B)** Two days of ara-C drug treatment revealed ara-C IC50 values of 1.7 x 10^{-9} M (control) and 5.3 x 10^{-10} M (*POLA2* siRNA). **C)** Three days of ara-C drug treatment revealed ara-C IC50 values of 3.9 x 10^{-8} M (control) and 3.7 x 10^{-10} M (*POLA2* siRNA). **D)** Four days of ara-C drug treatment revealed ara-C IC50 values of 5.0 x 10^{-7} M (control) and 1.3 x 10^{-9} M (*POLA2* siRNA). **E)** Five days of ara-C drug treatment revealed ara-C IC50 values of 3.9 x 10^{-7} M (control) and 7.2 x 10^{-9} M (*POLA2* siRNA). Nonlinear regression analysis was used to fit dose-response curves and data points were averaged from technical duplicates.

3.3.2 *Impact of POLA2 on ara-C-induced cell death mechanism:*

Having confirmed that altered *POLA2* expression render THP-1 cells more susceptible to ara-C-induced cell death, we next sought to examine whether decreased expression of *POLA2* impact the mechanism of cell death. Previous published studies from our lab identified a cell death mechanism called Parthanatos as a clinically favourable mechanism of cell death [53]. It was found that while the ara-C/ida regimen can induce either apoptosis or parthanatos in AML cells, a 3-fold improvement in survival rates was correlated with parthanatos-positive versus -negative patient groups [53]. Thus, we were interested to discover whether the increase in ara-C sensitivity is accompanied by an increase in favourable parthanatos cell death.

The presence of parthanatos cell death can be identified by a few distinct features namely, PARP-dependent changes in drug sensitivity and characteristic nuclear ‘‘ring’’ cell morphologies [53]. We chose to evaluate the presence/absence of parthanatos cell death by visualizing nuclear fragmentation patterns using DAPI nuclei staining combined with confocal microscopy. On the other hand, apoptotic bodies could be identified by a characteristic globular nuclear fragmentation pattern. Our confocal microscopy images demonstrate the clear presence of parthanatos “ring”-like nuclear fragmentation patterns in THP-1 cells (Figure 31). This reinforces the results of our lab’s previous work where THP-1 was identified as a Parthanatos-positive cell line. Interestingly, the presence of parthanatos rings was detected in all ara-C/ida-treated cell samples independent of changes in *POLA2* expression (Figure 31). Thus, these results suggest that *POLA2* knockdown does not impact the type of cell death mechanism induced by ara-C/ida treatment in THP-1 cells.

To gain insight into the quantity of cell death incurred in cells with reduced *POLA2* versus control cells, we analyzed our microscopy data in a semi-quantitative manner. This was done by

counting the number of dead and live cells, indicated by parthanatos rings and healthy cell morphology, respectively. A slight increase of ~4–10% in the number of parthanatos rings was observed in the *POLA2* siRNA-treated THP-1 cells as compared to the control cells (Figure 31). To illustrate, ~54% of cells observed in the control 0.5 μM ara-C-treated group exhibited parthanatos cell death whereas ~64% of the *POLA2* knockdown subjected to the same ara-C treatment showed parthanatos morphology (Figure 31). Similarly, in samples treated with a higher concentration of ara-C (1 μM), this trend remained consistent with *POLA2* knockdown cells exhibiting a higher percentage of parthanatos rings (~68%) compared to the control siRNA-treated cells (~64%) (Figure 31). However, it must be noted that a possible limitation in the collection of this data was the number of cells that were counted per sample (n=150). It is possible that this cell population size may not have been sufficient to capture the effect of altered *POLA2* expression on quantity of leukemic cell death. Nonetheless, these microscopy results corroborate previous studies identifying THP-1 cells as a parthanatos-positive cell line and support our earlier dose-response findings in correlating reduced *POLA2* expression with increase cell sensitivity to ara-C.

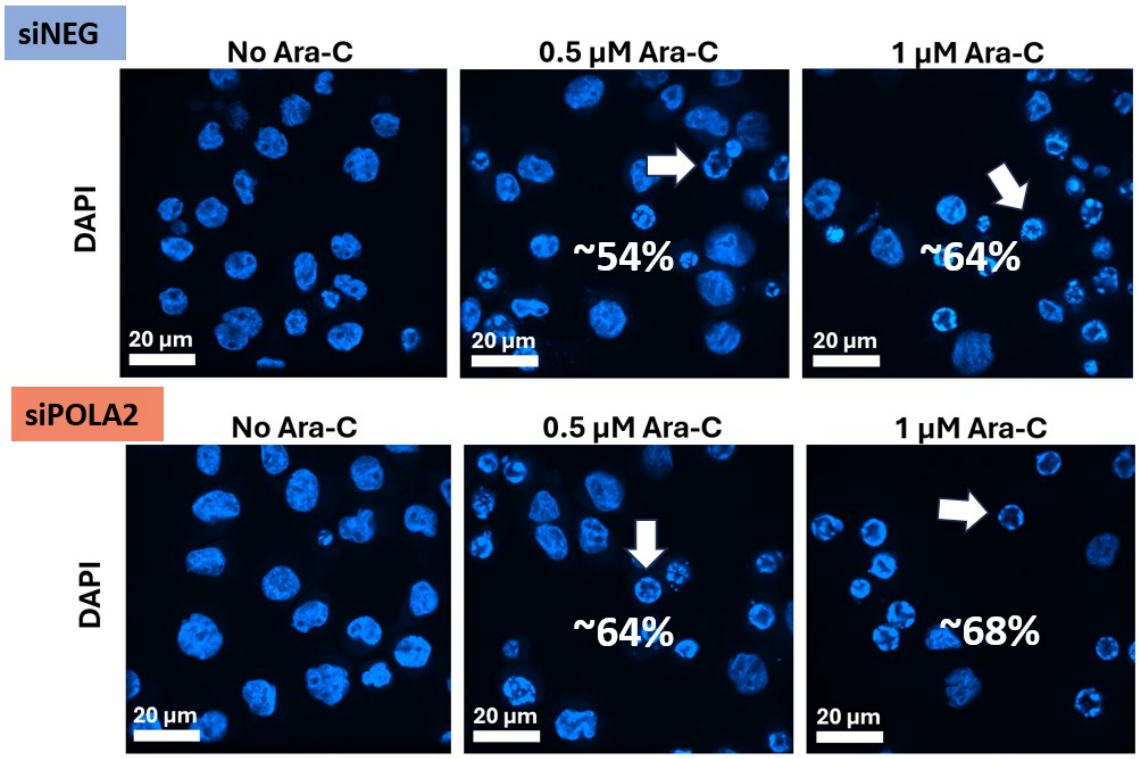

Figure 31: Confocal microscopy images depicting ara-C/ida-induced parthanatos rings in *POLA2* knockdown and control THP-1 cells. DAPI nuclei staining and microscopy revealed parthanatos ring-like nuclear fragmentation patterns in all ara-C/ida-treated samples regardless of changes in *POLA2* expression. The *POLA2* siRNA-treated cells (bottom) showed slightly increased numbers of dead parthanatos cells (0.5 µM ara-C: ~64%; 1 µM ara-C: ~68%) as compared to the negative control siRNA-treated cells (top) (0.5 µM ara-C: ~54%; 1 µM ara-C: ~64%). Parthanatos/live cell counts were performed on groups of 150 THP-1 cells/sample (n=150).

3.3.3 *Impact of POLA2 on ara-C incorporation:*

Given the compelling studies that recently suggested an important role for the POL-PRIM complex, specifically the polymerase domain, in variable ara-C incorporation, we aimed to explore the role of *POLA2*, specifically, in the variable incorporation of ara-C into DNA versus RNA [18]. To this end, we adopted one of the experimental strategies outlined in this study – Cu(I)-Catalyzed Azide−Alkyne Cycloaddition (CuAAC) staining. Briefly, THP-1 cell cultures were incubated with ara-C analog, AzC, then they were washed, fixed, and some were treated with either DNase I or RNase H prior to CuAAC "click" staining. To visualize DNA/RNA incorporation of AzC in the

cells, the chemical reaction between the azide-containing AzC drug and a fluorescent alkyne-derivatized silicon rhodamine dye was exploited. THP-1 cells were either transfected with *POLA2* or control siRNA for 72 hours prior to AzC treatment, enzyme digest, DAPI staining, CuAAC staining and confocal microscopy analysis. Surprisingly, no visible difference in green fluorescence representing AzC incorporation was observed between *POLA2* knockdown and control cells treated with AzC drug (Figure 32, and 33). The samples exposed to enzyme digest corroborate the findings reported in literature in that only RNase H was able to reduce AzC staining to background levels (Figure 32, and 33). This corroborates the evidence in literature that AzC is incorporated into the RNA of RNA/DNA hybrid duplexes. Together, these results suggest that while knockdown of *POLA2* appears to increase cell sensitivity to ara-C, it does not exert this effect by altering the cellular incorporation of the drug. Based on these findings as well as our previous dose-response data, it is more likely that *POLA2* impacts ara-C efficacy in AML cells by influencing DNA damage-related pathways downstream of drug incorporation. It is possible that once ara-C is incorporated into RNA, then knockdown of *POLA2* potentiates the cell death response, especially given its reported role in double strand break (DSB) repair [73].

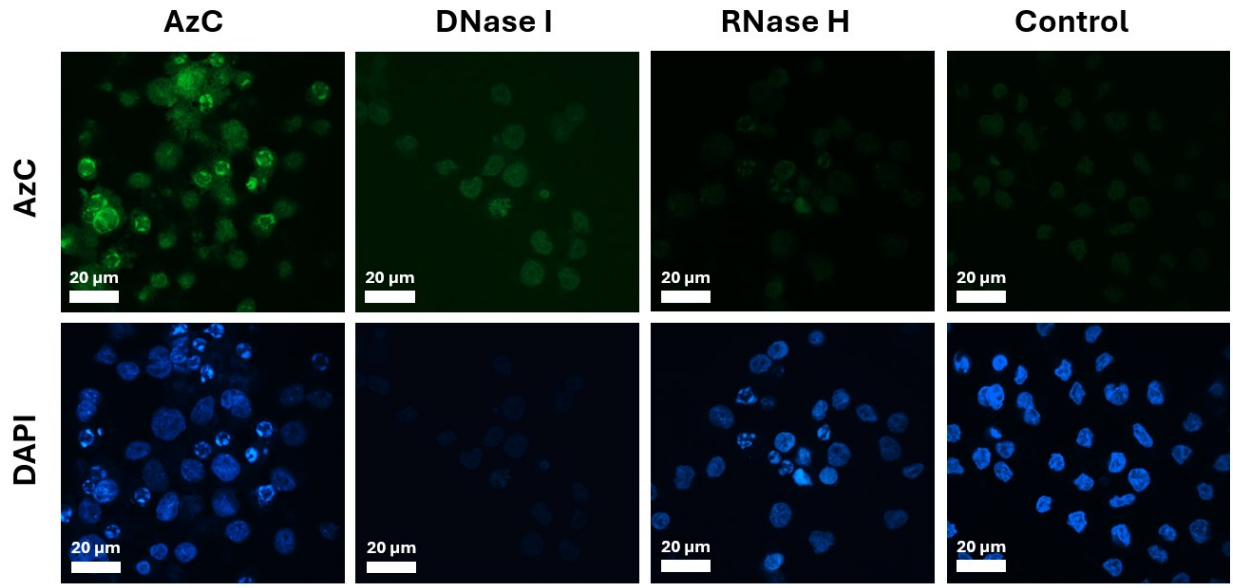

Figure 32: CuAAC click staining microscopy images revealing fluorescent AzC incorporation in *POLA2* knockdown THP-1 cells. Cells were incubated with 15 µM of AzC for 8–10 h, washed, fixed, treated with 1 mg/mL DNase, or 250 units/ml RNase H, and subsequently stained with an alkyne-derivatized silicon rhodamine dye by CuAAC, and DAPI prior to confocal microscopic analyses.

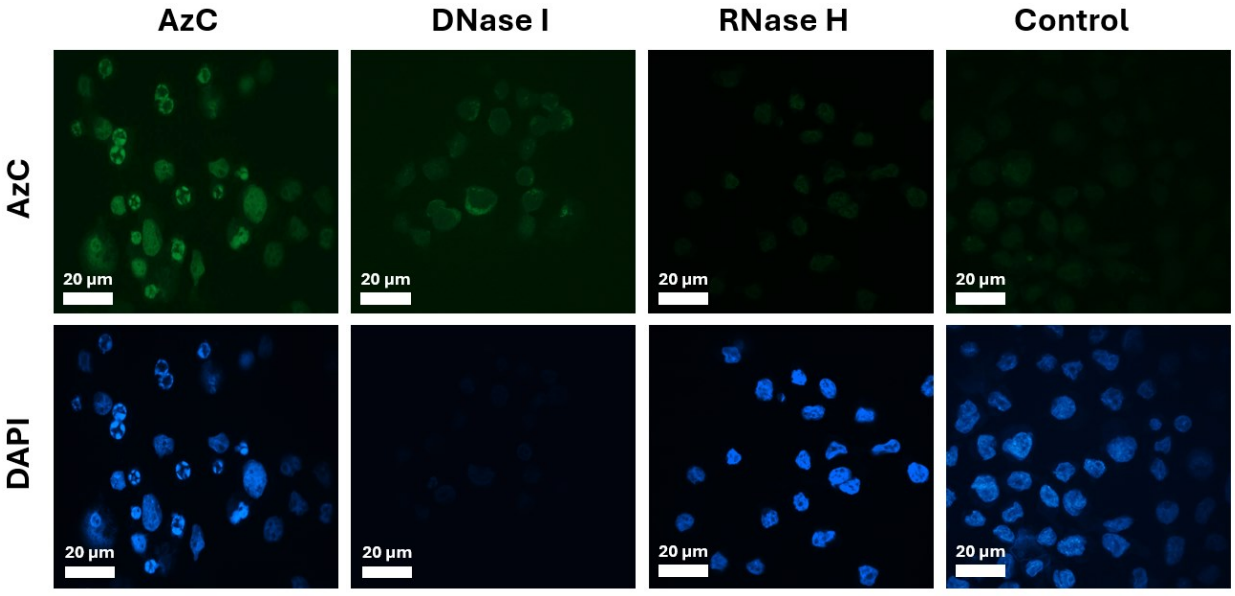

Figure 33: CuAAC click staining microscopy images revealing fluorescent AzC incorporation in control THP-1 cells. Cells were incubated with 15 µM of AzC for 8–10 h, washed, fixed, treated with 1 mg/mL DNase, or 250 units/ml RNase H, and subsequently stained with an alkyne-derivatized silicon rhodamine dye by CuAAC, and DAPI prior to confocal microscopic analyses.

In conclusion we found that siRNA knockdown of *POLA2* increased ara-C sensitivity in THP-1 cells but did not impact the parthanatos cell death mechanism triggered and did not influence variable drug incorporation. For these reasons, we hypothesize that role of *POLA2* in affecting cytarabine's killing of leukemic cells concerns downstream DNA damage-related mechanisms that occur after ara-C incorporation into RNA or DNA. One important limitation in these studies is that only one AML cell line was tested. The use of THP-1 cells was critical in these experiments because earlier work in aim 2 revealed that the most effective siRNA knockdown of *POLA2* could be achieved this cell line. Thus, this cell line model was chosen to maximize the downregulation of *POLA2* expression in AML cells, bolstering our capacity to detect the effect of altered *POLA2* expression on our chosen in vitro endpoints. Another important experimental limitation for the studies in aim 3, was the level of *POLA2* knockdown that was achievable via previously identified transfection methods. While the degree of *POLA2* knockdown achieved via INTERFERin transfection should be sufficient for inducing biological changes, it may not be enough to capture the maximal effect of altered *POLA2* on the various endpoints studied.

3.4 – Experimental Limitations & Confounding Factors:

i) Variability in AML Datasets:

For the bioinformatic analyses performed in aim 1, AML patient data was obtained from TCGA and HOVON trials datasets. However, it must be noted that these datasets are subject to variability in sample collection, handling, and processing methods. Moreover, confounding factors, such as differences in patient demographics, treatment regimens, and comorbidities, may have influenced the observed survival trends.

ii) Limitations of Cell Line Models:

While the THP-1 cell line was chosen for the drug incorporation and dose-response studies conducted in aim 3 due to their higher transfection efficiency, these cells do not reflect the heterogeneity of primary AML samples. The genetic and epigenetic profiles of these cells may act as confounding factors and limit the generalizability of results to the broader AML patient population. Thus, the results presented here do not necessarily reflect AML patient outcomes and their clinical relevance is limited. The use of primary AML cells or patient-derived xenografts in future studies would help overcome this limitation.

iii) Statistical Analysis:

Some assays, including the trypan blue exclusion assay lacked statistical significance due to limited resources or assays with highly variable outputs. This limits the strength and interpretation of conclusions. To extract more robust conclusions, statistical tests could be incorporated in future experiments.

iv) Variability between AzC and Ara-C:

Although AzC was reported to have a very similar biological profile as ara-C, exhibiting similar potencies, some slight differences between the two compounds may introduce confounding factors into the CuAAC click experiment. For example, potential differences in the AzC analog's intracellular metabolism compared to Ara-C, may have an influence on the differences in AzC incorporation observed.

v) Qualitative Analysis of Cell Death:

Confocal microscopy was employed to identify apoptotic and parthanatos features in treated cells; however, these observations were largely qualitative. Variability in the interpretation

of nuclear morphologies and reliance on subjective assessments may serve as a limitation in these cell death experiments.

vi) Impact of Drug Treatment:

For some dose-response and mechanistic cell death experiments, a clinically relevant (17:1) combination of cytarabine-to-idarubicin was used, while in other studies, idarubicin was excluded from specific assays to isolate the effects of cytarabine. In studies using combined ara-C/ida treatment, idarubicin's inherent cytotoxicity may confound the assessment of *POLA2*'s effect on cytarabine endpoints. Meanwhile, the exclusion of idarubicin may overlook potential interactions between the drugs that could reveal a more clinically-relevant impact on cell sensitivity and the mechanisms of cell death.

Chapter 4 - Conclusions and Future Objectives:

To improve the efficacy of the frontline cytarabine treatment in AML patients, the mechanism of this drug as well as genetic factors influencing its potency, incorporation and induction of leukemic cell death needs to be better understood. The goal of this thesis was to interrogate the role of the POL-alpha-PRIM complex in AML by examining the relationship between one of its critical subunits, *POLA2*, and AML cytarabine incorporation and sensitivity. First, expressional data of each subunit of the DNA polymerase alpha primase complex was compared for trends in AML patient survival. Secondly, a comprehensive screening of chemical transfection methods for siRNA delivery in difficult-to-transfect AML cells was performed to enable siRNA probing of *POLA2*. Finally, utilizing the methods developed in aim 2, the impact of altered *POLA2* expression on AML cell death and cytarabine incorporation into RNA vs DNA was investigated.

Towards my first aim, an extensive bioinformatic analysis of POL-PRIM subunit expression using TCGA RNA-seq data and HOVON clinical trials data revealed the impact of the *POLA2* gene on AML patient survival to be the most significant. These results established the *POLA2* subunit as a potential therapeutic target and biomarker for predicting patient survival in response to ara-C/anthracycline treatment. To address my second objective, siRNA transection methods with up to ~63% transfection efficiency in THP-1 and OCI-AML3 cell lines were established and functionally validated. Future studies will directly utilize these methods for the screening of RNA drug candidates in AML cell lines. Harnessing the methods established in aim 2, the impact of *POLA2* expression on cytarabine-induced AML cell death and ara-C incorporation was interrogated. Changes in quantity but not mechanism of ara-C-induced AML cell death, in

addition to lack of alteration of ara-C incorporation, demonstrated that while lower *POLA2* levels were associated with higher ara-C sensitivity, this effect was not due to any changes in drug incorporation or in the type of cell death triggered.

This thesis study exposed key insights into role of *POLA2* in AML treatment and will aid in furthering our knowledge of cytarabine's therapeutic mechanism of action following variable RNA/DNA incorporation. Given the unveiled impact of *POLA2* knockdown on AML cell sensitivity to cytarabine, this protein may be further investigated as a potential therapeutic target. Future studies may also investigate the relationship between each POL-PRIM subunit and ara-C efficacy as well as incorporation in a larger panel of diverse AML cell types representing different levels of subunit expression. For more clinically relevant insights, the effects of the POL-PRIM subunits on cytarabine activity could be evaluated in peripheral blood monocytes (PBMCs) collected from AML patients. The transfection work completed in aim 2 has established working protocols for the transfection of RNA in AML cells. This opens the door for the screening and development of novel therapeutic RNAs for known AML targets. Ultimately, we hope that characterizing the unexplored mechanisms of cytarabine-induced leukemic cell death using therapeutic RNA will also facilitate the development of new co-treatment strategies to ameliorate long-term AML outcomes.

Appendix:

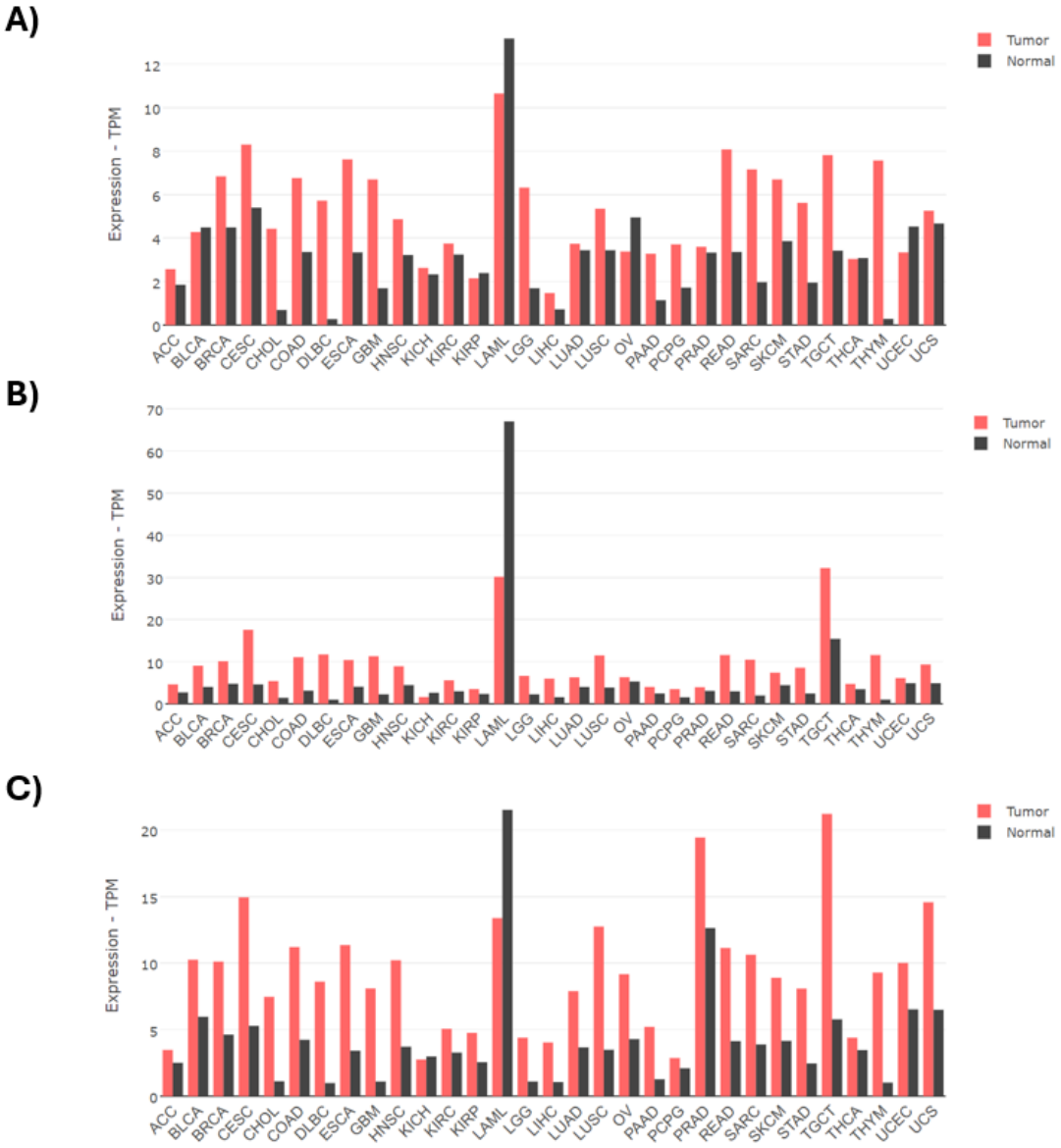

Supplementary Figure S1: *POLA1/PRIM1/PRIM2* gene expression profile produced using TCGA AML dataset using GEPIA2. The height of each bar represents the median gene expression of a certain tumour type or normal tissue. The AML dataset represents 173 AML tumour samples and paired normal tissues samples. **A)** AML tumour samples reveal a lower median *POLA1* expression (10.65 TPM) compared to matched normal tissue (13.18 TPM). **B)** AML tumour samples reveal a lower median *PRIM1* expression (30.16 TPM) compared to matched normal tissue (67.03 TPM). **C)** AML tumour samples reveal a lower median *PRIM2* expression (13.39 TPM) compared to matched normal tissue (21.52 TPM).

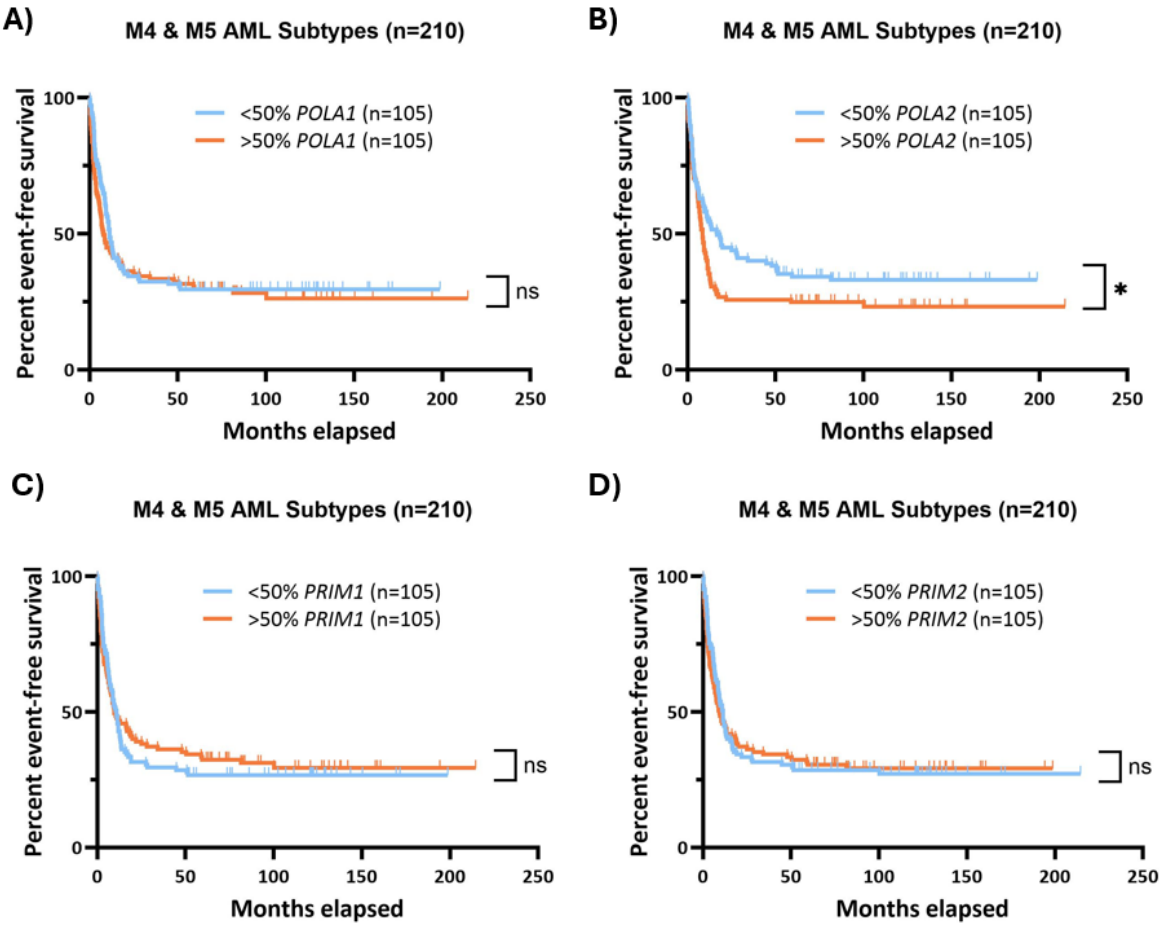

Supplementary Figure S2: Kaplan Meier event-free survival curves for M4/M5 HOVON trials patient groups with high/low POL-PRIM subunit expression. Significant difference in event-free survival between the lower-expressing POL-PRIM subunit patient population (n=210; blue) and the higher-expressing group (n=210; red) were identified only for *POLA2*. **A)** Log-rank and Gehan-Breslow-Wilcoxon tests revealed no correlation between *POLA1* levels and EFS (Gehan-Breslow-Wilcoxon, p=0.1355; log-rank, p=0.3733; HR (high) (Mantel-Haenszel) = 1.157). **B)** Statistically significant correlation was found between low *POLA2* levels and higher EFS (Gehan-Breslow-Wilcoxon, p=0.0505; log-rank, p=0.0462; HR (high) (Mantel-Haenszel) =1.39). **C)** No significant correlation was identified between *PRIM1* expression and EFS (Gehan-Breslow-Wilcoxon, p=0.9185; log-rank, p=0.7254; HR (high) (Mantel-Haenszel) =0.9441). **D)** EFS analysis in the context of *PRIM2* levels also failed to produce a significant correlation (Gehan-Breslow-Wilcoxon, p=0.5195; log-rank, p=0.8875; HR (high) (Mantel-Haenszel) = 1.023).

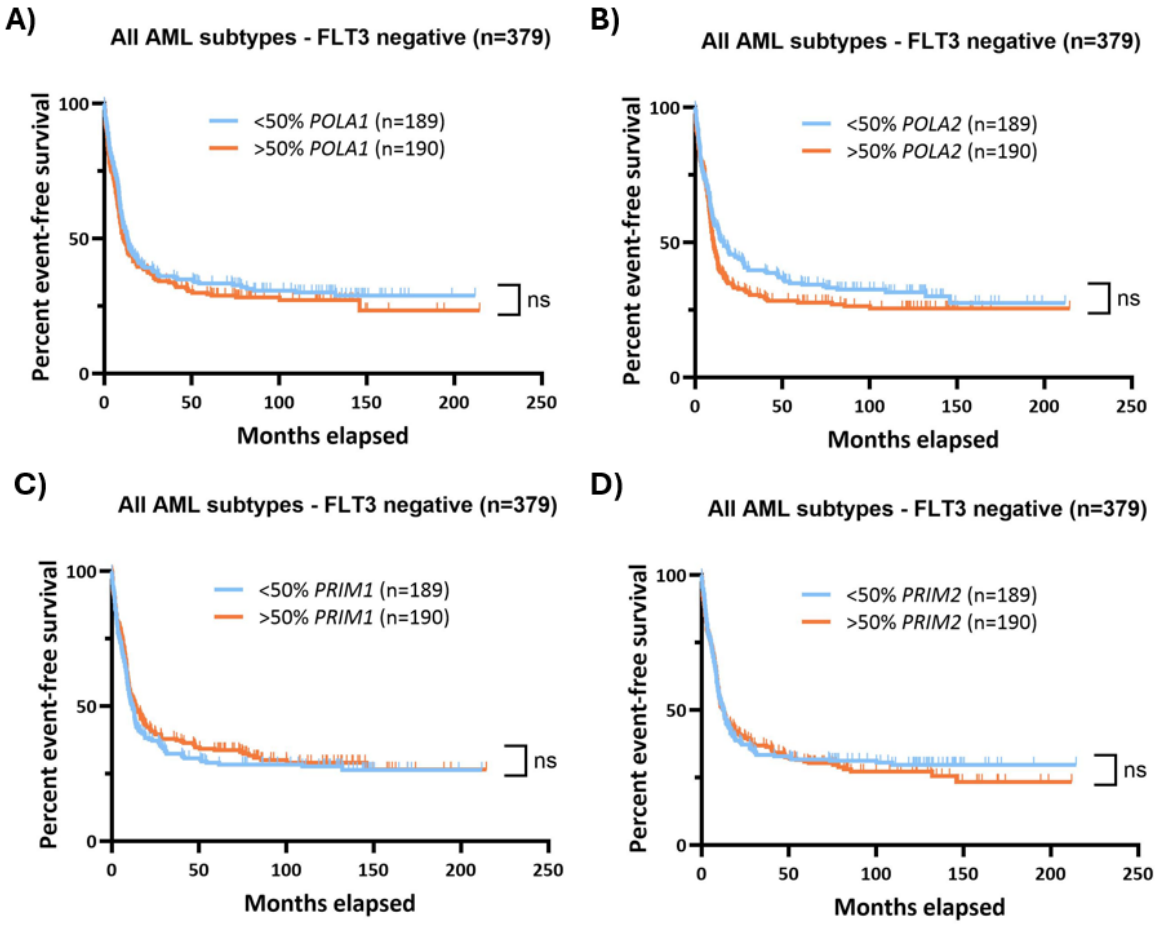

Supplementary Figure S3: Kaplan Meier event-free survival curves for FLT3/ITD-negative HOVON trials patient groups with high/low POL-PRIM subunit expression. Significant difference in event-free survival between the lower-expressing POL-PRIM subunit patient population (n=189; blue) and the higher-expressing group (n=190; red) was not identified for any of the POL-PRIM subunits. **A)** Log-rank and Gehan-Breslow-Wilcoxon tests revealed no correlation between *POLA1* levels and EFS (Gehan-Breslow-Wilcoxon, p=0.2586; log-rank, p=3354; HR (high) (Mantel-Haenszel) = 1.125). **B)** Similarly, the correlation between low *POLA2* levels and higher EFS was not significant (Gehan-Breslow-Wilcoxon, p=0.0979; log-rank, p=0.1219; HR (high) (Mantel-Haenszel) =1.209). **C)** No significant correlation was identified between *PRIM1* expression and EFS (Gehan-Breslow-Wilcoxon, p=0.3968; log-rank, p=0.4763; HR (high) (Mantel-Haenszel) =0.9167). **D)** EFS analysis in the context of *PRIM2* levels also failed to produce a significant correlation (Gehan-Breslow-Wilcoxon, p=0.9521; log-rank, p=0.7397; HR (high) (Mantel-Haenszel) = 1.041).

References:

1. De Kouchkovsky, I. and M. Abdul-Hay, *'Acute myeloid leukemia: a comprehensive review and 2016 update'.* Blood Cancer J, 2016. **6**(7): p. e441.
2. Dong, Y., et al., *Leukemia incidence trends at the global, regional, and national level between 1990 and 2017.* Exp Hematol Oncol, 2020. **9**: p. 14.
3. Vakiti, A., et al., *Acute Myeloid Leukemia (Nursing)*, in *StatPearls*. 2024: Treasure Island (FL).
4. Dhakal, P., et al., *Early mortality and overall survival in acute promyelocytic leukemia: do real-world data match results of the clinical trials?* Leuk Lymphoma, 2021. **62**(8): p. 1949-1957.
5. Yilmaz, M., H. Kantarjian, and F. Ravandi, *Acute promyelocytic leukemia current treatment algorithms.* Blood Cancer J, 2021. **11**(6): p. 123.
6. Patel, A., et al., *Outcomes of Patients With Acute Myeloid Leukemia Who Relapse After 5 Years of Complete Remission.* Oncol Res, 2021. **28**(7): p. 811-814.
7. Ravandi, F., *Relapsed acute myeloid leukemia: why is there no standard of care?* Best Pract Res Clin Haematol, 2013. **26**(3): p. 253-9.
8. Thol, F. and A. Ganser, *Treatment of Relapsed Acute Myeloid Leukemia.* Curr Treat Options Oncol, 2020. **21**(8): p. 66.
9. Gamal, A.-H., *Classification of Acute Leukemia*, in *Acute Leukemia*, A. Mariastefania, Editor. 2011, IntechOpen: Rijeka. p. Ch. 1.
10. Costa, A.F.O., et al., *Role of new Immunophenotypic Markers on Prognostic and Overall Survival of Acute Myeloid Leukemia: a Systematic Review and Meta-Analysis.* Sci Rep, 2017. **7**(1): p. 4138.
11. Kantarjian, H.M., et al., *Acute myeloid leukemia: Treatment and research outlook for 2021 and the MD Anderson approach.* Cancer, 2021. **127**(8): p. 1186-1207.
12. Daver, N., et al., *New directions for emerging therapies in acute myeloid leukemia: the next chapter.* Blood Cancer J, 2020. **10**(10): p. 107.
13. Wiernik, P.H., et al., *Cytarabine plus idarubicin or daunorubicin as induction and consolidation therapy for previously untreated adult patients with acute myeloid leukemia.* Blood, 1992. **79**(2): p. 313-9.
14. Yates, J., et al., *Cytosine arabinoside with daunorubicin or adriamycin for therapy of acute myelocytic leukemia: a CALGB study.* Blood, 1982. **60**(2): p. 454-62.
15. Li, Z., et al., *Exploring the Antitumor Mechanism of High-Dose Cytarabine through the Metabolic Perturbations of Ribonucleotide and Deoxyribonucleotide in Human Promyelocytic Leukemia HL-60 Cells.* Molecules, 2017. **22**(3).
16. El-Subbagh, H.I. and A.A. Al-Badr, *Chapter 2 - Cytarabine*, in *Profiles of Drug Substances, Excipients and Related Methodology*, H.G. Brittain, Editor. 2009, Academic Press. p. 37-113.
17. Avendaño López, C. and J.C. Menendez, *Medicinal Chemistry of Anticancer Drugs: Second Edition.* Medicinal Chemistry of Anticancer Drugs: Second Edition, 2015: p. 1-740.
18. Messikommer, A., et al., *RNA Targeting in Acute Myeloid Leukemia.* ACS Pharmacol Transl Sci, 2020. **3**(6): p. 1225-1232.
19. Geisberg, C.A. and D.B. Sawyer, *Mechanisms of anthracycline cardiotoxicity and strategies to decrease cardiac damage.* Curr Hypertens Rep, 2010. **12**(6): p. 404-10.

20. Perl, A.E., *Which novel agents will have a clinically meaningful impact in AML at diagnosis?* Best Pract Res Clin Haematol, 2021. **34**(1): p. 101257.
21. Krug, U., et al., *The treatment of elderly patients with acute myeloid leukemia.* Dtsch Arztebl Int, 2011. **108**(51-52): p. 863-70.
22. Negotei, C., et al., *A Review of FLT3 Kinase Inhibitors in AML.* J Clin Med, 2023. **12**(20).
23. Wouters, B.J., *Targeting IDH1 and IDH2 Mutations in Acute Myeloid Leukemia: Emerging Options and Pending Questions.* Hemasphere, 2021. **5**(6): p. e583.
24. Xu, J., et al., *Current Advances and Future Strategies for BCL-2 Inhibitors: Potent Weapons against Cancers.* Cancers (Basel), 2023. **15**(20).
25. Illangeswaran, R.S.S., et al., *A personalized approach to acute myeloid leukemia therapy: current options.* Pharmgenomics Pers Med, 2019. **12**: p. 167-179.
26. Döhner, H., A.H. Wei, and B. Löwenberg, *Towards precision medicine for AML.* Nature Reviews Clinical Oncology, 2021. **18**(9): p. 577-590.
27. Kim, Y.K., *RNA therapy: rich history, various applications and unlimited future prospects.* Exp Mol Med, 2022. **54**(4): p. 455-465.
28. Shi, Y., et al., *Chemically Modified Platforms for Better RNA Therapeutics.* Chem Rev, 2024. **124**(3): p. 929-1033.
29. Zhu, Y., et al., *RNA-based therapeutics: an overview and prospectus.* Cell Death Dis, 2022. **13**(7): p. 644.
30. Saw, P.E. and E. Song, *Advancements in clinical RNA therapeutics: Present developments and prospective outlooks.* Cell Rep Med, 2024. **5**(5): p. 101555.
31. Esendagli, G., et al., *Transfection of myeloid leukaemia cell lines is distinctively regulated by fibronectin substratum.* Cytotechnology, 2009. **61**(1-2): p. 45-53.
32. Jin, J., et al., *Clustering of endocytic organelles in parental and drug-resistant myeloid leukaemia cell lines lacking centrosomally organised microtubule arrays.* Int J Biochem Cell Biol, 2008. **40**(10): p. 2240-52.
33. Vadeikiene, R., et al., *Systemic Optimization of Gene Electrotransfer Protocol Using Hard-to-Transfect UT-7 Cell Line as a Model.* Biomedicines, 2022. **10**(11).
34. Larsen, H.O., et al., *Nonviral transfection of leukemic primary cells and cells lines by siRNA-a direct comparison between Nucleofection and Accell delivery.* Exp Hematol, 2011. **39**(11): p. 1081-9.
35. Sherba, J.J., et al., *The effects of electroporation buffer composition on cell viability and electro-transfection efficiency.* Sci Rep, 2020. **10**(1): p. 3053.
36. Kovecses, O., F.E. Mercier, and M. McKeague, *Nucleic acid therapeutics as differentiation agents for myeloid leukemias.* Leukemia, 2024. **38**(7): p. 1441-1454.
37. Dume, B., E. Licarete, and M. Banciu, *Advancing cancer treatments: The role of oligonucleotide-based therapies in driving progress.* Mol Ther Nucleic Acids, 2024. **35**(3): p. 102256.
38. Cortes, J., et al., *Phase 2 randomized study of p53 antisense oligonucleotide (cenersen) plus idarubicin with or without cytarabine in refractory and relapsed acute myeloid leukemia.* Cancer, 2012. **118**(2): p. 418-27.
39. Ohanian, M., et al., *Liposomal Grb2 antisense oligodeoxynucleotide (BP1001) in patients with refractory or relapsed haematological malignancies: a single-centre, open-label, dose-escalation, phase 1/1b trial.* Lancet Haematol, 2018. **5**(4): p. e136-e146.

40. Van den Avont, A. and N. Sharma-Walia, *Anti-nucleolin aptamer AS1411: an advancing therapeutic.* Front Mol Biosci, 2023. **10**: p. 1217769.
41. Walker, A.R., et al., *Phase 3 randomized trial of chemotherapy with or without oblimersen in older AML patients: CALGB 10201 (Alliance).* Blood Adv, 2021. **5**(13): p. 2775-2787.
42. Walker, C.J., et al., *Genetic Characterization and Prognostic Relevance of Acquired Uniparental Disomies in Cytogenetically Normal Acute Myeloid Leukemia.* Clin Cancer Res, 2019. **25**(21): p. 6524-6531.
43. Yin, J., et al., *Evaluation of event-free survival as a robust end point in untreated acute myeloid leukemia (Alliance A151614).* Blood Adv, 2019. **3**(11): p. 1714-1721.
44. Tan, C.P., et al., *RNA Activation-A Novel Approach to Therapeutically Upregulate Gene Transcription.* Molecules, 2021. **26**(21).
45. Hu, B., et al., *Therapeutic siRNA: state of the art.* Signal Transduction and Targeted Therapy, 2020. **5**(1): p. 101.
46. Wang, Y., et al., *Use of polymeric CXCR4 inhibitors as siRNA delivery vehicles for the treatment of acute myeloid leukemia.* Cancer Gene Ther, 2020. **27**(1-2): p. 45-55.
47. Karami, H., et al., *Therapeutic Effects of Myeloid Cell Leukemia-1 siRNA on Human Acute Myeloid Leukemia Cells.* Adv Pharm Bull, 2014. **4**(3): p. 243-8.
48. Sarker, D., et al., *MTL-CEBPA, a Small Activating RNA Therapeutic Upregulating C/EBP-alpha, in Patients with Advanced Liver Cancer: A First-in-Human, Multicenter, Open-Label, Phase I Trial.* Clin Cancer Res, 2020. **26**(15): p. 3936-3946.
49. Hofman, C.R. and D.R. Corey, *Targeting RNA with synthetic oligonucleotides: Clinical success invites new challenges.* Cell Chem Biol, 2024. **31**(1): p. 125-138.
50. Kim, H., et al., *Oligonucleotide therapeutics and their chemical modification strategies for clinical applications.* Journal of Pharmaceutical Investigation, 2024. **54**(4): p. 415-433.
51. Grosjean-Raillard, J., et al., *Erratum to: Flt3 receptor inhibition reduces constitutive NFkappaB activation in high-risk myelodysplastic syndrome and acute myeloid leukemia.* Apoptosis, 2015. **20**(12): p. 1666-7.
52. Tyner, J.W., et al., *RNAi screen for rapid therapeutic target identification in leukemia patients.* Proc Natl Acad Sci U S A, 2009. **106**(21): p. 8695-700.
53. Maru, B., et al., *PARP-1 improves leukemia outcomes by inducing parthanatos during chemotherapy.* Cell Rep Med, 2023. **4**(9): p. 101191.
54. Zheng, L., et al., *RNA activation: promise as a new weapon against cancer.* Cancer Lett, 2014. **355**(1): p. 18-24.
55. Watts, J.K. and D.R. Corey, *Silencing disease genes in the laboratory and the clinic.* (1096-9896 (Electronic)).
56. Fleischmann, K.K., et al., *RNAi-mediated silencing of MLL-AF9 reveals leukemia-associated downstream targets and processes.* Mol Cancer, 2014. **13**: p. 27.
57. Kwok, A., N. Raulf, and N. Habib, *Developing small activating RNA as a therapeutic: current challenges and promises.* Ther Deliv, 2019. **10**(3): p. 151-164.
58. Voutila, J., et al., *Gene Expression Profile Changes After Short-activating RNA-mediated Induction of Endogenous Pluripotency Factors in Human Mesenchymal Stem Cells.* Molecular Therapy - Nucleic Acids, 2012. **1**.
59. Small, S., T.S. Oh, and L.C. Platanias, *Role of Biomarkers in the Management of Acute Myeloid Leukemia.* Int J Mol Sci, 2022. **23**(23).

60. Cheng, W.Y., et al., *Transcriptome-based molecular subtypes and differentiation hierarchies improve the classification framework of acute myeloid leukemia.* Proc Natl Acad Sci U S A, 2022. **119**(49): p. e2211429119.
61. Nguyen, N.H.K., et al., *Global Proteomic Profiling of Pediatric AML: A Pilot Study.* Cancers (Basel), 2021. **13**(13).
62. Qin, Y., et al., *Machine learning-based biomarker screening for acute myeloid leukemia prognosis and therapy from diverse cell-death patterns.* Sci Rep, 2024. **14**(1): p. 17874.
63. Jiang, Z. and Y. Zhou, *Using bioinformatics for drug target identification from the genome.* Am J Pharmacogenomics, 2005. **5**(6): p. 387-96.
64. Chen, S., et al., *Bioinformatics Analysis Identifies Key Genes and Pathways in Acute Myeloid Leukemia Associated with DNMT3A Mutation.* Biomed Res Int, 2020. **2020**: p. 9321630.
65. Xu, X., et al., *Comprehensive bioinformatic analysis of the expression and prognostic significance of TSC22D domain family genes in adult acute myeloid leukemia.* BMC Med Genomics, 2023. **16**(1): p. 117.
66. Han, H., et al., *Identification of two key biomarkers CD93 and FGL2 associated with survival of acute myeloid leukaemia by weighted gene co-expression network analysis.* J Cell Mol Med, 2024. **28**(14): p. e18552.
67. Hoogenboezem, E.N., et al., *Structural optimization of siRNA conjugates for albumin binding achieves effective MCL1-directed cancer therapy.* Nat Commun, 2024. **15**(1): p. 1581.
68. Shinohara, F., et al., *siRNA potency enhancement via chemical modifications of nucleotide bases at the 5'-end of the siRNA guide strand.* RNA, 2021. **27**(2): p. 163-173.
69. Bowes, J., et al., *Reducing safety-related drug attrition: the use of in vitro pharmacological profiling.* Nat Rev Drug Discov, 2012. **11**(12): p. 909-22.
70. Vicens, Q. and E. Westhof, *Brief considerations on targeting RNA with small molecules.* Fac Rev, 2022. **11**: p. 39.
71. Triemer, T., et al., *Superresolution imaging of individual replication forks reveals unexpected prodrug resistance mechanism.* Proc Natl Acad Sci U S A, 2018. **115**(7): p. E1366-E1373.
72. He, Q., et al., *Structures of the human CST-Polalpha-primase complex bound to telomere templates.* Nature, 2022. **608**(7924): p. 826-832.
73. Dang, T.T. and J.C. Morales, *Involvement of POLA2 in Double Strand Break Repair and Genotoxic Stress.* Int J Mol Sci, 2020. **21**(12).
74. Yang, H., et al., *PolA2 is required for embryo development in ArabidopsisThis paper is one of a selection of papers published in a Special Issue from the National Research Council of Canada – Plant Biotechnology Institute.* Botany, 2009. **87**(6): p. 626-634.
75. Liu, L., et al., *Overexpression of POLA2 in hepatocellular carcinoma is involved in immune infiltration and predicts a poor prognosis.* Cancer Cell Int, 2023. **23**(1): p. 138.
76. Teng, Y. and R. Liu, *E2F-mediated POLA2 upregulation is correlated with macrophage infiltration and poor prognosis in hepatocellular carcinoma.* Transl Cancer Res, 2024. **13**(4): p. 1848-1860.
77. Yang, Z., et al., *The Biological Function of POLA2 in Hepatocellular Carcinoma.* Comb Chem High Throughput Screen, 2024. **27**(12): p. 1758-1775.
78. Kim, T.Y., et al., *DNA Polymerase Alpha Subunit B Is a Binding Protein for Erlotinib Resistance in Non-Small Cell Lung Cancer.* Cancers (Basel), 2020. **12**(9).

79. Koh, V., et al., *Knockdown of POLA2 increases gemcitabine resistance in lung cancer cells.* BMC Genomics, 2016. **17**(Suppl 13): p. 1029.
80. Willis, S., et al., *Single Gene Prognostic Biomarkers in Ovarian Cancer: A Meta-Analysis.* PLoS One, 2016. **11**(2): p. e0149183.
81. Kang, G., et al., *Integrated genomic analyses identify frequent gene fusion events and VHL inactivation in gastrointestinal stromal tumors.* Oncotarget, 2016. **7**(6): p. 6538-51.
82. Skopek, R.A.-O., et al., *Choosing the Right Cell Line for Acute Myeloid Leukemia (AML) Research. LID - 10.3390/ijms24065377 [doi] LID - 5377.* (1422-0067 (Electronic)).
83. Levis, M., *FLT3/ITD AML and the law of unintended consequences.* Blood, 2011. **117**(26): p. 6987-6990.
84. Bodbin, S.A.-O., C.A.-O. Denning, and D.A.-O. Mosqueira, *Transfection of hPSC-Cardiomyocytes Using Viafect™ Transfection Reagent. LID - 10.3390/mps3030057 [doi] LID - 57.* (2409-9279 (Electronic)).
85. Kawaai, K., et al., *Optimization of Transfection Conditions for Gene Expression, siRNA Knock-Down, and Live Cell Imaging Using FuGENE® HD Transfection Reagent.* BIOCHEMICA-MANNHEIM-, 2008. **1**: p. 21.
86. Jensen, K., J.A. Anderson, and E.J. Glass, *Comparison of small interfering RNA (siRNA) delivery into bovine monocyte-derived macrophages by transfection and electroporation.* Veterinary Immunology and Immunopathology, 2014. **158**(3): p. 224-232.
87. Böttger, J., et al., *RNAi in murine hepatocytes: the agony of choice--a study of the influence of lipid-based transfection reagents on hepatocyte metabolism.* (1432-0738 (Electronic)).
88. Alshamsan, A., et al., *Formulation and Delivery of siRNA by Oleic Acid and Stearic Acid Modified Polyethylenimine.* Molecular Pharmaceutics, 2009. **6**(1): p. 121-133.
89. Yan, F., et al., *Fatty acid-binding protein FABP4 mechanistically links obesity with aggressive AML by enhancing aberrant DNA methylation in AML cells.* Leukemia, 2017. **31**(6): p. 1434-1442.
90. Lacroix, A., et al., *Uptake and Fate of Fluorescently Labeled DNA Nanostructures in Cellular Environments: A Cautionary Tale.* ACS Central Science, 2019. **5**(5): p. 882-891.
91. Chong, Z.X., S.A.-O. Yeap, and W.Y. Ho, *Transfection types, methods and strategies: a technical review.* (2167-8359 (Print)).
92. Kasai, H., et al., *Efficient siRNA delivery and gene silencing using a lipopolypeptide hybrid vector mediated by a caveolae-mediated and temperature-dependent endocytic pathway.* Journal of Nanobiotechnology, 2019. **17**(1): p. 11.
93. Wallenstein, E.J., et al., *Serum starvation improves transient transfection efficiency in differentiating embryonic stem cells.* Biotechnology Progress, 2010. **26**(6): p. 1714-1723.
94. Tarakanchikova, Y.V., et al., *Boosting transfection efficiency: A systematic study using layer-by-layer based gene delivery platform.* Materials Science and Engineering: C, 2021. **126**: p. 112161.
95. Napirei, M., et al., *Murine serum nucleases – contrasting effects of plasmin and heparin on the activities of DNase1 and DNase1-like 3 (DNase1l3).* The FEBS Journal, 2009. **276**(4): p. 1059-1073.
96. Barnaby, S.N., A. Lee, and C.A. Mirkin, *Probing the inherent stability of siRNA immobilized on nanoparticle constructs.* (1091-6490 (Electronic)).